

Russian Original Vol. 48, No. 2, February, 1980

August, 1980

FILE

SATEAZ 48(2) 71-152 (1980)

5 - NOV 1980

SOVIET ATOMIC ENERGY

АТОМНАЯ ЭНЕРГИЯ
(ATOMNAYA ÉNERGIYA)

TRANSLATED FROM RUSSIAN

CONSULTANTS BUREAU, NEW YORK

SOVIET ATOMIC ENERGY

Soviet Atomic Energy is a translation of *Atomnaya Énergiya*, a publication of the Academy of Sciences of the USSR.

An agreement with the Copyright Agency of the USSR (VAAP) makes available both advance copies of the Russian journal and original glossy photographs and artwork. This serves to decrease the necessary time lag between publication of the original and publication of the translation and helps to improve the quality of the latter. The translation began with the first issue of the Russian journal.

Consultants Bureau journals appear about six months after the publication of the original Russian issue. For bibliographic accuracy, the English issue published by Consultants Bureau carries the same number and date as the original Russian from which it was translated. For example, a Russian issue published in December will appear in a Consultants Bureau English translation about the following June, but the translation issue will carry the December date. When ordering any volume or particular issue of a Consultants Bureau journal, please specify the date and, where applicable, the volume and issue numbers of the original Russian. The material you will receive will be a translation of that Russian volume or issue.

Subscription (2 volumes per year)

Vols. 46 & 47: $147.50 per volume (6 Issues)
Vols. 48 & 49: $167.50 per volume (6 Issues)

Single Issue: $50
Single Article: $7.50

Prices somewhat higher outside the United States.

Soviet Atomic Energy is abstracted or indexed in *Chemical Abstracts, Chemical Titles, Pollution Abstracts, Science Research Abstracts, Parts A and B, Safety Science Abstracts Journal, Current Contents, Energy Research Abstracts,* and *Engineering Index.*

CONSULTANTS BUREAU, NEW YORK AND LONDON

c/b
227 West 17th Street
New York, New York 10011

Published monthly. Second-class postage paid at Jamaica, New York 11431.

SOVIET ATOMIC ENERGY

A translation of *Atomnaya Énergiya*

August, 1980

Volume 48, Number 2 February, 1980

CONTENTS

CONTENTS

(continued)

The Russian press date (podpisano k pechati) of this issue was 1/23/1980. Publication therefore did not occur prior to this date, but must be assumed to have taken place reasonably soon thereafter.

ARTICLES

DEPENDENCE OF ^{232}U FORMATION IN NUCLEAR FUEL ON NEUTRON SPECTRUM

T. S. Zaritskaya, S. M. Zaritskii,
A. K. Kruglov, L. V. Matveev,
A. P. Rudik, and É. M. Tsenter

UDC 621.039.516.22

In the combustion of nuclear fuel, ^{232}U is formed, which is extremely undesirable since its presence in regenerated uranium may lead to marked deterioration in the radiational set-up at all stages of the fuel cycle. In fact, ^{232}U itself is a weak γ emitter, but its decay chain (Fig. 1) includes ^{208}Tl, which intensely emits high-energy γ radiation at an energy of 2.61 MeV.

The time dependence of the exposure dose rate at a distance of 1 m from a point source initially containing 1 mg of pure ^{232}U is shown in Fig. 2. The dose rate reaches a maximal value of 12.9 mR/h after 10.3 years (1 R = $2.58 \cdot 10^{-4}$ Ci/kg). The exposure dose rate from uranium with 1, 3, and 6% enrichment with ^{235}U in the absence of protection doubles if the uranium contains, respectively, $3 \cdot 10^{-8}$, $5 \cdot 10^{-8}$, and $9 \cdot 10^{-8}$ mass % ^{232}U.

When, in working with regenerated uranium, release of the uranium into the air is possible, the ^{232}U content should be established on the basis of the permitted concentrations of ^{232}U and natural uranium in the air of mineshafts [1]: $6.1 \cdot 10^{-13}$ and $8.8 \cdot 10^{-5}$ mg/liter, respectively. The internal irradiation of personnel doubles if in natural uranium there is $7 \cdot 10^{-7}$ mass % ^{232}U ($6.1 \cdot 10^{-13}/8.8 \cdot 10^{-5}$). The additional radiational danger associated with ^{232}U is due to the release of the gaseous decay product thoron (^{220}Rn) into the air of mineshafts.

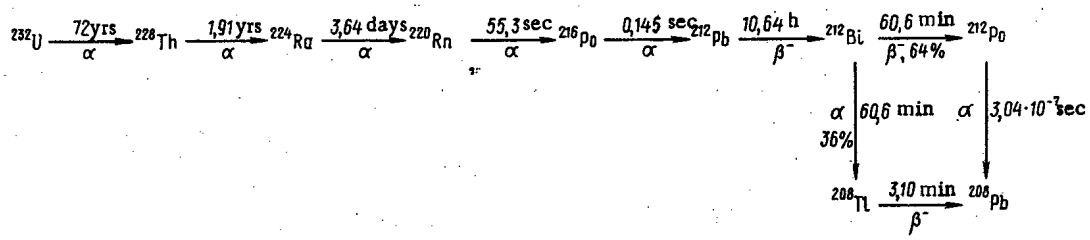

Fig. 1. Decay chain for ^{232}U.

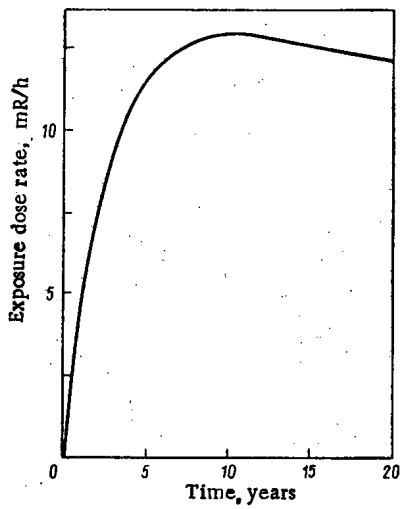

Fig. 2. Time dependence of exposure dose rate from a point source containing 1 mg of pure ^{232}U initially.

Translated from Atomnaya Énergiya, Vol. 48, No. 2, pp. 67-70, February, 1980. Original article submitted May 28, 1979.

0038-531X/80/4802-0071 $07.50

Decay Chain Forming ^{232}U

The decay chains forming ^{232}U in nuclear-reactor fuel may be divided into two groups. The first contains chains including the reaction (n, γ)

$$^{235}U\ (n, \gamma)\ ^{236}U\ (n, \gamma)\ ^{237}U\ (\beta^-)\ ^{237}Np\ (n, 2n)\ ^{236}Np\ (50\%,\ \beta^-)\ ^{236}Pu\ (\alpha)\ ^{232}U; \quad (1.1)$$

$$^{234}U\ (\alpha)\ ^{230}Th\ (n, \gamma)\ ^{231}Th\ (\beta^-)\ ^{231}Pa\ (n, \gamma)\ ^{232}Pa\ (\beta^-)\ ^{232}U; \quad (1.2)$$

$$^{235}U\ (\alpha)\ ^{231}Th\ (\beta^-)\ ^{231}Pa\ (n, \gamma)\ ^{232}Pa\ (\beta^-)\ ^{232}U. \quad (1.3)$$

If the fuel is produced from regenerated uranium, it will contain a certain amount of ^{236}U. Irradiation of ^{236}U also leads to the formation of ^{232}U

$$^{236}U\ (n, \gamma)\ ^{237}U\ (\beta^-)\ ^{237}Np\ (n, 2n)\ ^{236}Np\ (50\%,\ \beta^-)\ ^{236}Pu\ (\alpha)\ ^{232}U. \quad (1.4)$$

Fuel that has not been subjected to gas-diffusion enrichment always includes a certain amount of ^{232}Th, ^{230}Th, and ^{231}Pa. These nuclides at first give the following chain for the formation of ^{232}U:

$$^{232}Th\ (n, 2n)\ ^{231}Th\ (\beta^-)\ ^{231}Pa\ (n, \gamma)\ ^{232}Pa\ (\beta^-)\ ^{232}U; \quad (1.5)$$

$$^{232}Th\ (n, \gamma)\ ^{233}Th\ (\beta^-)\ ^{233}Pa\ (n, 2n)\ ^{232}Pa\ (\beta^-)\ ^{232}U; \quad (1.6)$$

$$^{230}Th\ (n, \gamma)\ ^{231}Th\ (\beta^-)\ ^{231}Pa\ (n, \gamma)\ ^{232}Pa\ (\beta^-)\ ^{232}U; \quad (1.7)$$

$$^{231}Pa\ (n, \gamma)\ ^{232}Pa\ (\beta^-)\ ^{232}U; \quad (1.8)$$

$$^{232}Th\ (n, \gamma)\ ^{233}Th\ (\beta^-)\ ^{233}Pa\ (\beta^-)\ ^{233}U\ (n, 2n)\ ^{232}U. \quad (1.9)$$

The products of gas-diffusion plants do not include protactinium and thorium. However, in time, a certain amount of ^{230}Th and ^{231}Pa may accumulate in the fuel as a result of the decay of ^{234}U and ^{235}U.

The second group contains processes that do not involve the reaction (n, γ)

$$^{234}U\ (n, 3n)\ ^{232}U; \quad (2.1)$$

$$^{238}U\ (n, 2n)\ ^{237}U\ (\beta^-)\ ^{237}Np\ (n, 2n)\ ^{236}Np\ (50\%,\ \beta^-)\ ^{236}Pu\ (\alpha)\ ^{232}U. \quad (2.2)$$

If the regenerated fuel includes neptunium as an impurity, an additional chain that forms ^{232}U appears

$$(2.3)\ ^{237}Np\ (n, 2n)\ ^{236}Np,\ (50\%,\ \beta^-)\ ^{236}Pu\ (\alpha)\ ^{232}U. \quad (2.3)$$

Rate of Formation of ^{232}U

The reactions (n, 2n) and (n, 3n) are characterized by fairly high energy thresholds: 6-8 and ~13 MeV, respectively. Therefore, it is assumed that the effective rate of the reactions (n, 2n) and (n, 3n) – $\Phi\sigma^{eff}(n, 2n)$ – does not depend on the neutron spectrum in the reactor

$$\Phi\sigma^{eff}(n, 2n) = \frac{\nu W}{E_f}\sigma(n, 2n)F, \quad (1)$$

where Φ is the neutron flux density; σ(n, 2n), microscopic cross section of the reaction (n, 2n); ν, number of neutrons in one fission act; W, specific power associated with the nuclear fuel; E_f, energy liberated in fission;

TABLE 1. Physical Characteristics of Nuclides

Nuclide	Reaction	σ, b	I, b	$T_{1/2}$
^{230}Th	(n, γ)	23,2	1010	$8{,}0\cdot10^4$ yr
^{231}Th	β^-	—	—	25,52 h
^{231}Pa	(n, γ)	210	1500	$3{,}25\cdot10^4$ yr
^{232}Pa	β^-	—	—	1,3 day
^{232}U	α	—	—	72 h
^{235}U	f	582,2	275	$7{,}1\cdot10^8$ yr
	(n, γ)	98,6	144	
^{236}U	(n, γ)	5,2	365	$2{,}39\cdot10^7$ yr
^{237}U	β^-	—	—	6,75 day
^{237}Np	(n, γ)	169	660	$2{,}14\cdot10^6$ yr
	$(n, 2n)$	—	$0{,}82\cdot10^{-2}$	

* 1 b = 10^{-28} m^2.

TABLE 2. Probability of Nuclide Formation

Nuclide	Chain	Probability
^{237}Np	(1.1)	$\frac{\sigma_{235U}(n, \gamma)}{\sigma_{235U}(f)}\frac{\sigma_{236U}(n, \gamma)}{\sigma_{235U}(f)}\frac{s^2}{2}$
	(1.4)	$\frac{\sigma_{236U}(n, \gamma)}{\sigma_{235U}(f)}s$
^{232}Pa	(1.7)	$\frac{\sigma_{230Th}(n, \gamma)}{\sigma_{235U}(f)}\frac{\sigma_{231Pa}(n, \gamma)}{\sigma_{235U}(f)}\frac{s^2}{2}$
	(1.8)	$\frac{\sigma_{231Pa}(n, \gamma)}{\sigma_{235U}(f)}s$

TABLE 3. Dependence of Cross-Sectional Ratio on Neutron-Spectrum Hardness

Cross-sectional ratio	γ					
	0,0	0,1	0,2	0,4	1,0	∞ *
$\sigma_{^{235}U}(n, \gamma)/\sigma_{^{235}U}(f)$	0.17	0.19	0.20	0.23	0.28	0.52
$\sigma_{^{236}U}(n, \gamma)/\sigma_{^{235}U}(f)$	0.0089	0.068	0.123	0.218	0.432	1.33
$\sigma_{^{230}Th}(n, \gamma)/\sigma_{^{235}U}(f)$	0.0040	0.204	0.353	0.617	1.21	3.67
$\sigma_{^{231}Pa}(n, \gamma)/\sigma_{^{235}U}(f)$	0.36	0.59	0.80	1.17	2.00	5.46
$\frac{\sigma_{^{235}U}(n, \gamma)}{\sigma_{^{235}U}(f)} \frac{\sigma_{^{236}U}(n, \gamma)}{\sigma_{^{235}U}(f)}$	0.0015	0.0127	0.0245	0.0493	0.122	0.700
$\frac{\sigma_{^{230}Th}(n, \gamma)}{\sigma_{^{235}U}(f)} \frac{\sigma_{^{231}Pa}(n, \gamma)}{\sigma_{^{235}U}(f)}$	0.014	0.123	0.283	0.722	2.40	20.0

* $\gamma = \infty$, i.e., in Eq. (2) $(2)\ U\sigma(n, \gamma) \ll \gamma IU$.

TABLE 4. Neutron-Spectrum Hardness in Power Reactors

Reaction type	^{235}U content in nuclear fuel mass, %	γ	Reaction type	^{235}U content in nuclear fuel mass, %	γ
VVÉR	1,6	0,23—0,33	BAÉS	1,5	0,2
	2,4	0,36—0,50		3,0	0,3
	3,6	0,56—0,73		5,75	0,44
RBMK	1,8	0,035—0,110	KS *	0,714	0,10—0,12

* Heavy-water power reactor with gas cooling, A-1 atomic power station, Czechoslovakia.

F, a geometric factor taking into account the fuel-element disposition and the properties of the moderator between them.

It is of interest to investigate the dependence of ^{232}U formation on the neutron spectrum for certain given depths of burnup and given initial compositions of the fuel. The only quantity sensitive to the neutron spectrum is the cross section of the reaction (n, γ). In power reactors of water-cooled–water-moderated (VVÉR) types, the rate of the reaction (n, γ) is given by the expression

$$\Phi\sigma^{\text{eff}}(n, \gamma) = U\sigma(n, \gamma) + \gamma IU, \tag{2}$$

where U is the thermal-neutron flux density; γ is a factor characterizing the ratio of neutron flux densities in the resonance and thermal parts of the spectrum (the rigidity of the spectrum) [2].

The dependence of ^{232}U formation on γ may be demonstrated for the example of the chains in Eqs. (1.1), (1.4), (1.7), and (1.8). Analogous estimates may easily be made for other chains. The probability of ^{232}U formation by the chains in Eqs. (1.1) and (1.4) is determined by the probability of ^{237}Np formation, and the probability for Eqs. (1.7) and (1.8) by the probability of ^{232}Pa formation. Table 1 shows the physical characteristics of the nuclides appearing in these chains (σ is the cross section at an energy E = 0.025 eV; I is the resonance integral for E = 0.5 eV; $T_{1/2}$ is the half life).

The probability of nuclide formation by a particular chain (Table 2) at small nuclear-fuel burnup [3] is taken to mean the ratio between the number of nuclei formed at burnup s to the initial number of nuclei in the first element of the chain, where $s = \sigma_{^{235}U}(f)\Phi t$. Table 3 gives the cross-sectional ratios appearing in the formation of Table 2, which are determined for different hardnesses of the neutron spectrum γ (the data of Table 1 are used). It follows from the data of Table 3 that the corresponding cross-sectional ratio increases practically linearly with rise in γ. In [3], rough values of γ for power reactors are given (Table 4).

TABLE 5. Probability of Nuclide Formation

Nuclide	Chain	γ	Burnup			
			0,5	1,0	1,5	2,0
^{237}Np	(1.1)	0,0	$1{,}48\cdot10^{-4}$	$4{,}77\cdot10^{-4}$	$8{,}70\cdot10^{-4}$	$1{,}27\cdot10^{-3}$
		0,1	$1{,}21\cdot10^{-3}$	$3{,}75\cdot10^{-3}$	$6{,}64\cdot10^{-3}$	$9{,}39\cdot10^{-3}$
		0,2	$2{,}30\cdot10^{-3}$	$6{,}92\cdot10^{-3}$	$1{,}19\cdot10^{-2}$	$1{,}63\cdot10^{-2}$
		∞	$3{,}63\cdot10^{-2}$	$6{,}18\cdot10^{-2}$	$5{,}97\cdot10^{-2}$	$4{,}59\cdot10^{-2}$
	(1.4)	0,0	$4{,}15\cdot10^{-3}$	$7{,}72\cdot10^{-3}$	$1{,}08\cdot10^{-2}$	$1{,}34\cdot10^{-2}$
		0,1	$3{,}05\cdot10^{-2}$	$5{,}47\cdot10^{-2}$	$7{,}36\cdot10^{-2}$	$8{,}83\cdot10^{-2}$
		0,2	$5{,}10\cdot10^{-2}$	$9{,}17\cdot10^{-2}$	0,119	0,138
		∞	0,264	0,216	0,135	$7{,}68\cdot10^{-2}$
^{232}Pa	(1.7)	0,0	$1{,}62\cdot10^{-3}$	$6{,}30\cdot10^{-3}$	$1{,}32\cdot10^{-2}$	$2{,}22\cdot10^{-2}$
		0,1	$1{,}32\cdot10^{-2}$	$4{,}65\cdot10^{-2}$	$9{,}25\cdot10^{-2}$	0,146
		0,2	$2{,}93\cdot10^{-2}$	$9{,}76\cdot10^{-2}$	0,184	0,276
		∞	0,647	0,931	0,988	0,998
	(1.8)	0,0	0,165	0,303	0,418	0,514
		0,1	0,256	0,446	0,588	0,693
		0,2	0,330	0,551	0,699	0,798
		∞	0,935	0,996	1,00	1,00

TABLE 6. Cross-Sectional Ratios for Fast Reactors

Cross-sectional ratio	Reaction with highly enriched fuel	"Large" reactor		
		active region	reproduction region	
			a	b
$\sigma_{^{235}U}(n, \gamma)/\sigma_{^{235}U}(f)_{AR}$	0,19	0,31	0,37	0,19
$\sigma_{^{236}U}(n, \gamma)/\sigma_{^{235}U}(f)_{AR}$	0,25	0,36	0,45	0,22
$\sigma_{^{231}Pa}(n, \gamma)/\sigma_{^{235}U}(f)_{AR}$	0,55	0,87	1,01	0,50

Using the data of Tables 2 and 3, the dependence of ^{232}U accumulation along the chains in Eqs. (1.1), (1.4), (1.7), and (1.8) on γ may be determined. The dependence of ^{232}U accumulation along the chains in Eqs. (1.1) and (1.4) is weaker than the dependence of the ^{237}Np yield on γ, since the quantity of ^{232}U is determined by the integral over time of the amount of ^{237}Np. The dependence of the total ^{232}U accumulation in the spent fuel on the neutron spectrum is determined by the relative contribution of chains of the first group to the total accumulation. The latter depends on the time elapsed from the moment of fuel-element manufacture to the onset of the operating cycle, on the duration of the operating cycle, and on the storage time of the spent fuel. At large nuclear-fuel burnup, the probability of nuclide formation is calculated by the method outlined in [3] (Table 5).

Fast Reactors

Equation (2) for the rate of the reaction (n, γ) is inapplicable for these reactors (formulas of this type are only valid for reactors with a relatively soft neutron spectrum). Table 6 shows cross-sectional ratios averaged over the spectra of different fast reactors with oxide fuel and sodium coolant; reactors with highly enriched fuel and small dimensions of the active region [4], and reactors of type BN-350 but of much larger power and dimensions – ~1600 MW (electrical). The neutron spectra differ significantly in degree of hardness, so that the data given in Table 6 characterize the limits within which these cross-sectional ratios may vary in fast oxide reactors with sodium coolant. The mean radiation-capture cross section is referred to the mean cross section for ^{235}U fission in the active region. For the reproduction region of the "large" reactor, data are given before (a) and after (b) taking account of the change in neutron-flux level in comparison with the active region. The multigroup cross sections used in averaging correspond to the BNAB-70 system of constants [5, 6]. Data on the radiational-capture cross section for ^{230}Th have not been published.

Comparing the data of Tables 6 and 3, and taking into account the dependence of γ on the type of reactor (Table 4) and the probability of ^{232}U formation (Table 2), it is found that, neglecting the different effective cross sections for the reaction (n, 2n) in reactors of different type, the probability of ^{232}U formation in fast reactors over the given chains is approximately the same as in power reactors of water-cooled – water-moderated type with an enrichment of 3.6% (it is assumed here that the burnup depth is the same).

Conclusions

As a result of the calculations, it has been established that for nuclear reactors of power type the amount of ^{232}U formed depends significantly on the neutron-spectrum hardness, while for fast reactors operating on uranium fuel this amount is close to the quantity of ^{232}U obtained in reactors of water-cooled – water-moderated type with 3.6% enrichment. The comparison is made for the same ^{235}U burnup depth, and the difference in effective cross sections of the reaction (n, 2n) is disregarded.

To determine the absolute amount of ^{232}U accumulation, it is necessary to take account of the reaction (n, 2n).

LITERATURE CITED

1. NRB-76 Radiation-Safety Standards [in Russian], Atomizdat, Moscow (1978).
2. A. D. Galanin, Theory of Thermal-Neutron Nuclear Reactors [in Russian], Atomizdat, Moscow (1959).
3. A. K. Kruglov and A. P. Rudik, Artificial Isotopes and Methods of Calculating Their Formation in Nuclear Reactors [in Russian], Atomizdat, Moscow (1977).
4. P. N. Alekseev, S. M. Zaritskii, and O. M. Kovalevich, in: Nuclear-Reactor Physics [in Russian], No. 6, Atomizdat, Moscow (1978).

5. L. P. Abagyan et al., Group Constants for Nuclear-Reactor Calculations [in Russian], Atomizdat, Moscow (1964).
6. L. P. Abagyan and V. M. Murogov, in: Bulletin of the Nuclear-Data Information Center [in Russian], No. 5, Atomizdat, Moscow (1968).

STRUCTURAL RELIABILITY OF ATOMIC POWER PLANT

A. I. Klemin and E. F. Polyakov

UDC 621.039.5.58

In 1978 the first specialized technical manual "Technique of Calculating the Structural Reliability of an Atomic Power Plant and Its Systems in the Design Stage was developed." The present article contains information about the main characteristics and capabilities of the manual.

General Propositions. This manual is intended for calculations, during the design stage, of the indices of structural reliability of a unit of an atomic power plant, and its parts and separate systems, including the safety system. Structural reliability is construed as the structural reliability of the system of the atomic power plant unit, its parts or systems with given reliability indices for the component elements, known functional relations between them, and a strategy adopted for routine maintenance. The manual gives recommendations concerning the calculations of the reliability of such specific systems as the reactor control and safety system (CSS), the system of instrumentation and automatic control (SIAC), and safety systems.

The manual is intended for atomic power plants with the following principal features:

maintenance of its complete capability to operate despite malfunctions of a separate piece of equipment as the result of redundancy;

a capability to function despite malfunctions of several pieces of equipment at power levels below the nominal value N_n;

presence of blocks of elements of one type, constituting a structure of the "m out of n" type;

the use of the atomic power plant at various power levels (this is particularly true of atomic power plants according to a variable load schedule);

performance of regular routine maintenance during operation;

a capability of operation in a basic regimen or according to a variable load schedule.

Underlying the manual are analytic methods of the modern theory of reliability with the use of the technique of minimum cross sections of complex systems [1, 2]. Calculations by the techniques of the manual permit a quantitative evaluation of the level of structural reliability, to reveal the weak points, to choose appropriate redundancy of the equipment, to distribute the requirements concerning the reliability of the atomic power plant over the component elements by means of variation calculation (in particular, to determine the reliability requirements pertaining to the component equipment), to make comparative estimations of the reliability of various variants of structural design of the atomic power plant, etc.

To take account of the internal and external factors which affect the value of the atomic plant's power, in a reliability analysis it is necessary to introduce the concept of available and required power, $N_a(t)$ and $N_r(t)$, respectively. The available power is the highest value of the power, determined by the totality of states of all elements of the equipment, which can be delivered by the atomic power plant at a given moment of time. The required power is the value of power which is necessary at a given moment of time and is determined by the demands of the system external to the atomic power plant.

For an atomic power plant as a complex system with more than two possible states, the manual introduces the concept of efficient and inefficient states, $N_a(t) \geq N$ and $N_a(t) < N_s$, respectively, in relation to a concrete power level. As a concrete set of discrete power levels the manual considers the nominal level N_n, the minimum level $N_m \neq 0$ below which the power plant is not operated, as well as a number of intermediate

Translated from Atomnaya Énergiya, Vol. 48, No. 2, pp. 70-73, February, 1980. Original article submitted May 28, 1979.

0038-531X/80/4802-0075$07.50

levels lying in the interval $[N_m, N_n]$, in which the atomic power plant can either operate in the event of the malfunction of a separate piece of equipment or should operate in accordance with a given load schedule $N_r(t)$.

In the calculation of the reliability of atomic power plants operating in the basic regimen, $N_r(t) = N_n$, a distinction is made between total and partial malfunctions in relation to set power levels. In the reliability calculation for atomic power plants operating according to a variable load schedule malfunctions are considered in relation to a set power level N_s and malfunctions caused by the required power surpassing the available power, $N_r > N_a$.

To calculate the reliability indices of any engineering system it is necessary to formulate the conditions for operational incapacity (or operational capacity). In the manual conditions of operational incapacity of atomic power plants are formulated separately for each set power level N_s in the form of a matrix of critical states of the atomic power plant. In this connection it is necessary that for each possible state of the plant the value of the available power be found from the state of its elements and that the unoperational states be distinguished, i.e., states for which the available power is below the level considered, and it is further necessary that critical states, i.e., those which are realized with the minimum number of malfunctioning units and elements in them, be selected from the set of unoperational states. In the case of a structure that is not made up of blocks,* in order to obtain the complete set of critical states it is necessary to construct the appropriate logical scheme, i.e., the "tree of malfunctions," and on the basis of an analysis of this scheme to distinguish all the minimal sets of malfunctioning elements, critical groups of elements (CGE) for which malfunctions of the plant occur. In this case the number of rows in the matrix corresponds to the number of CGE. The number of elements in each matrix row is equal to the number of elements in the plant. The elements in a CGE are labeled by 1 and the other elements by 0.

In the case of a plant with a block structure the conditions for operational incapacity are more conveniently written by using the concept of the critical group of block states (CGBS). This concept presupposes such a set of the minimum possible number of blocks of one-type elements (with a minimum number of malfunctioning elements responsible for the state of the block) which corresponds to the nonoperational state of the atomic power plant in relation to the set power level. In this case, the number of columns in the matrix of operational incapacity is equal to the number of blocks while the number of rows is equal to the set of CGBS. In each matrix row the nonzero elements denote the number of malfunctioning elements in the blocks in the concrete CGBS.

In turn, to isolate a CGBS from a CGE it is necessary to know the relation between the available power and the state of the elements, this relation being given by the so-called state functions. The state function $f_i(x_j)$ of a block is the contribution of the j-th block (in fractions of the nominal power of the atomic power plant) as a function of the number of malfunctioning elements in it while the remainder of the blocks are in good working order. The most general form in which the state functions are given is tabular. For convenience in analysis, in accordance with the functional purpose and the structure of the atomic power plant, the blocks of one-type elements, constituting a structure of the "m out of n" type, are combined into complexes (steam-generation loop, steam-piping complex, etc.).

The state functions of each complex are expressed in terms of the state functions of the blocks comprising that complex. This relation cannot in general be written in analytic form and is given with allowance for the recommendations in the manual, e.g., for complexes consisting of series-connected blocks,

$$\varphi_k(f_1^{(k)}, \ldots, f_j^{(k)}, \ldots, f_{\hat{j}}^{(k)}) = \min\{f_1^{(k)}, \ldots, f_j^{(k)}, \ldots, f_{\hat{j}}^{(k)}\};$$

while for parallel-connected blocks,

$$\psi_k(f_1^{(k)}, \ldots, f_{\hat{j}}^{(k)}) = \sum_{j=1}^{\hat{j}} f_j^{(k)}.$$

Once state functions have been assigned for the blocks and complexes for the atomic power plant, the state function of the power plant is assigned, representing the dependence of the allowable power (as a fraction of the nominal) on the state of the complexes,

$$N_p(\psi_1, \psi_2, \ldots, \psi_M).$$

The following data are necessary for calculating the reliability indices of an atomic power plant:

* If the plant does not contain blocks of single-type elements forming a system of the "m out of n" type.

a) complete sets of CGE or CGBS are given according to the conditions of operational incapacity;

b) data on the reliability of elements can be presented in two ways: by giving the distribution (density) laws of the time f(t) of malfunction-free operation and the settling time g(t) of the element or by giving the operational readiness $k_r(t)$ and the parameter $\omega(t)$ of the flux of malfunctions of the element. The second way is preferable if as an element we consider some subsystem with a complex structure, e.g., CSS, SIAC, whose malfunctions could result in a change in the available power. Recommendations concerning the calculation of the indices for these systems are given in special sections of the manual;

c) the initial data concerning planned maintenance of the atomic power plant and its equipment are given as the interval of time between running repairs and major overhauls of the atomic power plant and its equipment, the average time lost for running and major repairs of an element, and data about the make-up of the repair teams;

d) the manual considers two possible ways of giving the regimen for the required power: probabilistic and deterministic. The first is characterized by an average time for maintaining the power at a given level and a matrix of transitions from level to level. In the second method a change in the required power is given by a determinate diagram in power – time coordinates.

Nomenclature of Calculated Reliability Indices. The manual makes it possible to calculate a wide range of reliability indices, reflecting individually or collectively the properties of an atomic power plant being free of malfunctions or suitable for repairs. For atomic power plants operating in the basic regimen there are two groups of reliability indices: indices concerning an individual set power level and "integral" indices characterizing the reliability of the power plant with respect to all power levels. The first group comprises the operational readiness $k_r(N_S, t)$ and the average operational readiness $k_r(N_S)$, the parameter $\omega(N_S, t)$ of the malfunction flux and the average parameter $\omega(N_S)$ in the interval under consideration, the probability $R(N_S, t)$ of malfunction-free operation with respect to the given level, the mean operating time $T(N_S)$ between malfunctions for the given level. The second group comprises the following indices: the mean available power $\bar{N}_a(t)$ and the mean available energy production E(t) in some period of time, the mean total duration of repairs in some period [0, t] of operation, the coefficient $R_{t.u.}$ of technical utilization of the atomic power plant (ratio of mean operating time of atomic power plant on power to sum of that time and the mean duration of planned and unplanned repairs during that time), the coefficient of utilization of the installed capacity, etc.

For atomic power plants operating according to a variable load schedule other indices taken into consideration are those which characterize the reliability with allowance for the given regimen of power variation, i.e., taking account of malfunctions due to the available power dropping below the required level or by the required level rising above the available power. As a matter of convention we shall refer to malfunctions of this kind as regimen malfunctions. In the manual calculations are also made of reliability indices with respect to regimen malfunctions: the operational readiness and the mean operational readiness, the parameter ω_r of malfunction flux and the mean parameter of malfunction flux, the probability of malfunction-free operation, the power deficit, the mean energy production by the atomic power plant in a time t, the coefficient of delivery of the required energy production, etc.

In a separate chapter the manual expounds a technique for calculating the indices of an atomic power plant operating in the basic regimen by describing its functioning by a Markovian process. This is valid for those cases in which the elements are not restored during the given interval (the laws of the distribution of the time to malfunction of elements can be arbitrary) and if the distribution laws for the time to malfunction and the times in the interval under consideration are exponential.

In all other cases it is expedient to use the Markovian model for preliminary calculations of the reliability of an atomic power plant or its separate systems when the number of operational and nonoperational states, associated with restorable or nonrestorable elements, is no more than 50 in each case, respectively (in this case the computation time on a BÉSM-6 computer does not exceed 30 min, as a rule).

Calculation of the reliability indices by using the theory of Markovian processes is performed in the following sequence: the diagram of the states of the atomic power plant (or the individual system considered) is constructed, the systems of differential equations for the probabilities of the realization of all states found from the diagram are written and solved, and the reliability indices are calculated.

In the final three chapters the manual gives the reliability techniques for individual systems of an atomic power plant. In particular, Chapter 7 presents the technique for calculating the reliability index for the performance of the following functions by the CSS: maintenance of the reactor power at a given level, switching

of the reactor from one level to another, and emergency protection.

Chapter 8 gives the technique for estimating the reliability indices of the SIAC with allowance for the functions of monitoring and recording of the principal technological parameters, signaling their deviation beyond the allowable limits, and protection and control of the principal technological parameters of the process.

Chapter 9 presents the methodological problems of calculation of the indices of safety systems with account for the time taken to perform the given functions for various conditions and the rule for carrying out maintenance during power operation of the reactor.

In the addenda the manual presents brief data concerning the reliability of the equipment of an atomic power plant, the technique for estimating the reliability of piping, explanations pertaining to the construction of the "tree of malfunctions," and some other reference material.

To facilitate calculations according to the technique outlined in the manual, special programs have been written for the BÉSM-6 computer. The complete sets of CGE and CGBS for several typical structural schemes of atomic power plants are determined according to the FORONS program. The RAST-1 program realizes the technique of the manual for specifying the conditions of operational incapacity in terms of the CGE.

LITERATURE CITED

1. R. Barlow and F. Proschan, Mathematical Theory of Reliability, Wiley, New York (1965).
2. W. Vesely, Nucl. Eng. Design, 13, No. 2, 337 (1970).

ESTIMATING THE CARRYING CAPACITY OF ZIRCONIUM FUEL-ELEMENT SHELLS

V. I. Solyanyi and V. S. Yamnikov

UDC 621.039.54:539.4

In power reactors with water cooling, as a rule, fuel-element rods with shells made from zirconium-based alloys are used. For the design of these fuel elements, analysis of operational reliability, especially in transient conditions, and the investigation of this reliability in possible emergency situations, it is necessary to know the limiting strength characteristics of the shells in complex stress states over a broad temperature range.

The anisotropy of shells made from zirconium-based alloys is due, on the one hand, to the deformational anisotropy produced in the process of manufacture and, on the other, to the initial anisotropy of the α-zirconium single crystal. The usual experimental determination of the limiting stresses and strains of anisotropic shells in a complex stress state, by testing to failure under internal pressure and axial load, requires complex apparatus and is very demanding. However, the required characteristics may be obtained by a theoretical consideration of the carrying capacity of a cylindrical anisotropic fuel-element shell on the basis of the concept of plastic-deformation stability loss.

Since experimental verification has not confirmed [1] the possibility of using the Swift criterion modified for the case of anisotropic materials, it was decided to adopt the statics criterion [2], according to which plastic-deformation stability loss begins when a maximum of any external load is reached, and is characterized by infinitesimally small increments of this load being equal to zero.

Formulation of the Problem and Its Solution

Consider the short-term deformation of a very plastic shell under a simple load, assuming that Hill's theory of plastic anisotropy is valid [3], i.e., that the shell material has plastic orthogonal anisotropy (orthotropy) and isotropic strengthening. Note that, in tubes used for fuel-element manufacture, the texture is such that the normal to the basis plane lies in the cross-sectional plane. The anisotropy of such shells may be

Translated from Atomnaya Énergiya, Vol. 48, No. 2, pp. 73-76, February, 1980. Original article submitted May 18, 1977.

0038-531X/80/4802-0078$07.50

characterized by the factors R_θ and R_Z, defined as the ratio of the transverse strains under uniaxial extension of standard samples along the θ and z axes, respectively, i.e., as

$$R_\theta = \varepsilon_z/\varepsilon_r;\ R_z = \varepsilon_\theta/\varepsilon_r. \tag{1}$$

The basic relations of plasticity theory for an orthotropic metal with a plane stress state, when the principal axes of the stress tensor and the strain-increment tensor coincide, are written in the following form:

a) the relation between the stress and strain

$$\varepsilon_\theta = \frac{\bar{\varepsilon}}{A\bar{\sigma}}[(H+G)-Hm]\,\sigma_\theta; \tag{2a}$$

$$\varepsilon_z = \frac{\bar{\varepsilon}}{A\bar{\sigma}}[(H+F)\,m+H]\,\sigma_\theta; \tag{2b}$$

$$\varepsilon_r = -\frac{\bar{\varepsilon}}{A\bar{\sigma}}[G+Fm]\,\sigma_\theta, \tag{2c}$$

where $m = \sigma_Z/\sigma_\theta = \text{const}$ $(0 \le m < \infty)$; H, G, and F, anisotropy parameters; $A = (2/3)(H + G + F)$; $\bar{\sigma}$ and $\bar{\varepsilon}$, stress and strain intensities, which are uniquely interrelated, regardless of the stress – strain state, by the expression $\bar{\sigma} = f(\bar{\varepsilon})$;

b) the incompressibility condition

$$\varepsilon_\theta + \varepsilon_z + \varepsilon_r = 0. \tag{3}$$

From the definition of the factors R and Eq. (2), it follows that

$$R_\theta = H/G;\ R_z = H/F. \tag{4}$$

The expression for the stress intensity takes the form

$$\bar{\sigma} = \sqrt{\frac{\left[\left(1+\frac{1}{R_\theta}\right)-2m+\left(1+\frac{1}{R_z}\right)m^2\right]}{\frac{2}{3}\left(1+\frac{1}{R_z}+\frac{1}{R_\theta}\right)}}\,\sigma_\theta. \tag{5}$$

From Eqs. (2a) and (5), an expression for the strain intensity is obtained

$$\bar{\varepsilon} = \sqrt{\frac{2}{3}\left(1+\frac{1}{R_z}+\frac{1}{R_\theta}\right)\left[\left(1+\frac{1}{R_\theta}\right)-2m+\left(1+\frac{1}{R_z}\right)m^2\right]}\,\frac{\varepsilon_\theta}{1+\frac{1}{R_\theta}-m}. \tag{6}$$

On the basis of Eq. (2), the following notation is adopted

$$m_\varepsilon = \frac{\varepsilon_z}{\varepsilon_\theta} = \frac{\left(1+\frac{1}{R_z}\right)m-1}{1+\frac{1}{R_\theta}-m}. \tag{7}$$

The relation between the loads on an element of cylindrical shell and the stresses acting is described by the expressions

$$Q = \pi D t \sigma_z;\quad P = 2t\sigma_\theta/D, \tag{8}$$

where Q is the axial force; P, internal pressure; D and t, passing values of the diameter and shell thickness, respectively.

According to the statics criterion, plastic-deformation stability loss occurs

$$\text{when } \delta Q = 0 \tag{9}$$

or

$$\text{when } \delta P = 0. \tag{10}$$

From Eqs. (9) and (10) and Eqs. (3), (7), and (8), assuming that the strain increments along the axes θ, z, and r are $\delta\varepsilon_\theta = \delta D/D$, $\delta\varepsilon_Z = \delta L/L$, $\delta\varepsilon_r = \sigma t/t$, it is found that

$$\text{either } \delta\sigma_z/\delta\varepsilon_z = \sigma_z, \tag{11}$$

$$\text{or } \delta\sigma_\theta/\delta\varepsilon_\theta = (2+m_\varepsilon)\,\sigma_\theta. \tag{12}$$

Then, taking Eqs. (5) and (6) into account, it is found that

$$\text{either } \frac{\delta\bar{\sigma}}{\delta\bar{\varepsilon}}=\left\{\sqrt{\frac{\left(1+\frac{1}{R_z}\right)m-1}{\frac{2}{3}\left(1+\frac{1}{R_z}+\frac{1}{R_0}\right)\left[\left(1+\frac{1}{R_0}\right)-2m+\left(1+\frac{1}{R_z}\right)m^2\right]}}\right\}\bar{\sigma}, \tag{13}$$

$$\text{or } \frac{\delta\bar{\sigma}}{\delta\bar{\varepsilon}}=\left\{\sqrt{\frac{1+\frac{1}{R_0}-m}{\frac{2}{3}\left(1+\frac{1}{R_z}+\frac{1}{R_0}\right)\left[\left(1+\frac{1}{R_0}\right)-2m+\left(1+\frac{1}{R_z}\right)m^2\right]}}(2+m_\varepsilon)\right\}\bar{\sigma}. \tag{14}$$

From these relations, knowing the dependence $\bar{\sigma} = f(\bar{\varepsilon})$ and the anisotropy factors determined by uniaxial tests, the limiting values of the stress and strain leading to plastic-deformation stability loss may be obtained.

Here the dependence $\bar{\sigma} = f(\bar{\varepsilon})$ will be taken in the form of the most widespread approximation for the given alloys; as a power function

$$\bar{\sigma}=K(\bar{\varepsilon})^n, \tag{15}$$

where K is a proportionality factor, and n is the strength factor.

According to Eqs. (13) and (14), the following expressions are obtained: for breakdown along z

$$\sigma_{z\,\text{lim}}=Kn^n\left[\frac{2}{3}\left(1+\frac{1}{R_z}+\frac{1}{R_0}\right)\right]^{(n+1)/2}\frac{m\left[\left(1+\frac{1}{R_0}\right)-2m+\left(1+\frac{1}{R_z}\right)m^2\right]^{(n-1)/2}}{\left[\left(1+\frac{1}{R_z}\right)m-1\right]^n}; \tag{16}$$

$$\varepsilon_{z\,\text{lim}}=n; \tag{17}$$

for breakdown along θ

$$\sigma_{\theta\,\text{lim}}=Kn^n\left[\frac{2}{3}\left(1+\frac{1}{R_z}+\frac{1}{R_0}\right)\right]^{(n+1)/2}\frac{\left[\left(1+\frac{1}{R_0}\right)-2m+\left(1+\frac{1}{R_z}\right)m^2\right]^{(n-1)/2}}{\left[\left(1+\frac{1}{R_0}-m\right)(2+m_\varepsilon)\right]^n}, \tag{18}$$

$$\varepsilon_{\theta\,\text{lim}}=n/(2+m_\varepsilon). \tag{19}$$

The form of breakdown is determined by which of the two strains (ε_z or ε_θ) first reaches its limiting value in accordance with Eqs. (17) and (19).

Then, in the case

$$0\leqslant m<1+1/R_\theta \tag{20}$$

breakdown occurs due to plastic-deformation stability loss in the azimuthal direction, while in the case

$$1+1/R_\theta<m<\infty \tag{21}$$

the stability loss is in the axial direction.

Introducing the limiting stress for uniaxial extension along z

$$\sigma_{z\,\text{lim}}^{\text{uni}}=Kn^n\frac{\left[\frac{2}{3}\left(1+\frac{1}{R_z}+\frac{1}{R_0}\right)\right]^{(n+1)/2}}{\left(1+\frac{1}{R_z}\right)^{(n+1)/2}}, \tag{22}$$

Eqs. (16) and (18) give

$$\frac{\sigma_{z\,\text{lim}}}{\sigma_{z\,\text{lim}}^{\text{uni}}}=\left(1+\frac{1}{R_z}\right)^{(n+1)/2}\frac{m\left[\left(1+\frac{1}{R_0}\right)-2m+\left(1+\frac{1}{R_z}\right)m^2\right]^{(n-1)/2}}{\left[\left(1+\frac{1}{R_z}\right)m-1\right]^n}; \tag{23}$$

$$\frac{\sigma_{\theta\,\text{lim}}}{\sigma_{z\,\text{lim}}^{\text{uni}}}=\left(1+\frac{1}{R_z}\right)^{(n+1)/2}\frac{\left[\left(1+\frac{1}{R_0}\right)-2m+\left(1+\frac{1}{R_z}\right)m^2\right]^{(n-1)/2}}{\left[\left(1+\frac{1}{R_0}\right)2-1+\left(\frac{1}{R_z}-1\right)m\right]^n}. \tag{24}$$

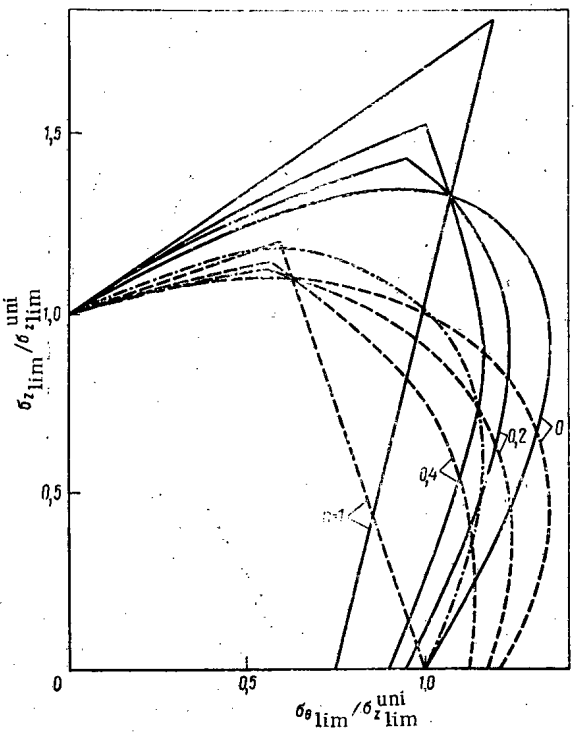

Fig. 1. Calculated curves of limiting stress with radial texture for $R_\theta = R_z = 2$ (continuous curve) and azimuthal texture for $R_\theta = 1$, $R_z = 0.5$ (dashed curve); the dash – dot curve corresponds to the isotropic case.

Results of Calculation and Discussion

Using Eqs. (17), (19), (23), and (24) obtained here, it is possible to construct, in dimensionless coordinates, the limiting curves characterizing the plastic-deformation stability loss of anisotropic shells. The index n may be taken to vary from 0 to 1, with n = 1 for an ideally elastic material and n = 0 for a rigid–plastic material.

The factors R_θ and R_z must be regarded as functions of the thermal and mechanical treatment in the course of manufacture [4, 5]. For shells with radial texture, R_θ and R_z vary in the range 2-5, while with azimuthal texture they are $R_z = 0.3$-0.7 and $R_\theta = 1$-1.7. For isotropic shells, $R_\theta = R_z = 1$. Curves calculated for the limiting stress for these textures are shown in Fig. 1.

Comparison with the isotropic case shows that ignoring the anisotropy may lead to considerable (up to 50%) discrepancy in the estimates of the carrying capacity. The shift in the limiting-stress curves for real isotropic shells ($0 < n < 0.3$) [6] is also observed for the anisotropic case: for $m > 1 + 1/R$ the shift is directed

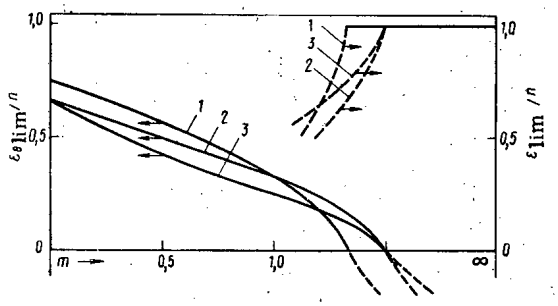

Fig. 2. Dependence of calculated curves for limiting uniform strains on load parameter m when $R_\theta = R_z = 2$ (1); $R_\theta = R_z = 1$ (2) (isotropic case); $R_\theta = 1$, $R_z = 0.5$ (3).

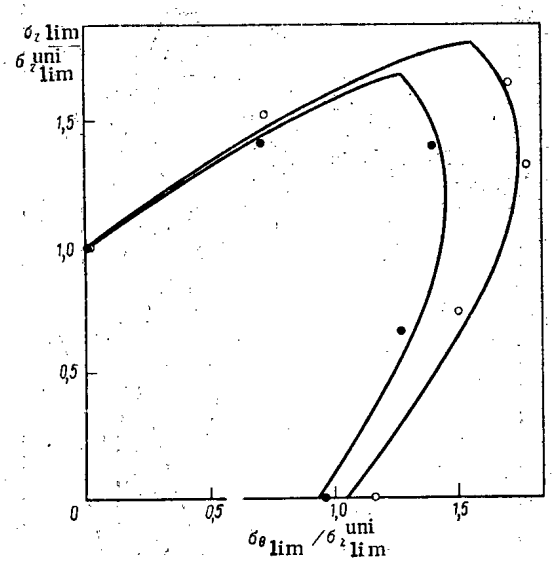

Fig. 3. Comparison of the results of calculational and experimental determinations of the limiting stress: ○) R_θ = 5.78, R_Z = 3.13, n = 0.15 [1]; ●) R_θ = 3.7, R_Z = 3.0, n = 1.15 [7].

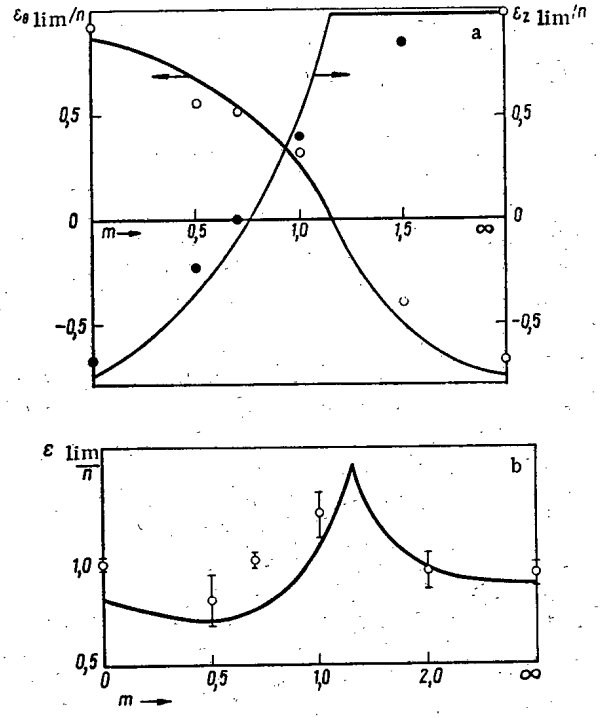

Fig. 4. Comparison of the results of calculational and experimental determinations, for R_θ = 5.78, R_Z = 3.13, and n = 0.15 [1], of the limiting uniform strain in the directions θ and z (a) and the intensity of the limiting uniform strain (b).

out of, and for $m < 1 + 1/R_\theta$ into, the region bounded by the curve for a rigid–plastic material.

Values of the limiting uniform stresses for analogous textures are shown in Fig. 2. Note that for m less than, but close to, $1 + 1/R_\theta$, breakdown occurs as a result of plastic-deformation stability loss in the azimuthal direction, although the azimuthal limiting uniform strain is close to zero. In other words, for such a stress ratio, localization of the strain and subsequent breakdown occurs with zero uniform strain in the azimuthal direction. This is evidently associated with the effect of the shell's geometric shape, since for plates nothing similar is observed [2].

Comparing the results of experimental determination [1, 7] of the limiting stresses and uniform strains of fuel-element shells of BWR type (diameter 12×0.8 mm) made from zircalloy-2 with the calculated values (Figs. 3 and 4), good qualitative and quantitative agreement is obtained, which confirms the applicability of the statics criterion of plastic-deformation stability loss for shells of zirconium alloy. Thus, in the design of rod fuel elements with shells made from zirconium-based alloys and the analysis of their operational reliability, it is necessary to take account of the geometric factor and anisotropy of the plastic deformation, which significantly affect the limiting stress and uniform strain of plastic shells under short-term loads.

LITERATURE CITED

1. Y. Miyamoto et al., J. Nucl. Mater., 61, 53 (1976).
2. V. D. Golovlev, Mashinoved., No. 2, 122 (1966).
3. R. Hill, Mathematical Theory of Plasticity [Russian translation], Gostekhteorizdat, Moscow (1956).
4. T. Andersson, J. Nucl. Mater., 62, 95 (1976).
5. P. Rittenhouse, J. Nucl. Mater., 24, 310 (1967).
6. V. I. Maksak, in: Elasticity and Inelasticity [in Russian], No. 1, Moscow State Univ. (1971), p. 159.
7. H. Maki et al., in: Proceedings of an International Conference on Nuclear Fuel Performance, London (1973), p. 621.

CRYSTAL STRUCTURE OF γ^S PHASE IN U – Mo, U – Re, AND U – Nb ALLOYS

N. T. Chebotarev and O. N. Utkina

UDC 548.7:669.822

The structure and properties of the initial elements in the actinide group are the result of the formation of hybrid 5f – 6d – 7s states and the emergency of interatomic bonds of a covalent–metallic nature, which in low-temperature modifications of uranium, neptunium, and plutonium is manifested in the form of four short bonds [1, 2]. In the transition from these low-temperature modifications to high-temperature ones there is a reduction of the overlapping of energy levels, a diminution of the covalent character of the bonds, and the gradual approach of the structure of the low-temperature modifications to that of a bcc lattice. The covalent component of the bond decreases not only as the temperature rises but also with alloying. When uranium is alloyed with molybdenum, e.g., a number of metastable phases (α', α'', γ^0) are formed and in these phases the covalent component of the bond decreases as the content of the alloying element grows. If it is assumed that the covalent component of the bond is partially conserved in the γ^S phase, then the cubic structure of the latter should be of a more complex character than the ideal bcc lattice.

Below we give the results of studies on the structure of the γ^S phase in U – Mo, U – Re, and U – Nb alloys, some of which had been published earlier [3].

Experimental Data. We studied single crystals of alloys of uranium with 12.4, 14.5, 15.4, 18.9, and 23.6 at. % Mo, 10.5 at. % Re, and 22.2 at. % Nb. The content of alloying elements in the alloys was determined from the melting charge and in the case of U – Mo was furthermore refined according to the dependence of the lattice constant on the concentration [4]. The cast specimens were rolled to a thickness of 1–1.5 mm at 850°C and then rolled without heating to a thickness of 0.2–0.4 mm. After the rolling the specimens were quenched

Translated from Atomnaya Énergiya, Vol. 48, No. 2, pp. 76–80, February, 1980. Original article submitted April 10, 1979.

0038-531X/80/4802-0083$07.50

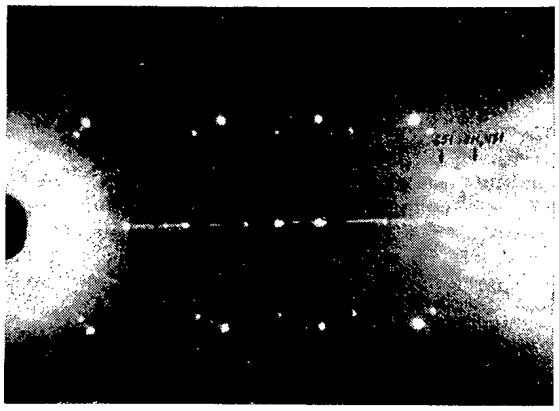

Fig. 1. Rotating-crystal x-ray pattern about [001] direction for single crystal of uranium alloy with 12.4 at. % Mo. The numbers indicate the most intensive superlattice reflections.

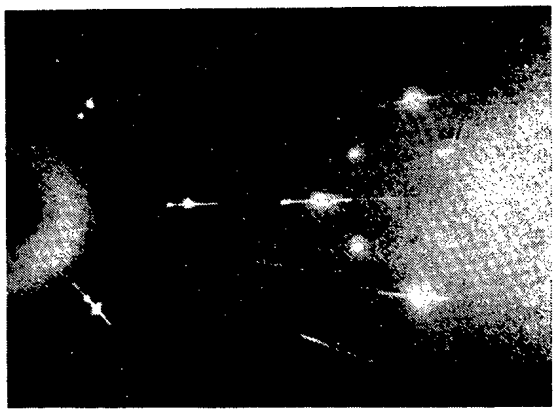

Fig. 2. Oscillating-crystal x-ray pattern of single crystal of alloy of uranium with 12.4 at. % Mo.

from the region of the γ phase and then the alloys with Mo were annealed for 50-300 h at 1100-1130°C, the alloy of uranium with 10.5% Re was annealed for 300 h at 1030°C, and the alloy with 22.2% Nb, for the same time but at 1200°C. Grains selected with the aid of an MBS-1 microscope were separated out electrolytically.

The single crystals obtained were oriented so that the [001] direction would be perpendicular to the x-rays and were then studied by the oscillating- and rotating-crystal methods in an RKV-86 camera in Cu Kα radiation. The intensity of the reflections in the oscillating- and rotating-crystal x-ray patterns was estimated by photometric measurements in an MF-4 microphotometer and from the blackening marks. Analysis of rotating-crystal patterns about the [001] direction for singles of the γ^S phase of the alloys of uranium with 12.4 at. % Mo, 10.5 at. % Re, and 22.2 at. % Nb showed that between the principal layer lines (for a bcc unit cell of two atoms) are secondary lines formed by low-intensity reflections (Fig. 1).

Sharper superlattice reflections from single crystals of the γ^S phase of alloys of uranium with 12.4% Mo, 10.5% Re, and 22.2% Nb were obtained on oscillating-crystal x-ray patterns (Fig. 2). Increasing the Mo content in the γ^S phase of alloys of the U – Mo system results in a decrease in the intensity and, finally, in the total disappearance of the superlattice reflections for alloys with 23.6 at. % Mo.

Results of the induction of superlattice reflections for an alloy with 12.4 at. % Mo are given in Table 1. The superlattice reflections correspond to a bcc unit cell of 16 atoms which is doubled along all axes and which has a constant of $3.442 \cdot 2 = 6.884$ Å.* Having studied the γ^S phase of uranium alloy with 16.6 at. % Nb and 5.64 at. % Zr, Yakel [5] came to the conclusion that the doubling of the lattice constant is due to displacement of atoms occupying the centers of the small unit cells, in the [100] direction by a value $\delta \approx 0.03 a_{\gamma^S}$. The

*1 Å = 0.1 nm.

TABLE 1. Superlattice Reflections in Rotating- and Oscillating-Crystal X-ray Patterns of Single Crystal of U – 12.4% Mo Alloy

Zero layer line, hk0	First layer line, hk1	Second layer line, hk2	Third layer line, hk3
420	211	112	213
600	321	312	323
550	411	402	413
640	431	332	433
730	521	512	523
820	611	442	613
750	541	532	543
	631	622	633
	721	712, 552	
	651	732	
	811, 741	802	
	831	662	
		752	

TABLE 2. Observed and Calculated Data Concerning Superlattice Reflections of γ^S Phase of U – 12.4% Mo Alloy

N	hk0, hk1	$\left(\frac{F^2_{hk0}}{F^2_{642}}\right)_{calc}$ %	$\left(\frac{F^2_{hk0}}{F^2_{642}}\right)_{exp}$ %	N	hk2, hk3	$\left(\frac{F^2_{hk2}}{F^2_{642}}\right)_{calc}$ %	$\left(\frac{F^2_{hk2}}{F^2_{642}}\right)_{exp}$ %
1	110	0,0008	—	1	222	0,02	—
2	200	0,003	—	2	312	0,7	0,5
3	310	0,005	—	3	402	0,05	*
4	330	0,04	—	4	332	0,6	*
5	420	0,05	*	5	512	0,5	*
6	510	0,01	—	6	442	0,2	*
7	530	0,08	—	7	532	0,5	*
8	600	0,12	*	8	622	0,2	*
9	710	0,01	—	9	712	0,3	*
10	550	0,18	*	10	552	0,5	*
11	640	0,19	*	11	732	0,4	*
12	730	0,11	*				
13	820	0,28	*				
1	301	0,005	—	1	103	0,005	—
2	231	0,67	0,59	2	213	0,7	0,4
3	411	2,4	2,1	3	303	0,04	—
4	501	0,01	2,1	4	323	0,6	0,5
5	431	2,0		5	413	2,0	1,9
6	521	0,5	*	6	433	1,8	1,6
7	611	3,7	4,6	7	503	0,08	—
8	541	1,5	2,7	8	523	0,5	*
9	631	3,2	2,9	9	613	3,2	3,0
10	701	0,01	—	10	543	1,4	1,6
11	721	0,3	*	11	633	2,9	2,2
12	651	2,6	4,8				
13	811	4,8	5,5				
14	741	1,1					
15	831	4,3	3,4				

*Weak reflections, appearing only on oscillating-crystal x-ray patterns.

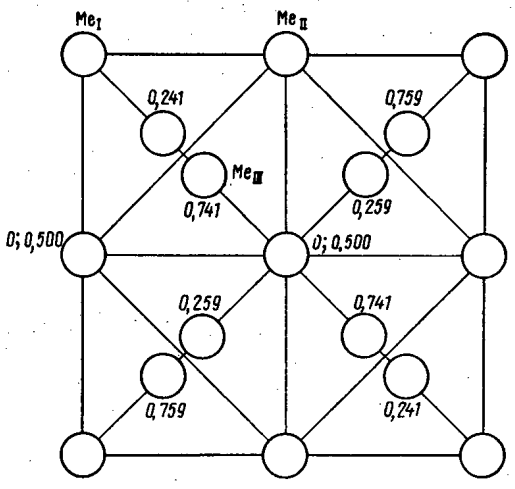

Fig. 3. Projection of unit cell of γ^S phase of uranium alloy with 12.4 at. % Mo on (001) plane.

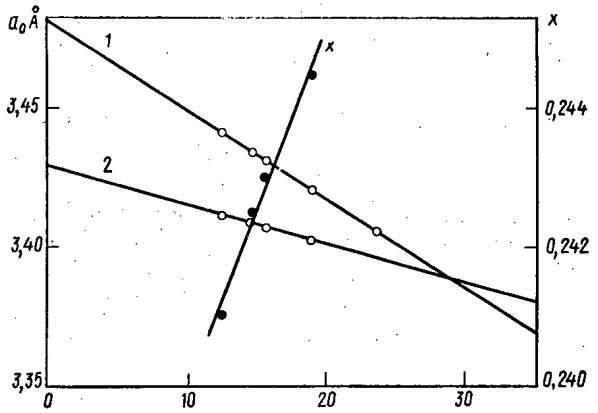

Fig. 4. Lattice constant of γ^S phase (1) and ideal bcc γ phase (2) vs molybdenum content.

structure falls in the space group T_d^3 [6] with the following atomic positions in the unit cell:

$$2 \text{ at.} - 2(a): 000, \tfrac{1}{2}\tfrac{1}{2}\tfrac{1}{2};$$

$$6 \text{ at.} - 6(b): 0\,\tfrac{1}{2}\tfrac{1}{2}, \tfrac{1}{2}\,0\,\tfrac{1}{2} \text{ etc.}$$

$$8 \text{ at.} - \tfrac{1}{3} \cdot 24(d): xxz \text{ etc.}$$

where $x = 0.250 \pm 0.001$; $z = 0.250 - \delta = 0.220 \pm 0.005$.

However, Yakel's assumptions concerning the atoms occupying only one-third of the 24 (d) positions and being displaced in the direction of the cube edges is not in accord with the cubic symmetry of the structure. In a cubic lattice eight atoms can experience displacement only in [111] directions. Analysis of the intensity of the superlattice reflections on the rotating- and oscillating-crystal x-ray patterns of a single crystals of the γ^S phase of the U – 12.4% Mo alloy showed that the atoms are arrayed statistically in the following positions of space group T_d^4:

$$\left.\begin{array}{l} 2(a): 000 \\ 6(b): 0\,\tfrac{1}{2}\tfrac{1}{2}, \tfrac{1}{2}\,0\,\tfrac{1}{2}, \tfrac{1}{2}\,\tfrac{1}{2}\,0 \\ 8(c): xxx, x\bar{x}\bar{x}, \bar{x}x\bar{x}, \bar{x}\bar{x}x \end{array}\right\} + \left(000, \tfrac{1}{2}\tfrac{1}{2}\tfrac{1}{2}\right).$$

The atomic parameter x can be found from the equality of the ratios of the squared structure factors of two reflections, superlattice and lattice, e.g., $(F^2_{631}/F^2_{642})_{exp} = (F^2_{631}/F^2_{642})_{calc}$. Proceeding from the value obtained for the atomic parameter $x = 0.241 \pm 0.001$, we found the square of the structure factors for the superlattice reflections. In the calculation we took the following factors into account: Lorentz factor, polarization factor, repetition period, and temperature factor; the absorption factor was not included (Table 2).

It is seen from Table 2 that the experimental values of the intensity of the superlattice reflections are in good agreement with the calculated values. The rotating-crystal x-ray patterns show only the strongest of the superlattice reflections, less strong reflections are seen in the oscillating-crystal patterns, while the very weak, theoretically possible reflections, such as 200, 310, 330, 510, etc., cannot be observed even in the oscillating-crystal patterns.

Figure 3 shows the projection of the unit cell of the γ^S phase of the U – 12.4% Mo alloy on the (001) plane. The complete analogy between the rotating- and oscillating-crystal x-ray diffraction patterns of single crystals of the γ^S phase of U – 10.5% Re, U – 22.2% Nb, and U – 12.4% Mo alloys permits the conclusion that the crystal structures of the γ^S phase of these alloys are also analogous. The atomic parameter x of the structure of the γ^S phase of the U – 10.5% Re and U – 22.2% Nb alloys is 0.241 ± 0.001. It should be pointed out that the Mo, Re, and Nb contents indicated are the minimum contents ensuring fixation of the γ^S phase.

The atomic parameter x was also found for the γ^S phase of alloys of uranium with 14.5, 15.4, and 18.9% Mo (Fig. 4); the dependence of x on the molybdenum content can be represented by the equation $x = 0.2344 \pm 0.00055$ C. It follows from this equation that with a Mo content of about 29% an ideal bcc lattice is formed with x = 0.250.

Proceeding from the values found for the atomic parameter x, we calculated the interatomic distances in the structure of the γ^S phase of uranium alloys with various molybdenum contents (Table 3).

TABLE 3. Interatomic Distances and Atomic Coordination in Structure of γ^S Phase of U – Mo Alloys

Mo content, at.%	Interatomic distance, Å								$d_{max} - d_{min}$, Å
	Mo_I		Mo_{II}		Mo_{III}				
	4 Mo_{III}	4 Mo_{III}	4 Mo_{III}	4 Mo_{III}	1 Mo_I	3 Mo_{II}	3 Mo_{II}	1 Mo_I	
12,4	2,87	3,09	2,95	3,02	2,87	2,95	3,02	3,09	0,22
14,5	2,89	3,06	2,95	3,01	2,89	2,95	3,01	3,06	0,17
15,4	2,89	3,06	2,95	3,00	2,89	2,95	3,00	3,06	0,17
18,9	2,90	3,03	2,94	2,99	2,90	2,94	2,99	3,03	0,13

TABLE 4. The Lengths of the Short Bonds, d_{min}, of the Structure of α-Uranium and the Metastable States of the U–Mo System

Mo content, %	Phase	Structure	d_{min}, Å
0	α	Rhombic	$2\ d_1 = 2{,}77$ $2\ d_2 = 2{,}85$
3	α'	"	$2\ d_1 = 2{,}77$ $2\ d_2 = 2{,}87$
9,4	α''	Monoclinic	$2\ d_1 = 2{,}78$ $2\ d_2 = 2{,}88$
10,5	γ^0	Tetragonal	$4\ d_1 = 2{,}86$
12,4 18,9	γ^s	Cubic	$4\ d_1 = 2{,}87$ $4\ d_2 = 2{,}95$ $4\ d_1 = 2{,}90$ $4\ d_2 = 2{,}94$

Discussion. As is clear in the cubic structure of the γ^S phase of a uranium alloy with Mo, Re, and Nb, four covalent bonds, characteristic of the structure of the metastable stages α', α'', and γ^0 of the system U–Mo, are particularly maintained. The lengths of the short bonds d_{min} of the structures are presented in Table 4.

Short bonds of two types exist in the γ^S phase of the alloy of uranium with 12.4 at. % Mo: $4d_1 = 2.87$ Å and $4d_2 = 2.95$ Å. As the molybdenum content in the γ^S phase increases, the length of the short bonds grows just as is the case in the α, α', α'', and γ^0 phases and the structure approaches the ideal bcc lattice ($d_{max} - d_{min} = 0$), for which $x = 0.250$.

The deviation of the structure of the γ^S phase from the ideal is accompanied by a reduction of the degree of compactness of the lattice, i.e., an increase in the lattice constant $a_{\gamma S}$ in comparison with that of the ideal bcc lattice, a_γ, in accordance with

$$a_{\gamma^s} = (1 + \delta)\, a_\gamma, \tag{1}$$

where $\delta = 0.250 - x$.

The dependence of the lattice constant of the γ^S phase of the U–Mo system is expressed [4] by

$$a_{\gamma^s} = 3.4808 - 0.00314\, C_{Mo} \tag{2}$$

and is shown in Fig. 4 (straight line 1).

The values of the lattice constant of the ideal bcc lattice of the phase of the compositions studied can be found from Eq. (1) by using the values obtained for the atomic parameter x. The pertinent equation is of the form

$$a_\gamma = 3.4283 - 0.00132\, C \tag{3}$$

and is also shown in Fig. 4 (straight line 2). It is seen from Fig. 4 that $a_{\gamma S} - a_\gamma = 0$ when the Mo content is about 29%.

In conclusion, it should be noted that the deviation of the structure of the γ^S phase from the ideal bcc lattice and the dependence of the degree of that deviation on the concentration of the alloying element and the temperature should affect the physical properties of the alloys studied. In particular, a reduction in the fraction of the covalent component of the interatomic bonds and an increase in the degree of compactness of the structure of the γ^S phase with a rise in temperature should result in the appearance of a negative component of the coefficient of thermal expansion and the temperature coefficient of electrical resistance.

LITERATURE CITED

1. N. T. Chebotarev, At. Energ., 10, No. 1, 43 (1961).
2. S. T. Konobeevskii and N. T. Chebotarev, At. Energ., 10, No. 1, 50 (1961).

3. N. T. Chebotarev and O. N. Utkina, in: Proc. Conf. "Plutonium 1975 and Other Actinides," North-Holland, Amsterdam (1976), p. 559.
4. A. Dwight, J. Nucl. Mater., 2, No. 1, 81 (1960).
5. H. Yakel, J. Nucl. Mater., 33, No. 3, 286 (1969).
6. International Tables for X-Ray Crystallography, Kynoch Press, Birmingham (1952).

POLYNOMIAL APPROXIMATION OF NEUTRON FLUX IN FIRST-COLLISION PROBABILITY METHOD

T. S. Poveshchenko and Ya. V. Shevelev

UDC 621.039.512.45

First-Collision Probability Method

This is a very popular method of solving the kinetic equation written in the form of the Peierls integral equation (e.g., [1])

$$\Phi(\mathbf{r}) = \int_V d\mathbf{r}' P(\mathbf{r} \leftarrow \mathbf{r}') \sigma_s(\mathbf{r}') \Phi(\mathbf{r}') + 4 \int_F d\mathbf{r}' \Omega'(\mathbf{r} \leftarrow \mathbf{r}') \mathbf{n}(\mathbf{r}') P(\mathbf{r} \leftarrow \mathbf{r}') I^+(\mathbf{r}'). \quad (1)$$

Here $\int_V d\mathbf{r}'$ is the integral over the volume of the studied region; $\int_F d\mathbf{r}'$, integral over its surface; $\mathbf{n}$, internal normal; Φ, neutron flux; I^+, neutron current through the surface into the region; σ_S, macroscopic scattering cross section; Ω', ray unit vector from $\mathbf{r}'$to $\mathbf{r}$; P, kernel of the first collision; and

$$\Omega'(\mathbf{r} \leftarrow \mathbf{r}') = (\mathbf{r} - \mathbf{r}')/|\mathbf{r} - \mathbf{r}'|; \quad (2)$$

$$P(\mathbf{r} \leftarrow \mathbf{r}') = (4\pi |\mathbf{r} - \mathbf{r}'|^2)^{-1} \exp[-\tau(\mathbf{r} \leftarrow \mathbf{r}')]; \quad (3)$$

$$\tau(\mathbf{r} \leftarrow \mathbf{r}') = \int_0^1 \sigma[\mathbf{r}' + s(\mathbf{r} - \mathbf{r}')] |\mathbf{r} - \mathbf{r}'| ds, \quad (4)$$

where σ is the total macroscopic cross section; τ is the optical path length.

Equation (1) is written for the simplest model: neutrons enter the studied region only through the surface, and are scattered isotropically and absorbed; the cross section is independent of the energy. A more general Peierls equation may be written for the case when the scattering index has a finite number of nonzero angular moments. A system of several integral equations for several angular moments of the neutron distribution function [2] will now be obtained. The number of kernels in these equations is found by multiplying P by polynomials of the components of Ω'. It is also simple to perform the generalization for multivelocity problems, and to introduce internal neutron sources. However, to illustrate the proposed improvement of the method, the simplest relation – Eq. (1) – is completely adequate.

The first-collision probability method is as follows. The region V is divided into small zones, in each of which the cross section is independent of the coordinate, and the flux Φ is relatively unchanging and may be replaced by a mean value.

Let $g_t(\mathbf{r})$ be a characteristic function of the region t, equal to unity inside the region and zero outside; Φ_t be the mean flux in zone t. Then the basic hypothesis of the method is expressed by the formula

$$\Phi(\mathbf{r}) = \sum_{t'} \Phi_{t'} g_{t'}(\mathbf{r}). \quad (5)$$

Substituting Eq. (5) into Eq. (1) gives, after multiplying by g and integrating, a system of equations for Φ_t

$$\Phi_t = \sum_{t'} \Phi_{t'} P_{t \leftarrow t'} + q_t, \quad (6)$$

Translated from Atomnaya Énergiya, Vol. 48, No. 2, pp. 80-84, February, 1980. Original article submitted January 8, 1979.

0038-531X/80/4802-0088 $07.50

where

$$P_{t\leftarrow t'}=\sigma_{st'}\int\limits_{V_{t'}} d\mathbf{r}'\int\limits_{V_t} d\mathbf{r}\,P(\mathbf{r}\leftarrow\mathbf{r}')/V_t; \tag{7}$$

$$q_t=4\int\limits_F d\mathbf{r}'\int\limits_{V_t} d\mathbf{r}P(\mathbf{r}\leftarrow\mathbf{r}')\,\Omega'(\mathbf{r}\leftarrow\mathbf{r}')\,\mathbf{n}(\mathbf{r}')\,I^+(\mathbf{r}')\Big/\int\limits_{V_t} d\mathbf{r}. \tag{8}$$

Here V_t is the volume of zone t.

Improvement in the First-Collision Probability Method

If the accuracy of the method is to be increased, the number of zones t must be increased. Then the accuracy of Eq. (5) is increased, and so is the accuracy with which the mean values Φ_t are calculated. However, this is not the only means of improving the method. The accuracy of Eq. (5) may be increased by replacing the constant Φ_t by a polynomial in the coordinate $\mathbf{r}$ with undetermined multipliers, for which a system of equations analogous to Eq. (6) for Φ_t is written.

Generally speaking, instead of the polynomial it is possible to take a linear combination of any functions allowing a good approximation of $\Phi(\mathbf{r})$ to be obtained. But polynomials have an important advantage: in calculating integrals of the type in Eqs. (7) and (8), the numerical integration forms only a minimal part of the total computational work.

Let

$$\Phi(\mathbf{r})=\sum_{t'}\sum_{\eta'}\varphi_{\eta't'}f_{\eta't}(\mathbf{r})\,g_{t'}(\mathbf{r}), \tag{9}$$

where $f_{\eta't'}$ is a set of approximating functions in the region t' (in particular, this may be the polynomials). Let $\Psi_{\eta t}(\mathbf{r})$ be a set of functions for the region t, mutually orthogonal with $f_{\eta't'}$, while

$$\int\psi_{\eta t}f_{\eta't'}g_tg_{t'}d\mathbf{r}=\delta_{\eta\eta'}V_t. \tag{10}$$

Substituting Eq. (9) into Eq. (1), multiplying by $\Psi_{\eta t}g_t$, and integrating, a system of equations for $\varphi_{\eta t}$ is obtained

$$\varphi_{\eta t}=\sum_{t'}\sum_{\eta'}\varphi_{\eta't'}P_{\eta\leftarrow\eta',\,t\leftarrow t'}+q_{\eta t}, \tag{11}$$

where

$$P_{\eta\leftarrow\eta',\,t\leftarrow t'}=\sigma_{st'}\int\limits_{V_{t'}} d\mathbf{r}'\int\limits_{V_t} d\mathbf{r}P(\mathbf{r}\leftarrow\mathbf{r}')\;\psi^{(r)}_{\eta t}f_{\eta't'}(\mathbf{r}')/V_t; \tag{12}$$

$$q_{\eta t}=4\int\limits_F d\mathbf{r}'\int\limits_{V_t} d\mathbf{r}P(\mathbf{r}\leftarrow\mathbf{r}')\;\Omega'(\mathbf{r}\leftarrow\mathbf{r}')\,\mathbf{n}(\mathbf{r}')\,I^+(\mathbf{r}')\,\psi_{\eta t}(\mathbf{r})/V_t. \tag{13}$$

Calculation of Generalized Probabilities for Polynomial Approximation

A quantity proportional to $P_{t\leftarrow t'}$ is called the first-collision probability of a neutron in zone t if it has previously experienced a collision in zone t'. The quantities $P_{\eta\leftarrow\eta',\,t\leftarrow t}$ may be called generalized first-collision probabilities. It will be shown how they may be calculated if $f_{\eta't'}$ and $\Psi_{\eta t}$ are polynomials of the Cartesian coordinates (x, y) in the reactor-channel cross section, i.e., in the cylindrical region with generatrices parallel to the z axis.

A great amount of work is required to calculate τ in a channel of complex geometry, since it is necessary to find all the points at which the beam from $\mathbf{r}'$ into $\mathbf{r}$ intersects the boundary of regions with different properties. Therefore, as in the WIMS program [3], new variables of integration are introduced, so that calculation of the boundary points is not repeated. This means that the pairs of points $(\mathbf{r}, \mathbf{r}')$ must be distributed over the straight lines on which they lie.

Let φ be the angle to the x axis formed by the projection of the beam from $\mathbf{r}'$ into $\mathbf{r}$ onto the (x, y) plane; x_φ, y_φ, z be coordinates of the point $\mathbf{r}$ in a system turned around the z axis by an angle φ; $x_\varphi, y'_\varphi, z'$ be the same for the point $\mathbf{r}'$; it is obvious that

$$y'_\varphi=y_\varphi;\;\; x\geqslant x'_\varphi. \tag{14}$$

The parameters φ, y_φ, x_φ, x'_φ, z, z' uniquely define the pair of points $\mathbf{r}$, $\mathbf{r}'$ and may serve as the new variables in place of x, y, z, x', y', z'.

It is expedient to introduce the notation

$$\lambda = (z - z')/(x_\varphi - x'_\varphi). \tag{15}$$

Then in the new variables

$$P = [4\pi (x_\varphi - x'_\varphi)^2 (1+\lambda^2)]^{-1} \exp[-\sqrt{1+\lambda^2}\,\tau_0 (x_\varphi, x'_\varphi, y_\varphi, \varphi)], \tag{16}$$

where τ_0 is the optical ray for the projection of the ray on the (x, y) plane. If the outer channel boundary is a circular cylinder of radius ρ, then

$$\mathbf{n}(\mathbf{r}')\,\Omega' = \frac{\sqrt{\rho^2 - y_\varphi^2}}{\rho\sqrt{1+\lambda^2}}. \tag{17}$$

Calculating the transformation Jacobian for the new variables, it is found that

$$P_{\eta\leftarrow\eta',\, t\leftarrow t'} = \int_{t'} dx'_\varphi \int_t dx_\varphi \int_0^\rho dy_\varphi \int_0^{2\pi} d\lambda\varphi \int_{-\infty}^{\infty} d\lambda \psi_{\eta t} f_{\eta' t'} \exp\left(-\sqrt{1+\lambda^2}\,\tau_0\right) \frac{1}{4\pi(1+\lambda^2)} \Big/ s_t \tag{18}$$

and when $I^+ = \text{const}$

$$q_{\eta t} = I^+ \int_t dx_\varphi \int_0^\rho dy_\varphi \int_0^{2\pi} d\varphi \int_{-\infty}^{\infty} d\lambda \exp\left(-\sqrt{1+\lambda^2}\,\tau_0\right) \frac{\psi_{\eta f}}{\pi (1+\lambda^2)^{3/2}} \Big/ s_t, \tag{19}$$

where s_t is the cross-sectional area of the region t.

In calculating integrals over x_φ and x'_φ, it is necessary to know the boundary of the region along the ray (y_φ, φ). The dependence of these boundaries on (y_φ, φ) completely corresponds to the channel outline. This dependence for a discrete set of values of y_φ and φ may be stored in the computer memory and recalled for recalculations connected with change in the physical properties of the region (change in neutron energy, temperature of the medium, density, etc.).

In calculating the first-collision probability, integrals over x_φ, x'_φ, and λ are reduced to tabular functions of a single variable [3]. This is because τ_0 is a linear function of x_φ and x'_φ

$$\frac{\partial \tau_0}{\partial x_\varphi} = \sigma_t; \quad \frac{\partial \tau_0}{\partial x'_\varphi} = -\sigma_{t'}, \tag{20}$$

so that, if $x_\varphi-$ and $x_\varphi+$ are the boundaries of zone t, while $x'_\varphi-$ and $x'_\varphi+$ are the boundaries of zone t', then

$$\int_{t'} dx'_\varphi \int_t dx_\varphi \exp\left(-\sqrt{1+\lambda^2}\,\tau_0\right) = \frac{1}{(1+\lambda^2)\,\sigma_t \sigma_{t'}} \times$$
$$\times \{\exp[-\sqrt{1+\lambda^2}\,\tau_0 (x_{\varphi+}, x'_{\varphi-}, \varphi_\varphi, \varphi] + \exp[-\sqrt{1+\lambda^2}\,\tau_0 (x_{\varphi-}, x'_{\varphi+}, y_\varphi, \varphi)] -$$
$$- \exp[-\sqrt{1+\lambda^2}\,\tau_0 (x_{\varphi+}, x'_{\varphi+}, \varphi_\varphi, \varphi)] - \exp[-\sqrt{1+\lambda^2}\,\tau_0 (x_{\varphi-}, x'_{\varphi-}, y_\varphi, \varphi)]\}. \tag{21}$$

Therefore, integrals over x_φ, x'_φ, and λ reduce to the function

$$Q_4(v) = \int_{-\infty}^{\infty} \exp\left(-\sqrt{1+\lambda^2}\,v\right) \frac{d\lambda}{(1+\lambda^2)^2}. \tag{22}$$

It remains to perform numerical integration over y_φ and φ, since v is a function of these variables. The calculation of q_t is analogous. Note only that the zones t and t' along the ray (y_φ, φ) may be multiply connected because of the channel symmetry. In this case, the formulas obtained are applicable for each combination including a connected subregion of t and a connected subregion of t'. The final result is obtained by summing similar expressions over all the possible combinations.

For arbitrary functions ψ and f, not double but quadruple numerical integration must be performed (the integral over λ may be tabulated as a function of τ_0). However, if ψ and f are polynomials of (x, y), then in contrast to the case when $\psi = f = 1$ all that is involved is an increase in the number of tabulated functions of v. In the general case, a function of the following form is needed [4]

$$Q_m(v) = \int_{-\infty}^{\infty} \exp\left(-\sqrt{1+\lambda^2}\,v\right) \frac{d\lambda}{(1+\lambda^2)^{m/2}} = \int_{-\pi/2}^{\pi/2} \exp\left(-\frac{v}{\cos\alpha}\right) \cos^{m-2}\alpha\, d\alpha. \tag{23}$$

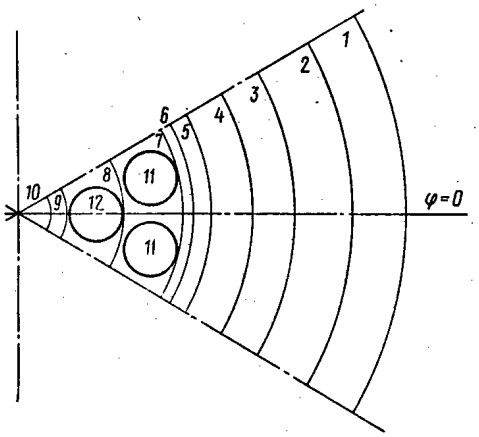

Fig. 1. Symmetry-sector zones of region with RBMK channel: 1-4) graphite; 5) zirconium; 6-10) water; 11, 12) uranium oxide.

In fact, the polynomial in (x, y) becomes, after transforming to the variables (x_φ, y_φ), a polynomial in x_φ with coefficients depending on y_φ and φ. Therefore, it is sufficient to calculate the integral

$$\int_{t'} x_\varphi^\nu dx'_\varphi \int_t x_\varphi^\mu dx_\varphi \int_{-\infty}^{\infty} \frac{\exp\left[-\sqrt{1+\lambda^2}\,\tau_0\right]}{1+\lambda^2} d\lambda = \int_{x'_{\varphi-}}^{x'_{\varphi+}} dx'_\varphi \int_{x_{\varphi-}}^{x_{\varphi+}} dx_\varphi x'^{\nu}_\varphi x^\mu_\varphi Q_2(\tau_0); \tag{24}$$

$$\int_t x_\varphi^\mu dx_\varphi \int_{-\infty}^{\infty} \exp\left(-\sqrt{1+\lambda^2}\,\tau_0\right) \frac{d\lambda}{(1+\lambda^2)^{3/2}} = \int_{x_{\varphi-}}^{x_{\varphi+}} dx_\varphi x^\mu_\varphi Q_3(\tau_0). \tag{25}$$

Integration by parts using Eq. (20) and the relation

$$dQ_m^{(\nu)}/dv = -Q_{m-1}(v) \tag{26}$$

allows the powers of x_φ and x'_φ to be reduced and, simultaneously, the order of the function Q_m to be increased, for example

$$\int_{x_{\varphi-}}^{x_{\varphi+}} dx_\varphi x^\mu_\varphi Q_2(\tau_0) = -\int_{x_{\varphi-}}^{x_{\varphi+}} \frac{x^\mu_\varphi}{\sigma_t} dQ_3(\tau_0) = -\frac{x^\mu_\varphi}{\sigma_t} Q_3(\tau_0)\Big|_{x_{\varphi-}}^{x_{\varphi+}} + \int_{x_{\varphi-}}^{x_{\varphi+}} \frac{\mu}{\sigma_t} x^{\mu-1}_\varphi Q_3(\tau_0).$$

Thus, Eqs. (24) and (25) may be reduced to a combination of functions $Q_m(v)$ with different m and different arguments.

Model of RBMK-Reactor Channel

A simplified RBMK-channel geometry is shown in Fig. 1. The simplification is that the coating attached to the fuel element is not assigned to a separate region, but is included with the uranium oxide. To the channel a graphite layer of thickness 4.6 cm is added. It is assumed that beyond the limits of this layer the neutron distribution may be described within the framework of the small-group P_1 approximation, using the Maxwell spectrum for the thermal group. The channel symmetry sector is divided into 12 zones. In each zone the functions ψ and f are taken in the form of linear functions of (x, y)

$$f_{0t} = 1,\ f_{xt} = x + A1(t),\ f_{yt} = y + A21(t)\,x + A22(t); \tag{27}$$

$$\psi_{0t} = B(t),\ \psi_{xt} = f_{xt} \cdot B1(t),\ yt = f_{yt} B2(t). \tag{28}$$

The constants A1, A21, A22, B1, B2, B are found from the condition of mutual orthonormality of the functions $f_{\eta t}$ and $\psi_{\eta t}$. For the other symmetry sectors, the functions take the same form in a coordinate system applied

TABLE 1. Cross Sections of Materials

Material	Total cross section	Scattering cross section, min	Material	Total cross section, min	Scattering cross section, min
C	0,03809	0,03809	UO_2	0,06114	0,03659
Zr	0,03485	0,03400	H_2O	0,21318	0,21243

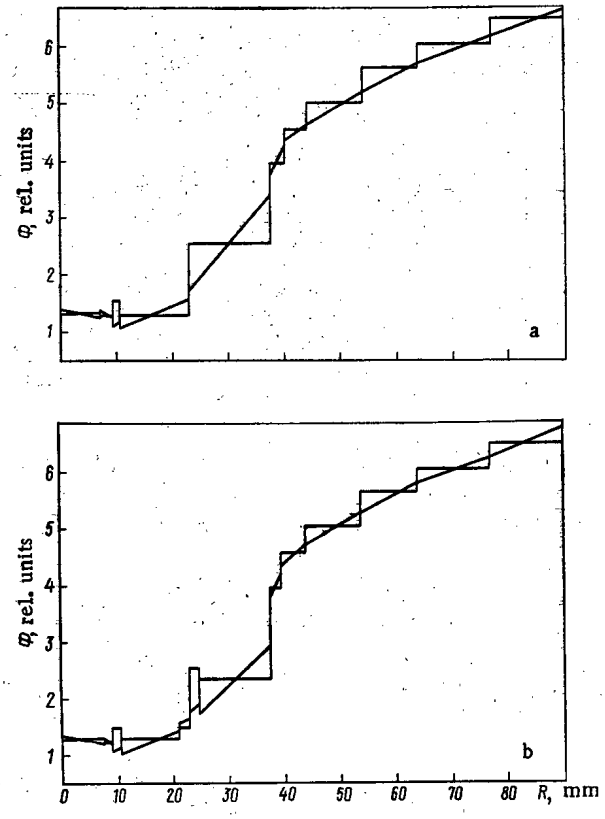

Fig. 2. Dependence of flux Φ on the radius in the cross sections $\varphi = \pi/12$ (a) and $\varphi = 0$ (b). The horizontal bars correspond to the mean values of the flux over the zone.

at some angle to the initial system. On passing to the initial system, the appropriate coordinate transformation is performed.

Solutions of Eq. (1) were obtained by the scheme outlined in two approximations: by the usual first-collision method and the improved method with the polynomials in Eqs. (27) and (28). The cross sections and the results of the calculations are shown in Tables 1 and 2 and Fig. 2. Comparison with the Monte Carlo method shows that the improved method is of high accuracy (Table 2). It is also of interest to compare the results with the usual first-collision method but with division into 16 zones (Table 2). The error of the usual method in calculating Φ with division into 12 zones amounts to 27.3%, the corresponding figure for the improved method being 3%. The difference in computation times is a factor of 4.5, whereas the number of unknowns (matrix elements) is increased by a factor of 9. It is seen in Fig. 2 that the linear functions f_{xt} and f_{yt} reduce the discontinuities of the flux Φ at the zone boundaries, but cannot eliminate them entirely.

It must be noted that division of the RBMK-channel symmetry sector into 12 zones with linear functions $f_{\eta t}$ is the optimum. A smaller number of layers can probably be introduced in the graphite layer. But

TABLE 2. Calculation of Φ in RBMK Channel by Different Methods

Zone No.	Material	Monte Carlo method		Division into 12 zones		Division into 16 zones		Linear approximation	
		$\Phi \cdot 10^3$	$\sigma \cdot 10^2$	$\Phi \cdot 10^3$	$\frac{\Phi - \Phi_{MC}}{\Phi_{MC}} \cdot 100\%$	$\Phi \cdot 10^3$	$\frac{\Phi - \Phi_{MC}}{\Phi_{MC}} \cdot 100\%$	$\Phi \cdot 10^3$	$\frac{\Phi - \Phi_{MC}}{\Phi_{MC}} \cdot 100\%$
1	C	6,491	0,006	6,424	—1,0	6,445	—0,7	6,454	—0,6
2	C	6,059	0,008	5,971	—0,2	6,005	—0,9	5,998	—1,0
3	C	5,577	0,010	5,496	—1,4	5,542	—0,6	5,530	—0,8
4	C	5,066	0,011	4,974	—1,8	5,037	—0,6	5,023	—0,8
5	Zr	4,592	0,012	4,484	—2,4	4,566	—0,7	4,556	—0,8
6	H_2O	4,000	0,011	3,867	—3,3	3,965	—0,9	3,986	—1,4
7	H_2O	2,594	0,009	2,646	+2,0	2,631	+1,4	2,570	—0,9
11	UO_2	2,348	0,008	2,418	+3,0	2,395	+2,0	2,362	+1,4
8	H_2O	1,543	0,010	1,810	+17,3	1,593	+3,2	1,516	—1,7
12	UO_2	1,328	0,009	1,633	+23,0	1,417	+6,7	1,320	—0,6
9	H_2O	1,298	0,016	1,651	+27,2	1,365	+5,2	1,267	—3,6
10	Zr	1,316	0,018	1,626	+23,6	1,368	+4,0	1,278	—2,9

additional division into small zones may perhaps be worthwhile between the series of fuel elements. On the other hand, the addition of quadratic terms in certain zones may eliminate the need to divide them.

CONCLUSIONS

The generalized first-collision method may prove useful in calculating channels with complicated geometry – e.g., RBMK channels. Then polynomials of different order may be used in different zones, taking into account, where necessary, the curvature of the neutron distribution by means of quadratic terms.

It remains to thank Yu. P. Elagina, A. S. Il'yashenko, and V. A. Lyul'ke for generally offering the possibility of comparing the results of the present work with results obtained with their program.

LITERATURE CITED

1. G. I. Marchuk and V. I. Lebedev, Numerical Methods in Neutron-Transfer Theory [in Russian], Atomizdat, Moscow (1971).
2. T. Taxeda and T. Sekiya, J. Nucl. Sci. Technol., 8, No. 12, 663 (1971).
3. J. Askew, E. Fayers, and P. Kemshell, J. Brit. Nucl. Energy Soc., 5, No. 4, 564 (1966).
4. W. Bikley and J. Nayler, Phil. Mag., 20, 343 (1935).

COST OPTIMIZATION IN CONNECTION WITH THE ACCUMULATION OF ISOTOPES OF THE TRANSURANIUM ELEMENTS

S. A. Nemirovskaya and A. P. Rudik

UDC 621.039.554

A system of equations has been proposed in [1] which describes cost redistribution in connection with the accumulation of isotopes of transuranium elements. The purpose of this article is to develop a formalism which permits optimizing the costs in connection with the accumulation of the isotopes of transuranium elements if the redistribution of these costs is described by the system of equations from [1].

The equations which describe depletion of isotopes are of standard form (e.g., see [2, 3]). Let us introduce the following notation: $x^{(i)}(t)$, number of nuclei of isotope i at time t; Σ_i, depletion rate of isotope i; Σ_i^{i-1}, formation rate of isotope i due to the depletion of isotope i – 1; λ_i, decay constant of isotope i; and λ_i^{i-1}, decay constant of isotope i – 1 with the formation of isotope i. Then

$$\frac{dx^{(i)}}{dt} = (\Sigma_i^{i-1} + \lambda_i^{i-1})\, x^{(i-1)} - (\Sigma_i + \lambda_i)\, x^i \equiv f^{(i)}, \tag{1}$$

with i = 1, . . . , n, where n is the number of isotopes in question; $\Sigma_1^0 = \lambda_1^0 = 0$.

If we arbitrarily separate (as has been done, e.g., in [2, 3]) the neutron flux density into a thermal part U and a resonant part ω, then one can represent the reaction rate Σ in the form

$$\Sigma = \sigma U + I\xi(x)\,\omega, \tag{2}$$

where σ and I are the thermal cross section and the resonant integral, and the factor ξ takes account of blocking of the resonant integral for the isotope x to which Σ corresponds.

Equations Which Describe Cost Redistribution. Let

$$y^{(k)}(t) = C_{k-n}(t)\, x^{(k-n)}(t), \quad k = n+1, \ldots, 2n \tag{3}$$

be the cost of all the nuclei of the isotope k – n at time t [then $C_{k-n}(t)$ is the cost of a single nucleus of isotope k – n], and correspondingly let $\bar{V}$ be the average cost of a single neutron. According to [1], the following system of equations occurs:

Translated from Atomnaya Énergiya, Vol. 48, No. 2, pp. 84-86, February, 1980. Original article submitted March 26, 1979.

0038-531X/80/4802-0093$07.50

$$\frac{dy^{(k)}}{dt} = (\Sigma_{k-n-1} + \lambda_{k-n-1})\, y^{(k-1)} + (\Sigma_{k-n} + \lambda_{k-n})\, y^{(k)} + \Sigma_{k-n-1}\bar{V}x^{(k-n-1)} \equiv g^{(k)}. \tag{4}$$

If we use Eq. (2) for Σ_{k-n-1}, the product $\Sigma_{k-n-1}\bar{V}$ is transformed to the form

$$\Sigma_{k-n-1}\bar{V} = \sigma_{k-n-1}V_U U + I_{k-n-1}\xi V_\omega \omega, \tag{5}$$

where V_U and V_ω are the costs of thermal and resonant neutrons, respectively.

Functional to be Analyzed. The systems of equations (1) and (4) should be supplemented with a functional J to be analyzed of the form

$$J = \int_0^T f^{(0)}\, dt. \tag{6}$$

Here T is the irradiation time, and the function $f^{(0)}$ depends on $x^{(i)}$ ($i = 1, \ldots, n$, $y^{(k)}$, $k = n+1, \ldots, 2n$) and the reaction rate.

Conjugate Functions and the Hamiltonian. Let us denote the conjugate functions in $x^{(i)}$ by Ψ_i and those in $y^{(k)}$ by χ_k. Then the Hamiltonian $\mathcal{H}$ of the systems of Eqs. (1) and (4) supplemented by the functional (6) is written in the form

$$\mathcal{H} = \psi_0 f^{(0)} + \sum_{i=1}^{n} \psi_i f^{(i)} + \sum_{k=n+1}^{2n} \chi_k g^{(k)}, \tag{7}$$

where ψ_0 is a nonpositive-definite constant and the conjugate functions ψ_i and χ_k satisfy the equations

$$\frac{d\psi_i}{dt} = -\frac{\partial \mathcal{H}}{\partial x^i}; \quad \frac{d\chi_k}{dt} = -\frac{\partial \mathcal{H}}{\partial y^k}. \tag{8}$$

If the reaction rate Σ has the form (2), Eqs. (8) are transformed to the form

$$\frac{d\psi_i}{dt} = -\psi_0 \frac{\partial f^{(0)}}{\partial x^{(i)}} + \psi_i \frac{\partial (\Sigma_i x^{(i)})}{\partial x^{(i)}} - \psi_{i+1} \frac{\partial (\Sigma_{i+1}^{i} x^{(i)})}{\partial x^{(i)}} + \chi_{i+n} y^{(i+n)} \frac{\partial \Sigma_i}{\partial x^{(i)}} - \chi_{i+n+1} \left[y^{(i+n)} \frac{\partial \Sigma_i}{\partial x^{(i)}} + \bar{V} \frac{\partial (\Sigma_i x^{(i)})}{\partial x^{(i)}} \right];$$
$$\frac{d\chi_k}{dt} = (\chi_k - \chi_{k+1})(\Sigma_{k-n} + \lambda_{k-n}) - \psi_0 \frac{\partial f^{(0)}}{\partial y^{(k)}}, \tag{9}$$

and the derivatives of the reaction rate with respect to the variable x are not equal to zero by virtue of the dependence of the blocking factor ξ on x.

Boundary Conditions. The systems of equations for the phase variables (1) and (4) and for their conjugate functions (8) or (9) should be supplemented with boundary conditions. All the quantities $x^{(i)}(0)$ and $y^{(k)}(0)$ are specified at the start of irradiation at t = 0. At the end of the irradiation at t = T usually neither $x^{(i)}(T)$ nor $y^{(k)}(T)$ are specified* and the boundary conditions are

$$\psi_i(T) = \chi_k(T) = 0; \; i = 1, \ldots, n; \; k = n+1, \ldots, 2n. \tag{10}$$

Perturbation Theory. Let the reaction rate be of the form (2) and let α be one of the functions U, ω, V_U, or V_ω or one of the parameters σ or I. Then if the systems of equations (1), (4), and (9) are solved for some value $\alpha(t)$ and the corresponding functional J is determined from Eq. (4), the variation δJ is expressed [4] in the following way in terms of the variation $\delta\alpha$:

$$\delta J = \int_0^T \frac{\partial \mathcal{H}}{\partial \alpha}\, \delta\alpha(t)\, dt, \tag{11}$$

with $\psi_0 = -1$.

Control in the Problems. We will assume that Σ has the form (2). Then U(t) or $\omega(t)$ can figure as the control in optimization problems. It is necessary to find such temporal variations of the function U(t) or $\omega(t)$ (which one is immaterial) which would result in a minimum of the functional J. It turns out [5] that the necessary condition for this to occur is the satisfaction of the maximum principle, which requires that the Hamiltonian as the control function attains a maximum. For the class of problems under discussion the Hamiltonian (7) is linear with respect to control and can be represented in the form

$$\mathcal{H} = F_1 + F_2 U + F_3 \omega, \tag{12}$$

* If some of the $x^{(i)}(T)$ and $y^{(k)}(T)$ are specified, the transversality condition (10) is modified in a standard way (e.g., see [4]).

TABLE 1. Main Physical Constants Entering into the Reaction Rate

Index	σ, b	I, b	Index	σ, b	I, b
1	18	1100	1→2	18	1100
2	90	2000	2→3	90	2000
3	12	720			

where the functions F_1, F_2, and F_3 depend only on the phase variables and the conjugate functions but do not depend on the controls. Therefore, satisfaction of the maximum principle requires either sign determinacy of the switching functions F_2 and F_3 for the limiting values of the corresponding controls or – in the case of special controls [6] – equating the switching functions to zero.

Two Types of Optimization Problems. The following types are evidently of greatest interest.

1. Minimization of costs for the production of a given isotope. In this case $J(T) = y^{(k)}(T)$ and the function $f^{(0)}$ can be selected in the form $f^{(0)} = g^{(k)}$.

2. Minimization of the costs for the production of the sum of all the isotopes appearing in Eq. (1). Then

$$\frac{d}{dt}\sum_{k=n+1}^{2n} y^{(k)} = \bar{V}\sum_{i=1}^{n}\Sigma_i x^{(i)} \tag{13}$$

follows* from the system (4). Thus minimization of the costs for the production of the sum of all the isotopes is determined only by the total number of absorbed neutrons. In this case

$$f^{(0)} = \bar{V}\sum_{i=1}^{n}\Sigma_i x^{(i)},$$

and consequently it is not necessary to discuss system (4) for solution of the optimization problem.

General Nature of the Solution of Eqs. (1), (4), and (9). Let us discuss the simplest example which has a purely methodological meaning. The most characteristic features of the solution of the systems of Eqs. (1), (4), and (9) will be clear from an analysis of it. Let us take ^{242}Pu as the initial isotope i = 1. Then the isotopes ^{243}Am and ^{244}Cm will correspond to the indices i = 2 and i = 3. The main physical constants entering into the reaction rate are given in Table 1.

To simplify matters we have assumed all $\xi = 1$. A specially written computer program has been used for the solution of the systems of Eqs. (1), (4), and (9). The calculations were carried out with $U = 10^{14}$ neutrons/cm$^2\cdot$sec, $\omega = 0.3\cdot 10^{14}$ neutrons/cm$^2\cdot$sec, and T = 1.2 years. We adopted $x^{(1)}(0) = 1$, $x^{(2)}(0) = x^{(3)}(0) = 0$ as the initial conditions for $x^{(i)}(0)$. The following alternative initial conditions were considered for $y^{(k)}(0)$ (with $V_U = V_\omega = 1$):

1) $y^{(4)}(0) = y^{(5)}(0) = y^{(6)}(0) = 0$;
2) $y^{(4)}(0) = 1$; $y^{(5)}(0) = y^{(6)}(0) = 0$;
3) $y^{(4)}(0) = 2$; $y^{(5)}(0) = y^{(6)}(0) = 0$,

$J = y^{(6)}(T)$ was selected as the functional to be analyzed. The dependences $x^{(3)}(t)$ and $y^{(6)}(t)$ and the switching functions $F_2(t)$ and $F_3(t)$ are given in Table 2 for the corresponding alternatives. The results obtained permit formulating the following conclusions within the framework of the example considered.

In the first place, it is completely natural that both $y^{(6)}(t)$ and $y^{(6)}/x^{(3)}$ increase as $y^{(4)}(0)$ increases. However, the ratio $[y^{(3)}(t)x^{(3)}(0)]/[y^{(6)}(0)x^{(3)}(t)]$ is, within the limits of computational error, a universal function of t, i.e., it does not depend on the alternative number.

In the second place, the temporal dependence of the switching functions F_1 and F_2 indicates that in order to reduce $y^{(6)}(T)$ the flux of thermal neutrons should be less at the end of the irradiation than at the start, and the flux of resonant neutrons should be less at the start of the irradiation than at the end. We note the universality of the functions $F_2(t)/F_2(0)$ and $F_3(t)/F_3(0)$.

*If the chain (1) is being considered for n isotopes, it is necessary to discard the term $(\Sigma_n + \lambda_n)y^{(2n)}$ in Eq. (4) for $y^{(2n)}$. We have the situation in mind in which we are speaking of a certain logical inconclusiveness of [1].

TABLE 2. Results of the Calculation of Alternatives 1-3

Alternative	Temporal function	t, years						
		0,0	0,2	0,4	0,6	0,8	1,0	1,2
For all alternatives	$x^{(3)}(t)$	0,000	0,037	0,113	0,197	0,271	0,330	0,371
1	$y^{(6)}(t)$	0,000	0,077	0,251	0,463	0,680	0,884	1,068
	$y^{(6)}/x^{(3)}$	2,000	2,081	2,221	2,350	2,509	2,679	2,879
	$F_2(t)$	—0,045	—0,051	—0,058	—0,068	—0,080	—0,094	—0,112
	$F_3(t)$	—2,723	—2,703	—2,677	—2,645	—2,606	—2,557	—2,497
2	$y^{(6)}(t)$	0,000	0,116	0,376	0,694	1,020	1,327	1,602
	$y^{(6)}/x^{(3)}$	3,000	3,135	3,327	3,523	3,764	4,021	4,318
	$F_2(t)$	—0,067	—0,076	—0,088	—0,102	—0,119	—0,141	—0,169
	$F_3(t)$	—4,084	—4,053	—4,015	—3,967	—3,909	—3,836	—3,745
3	$y^{(6)}(t)$	0,000	0,154	0,502	0,926	1,360	1,769	2,137
	$y^{(6)}/x^{(3)}$	4,000	4,162	4,442	4,700	5,018	5,361	5,760
	$F_2(t)$	—0,089	—0,101	—0,117	—0,136	—0,159	—0,188	—0,225
	$F_3(t)$	—5,445	—5,404	—5,353	—5,290	—5,211	—5,114	—4,993

The universal nature indicated above for the functions $[y^{(6)}(t)x^{(3)}(0)]/[y^{(6)}(0)x^{(3)}(t)]$, $F_2(t)/F_2(0)$, and $F_3(t)/F_3(0)$ is a rigorous law which is due to the form of Eqs. (1) and (4) and the initial conditions on $x^{(i)}(0)$ and $y^{(k)}(0)$.

In the third place, given the very same neutron flux alternatives, the larger the absolute value of the variation δJ of the functional is, the higher is the cost of the target material.

LITERATURE CITED

1. Yu. P. Kormushkin, A. V. Klinov, and Yu. G. Toporov, At. Energ., 41, No. 2, 102 (1976).
2. A. D. Galanin, The Theory of Nuclear Reactors Operating on Thermal Neutrons [in Russian], Atomizdat, Moscow (1959).
3. A. K. Kruglov and A. P. Rudik, Artificial Isotopes and a Method for Calculation of Their Formation in Nuclear Reactors [in Russian], Atomizdat, Moscow (1977).
4. A. P. Rudik, Nuclear Reactors and Pontryagin's Maximum Principle [in Russian], Atomizdat, Moscow (1971).
5. A. S. Pontryagin et al., The Mathematical Theory of Optimal Processes [in Russian], Fizmatgiz, Moscow (1965).
6. R. Gabasov and F. M. Kirillova, Special Optimal Controls [in Russian], Nauka, Moscow (1973).

MEASUREMENT OF THE CROSS SECTIONS FOR RADIATIVE CAPTURE OF NEUTRONS BY ^{238}U AND ^{197}Au RELATIVE TO THE CROSS SECTION FOR THE ELASTIC SCATTERING OF NEUTRONS BY PROTONS

A. N. Davletshin, S. V. Tikhonov,
A. O. Tipunkov, and V. A. Tolstikov

UDC 539.125.5

The study of the cross sections for the radiative capture of fast neutrons by ^{238}U and ^{197}Au is of interest mainly because of the practical requirements of fast reactor calculations involving the breeding of nuclear fuel. The differences in the results obtained by various experimenters who have investigated these cross sections are still rather large. Most of the measurements have been made relative to standard cross sections which have a complex structure, and this can introduce further errors. In order to obtain more accurate experimental data we have measured the ^{238}U and ^{197}Au capture cross sections relative to the smoothly varying $n-p$ scattering cross section for neutron energies from 0.35 to 1.4 MeV.

Bombardment of Samples. Samples were bombarded at an electrostatic accelerator using the $T(p, n)^3He$ and $^7Li(p, n)^7Be$ reactions. Figure 1 shows schematically the geometry of the placement of the sample and the hydrogen-filled counter during bombardment. The sample and counter were located at an angle of 0° with respect to the proton beam.

The neutron flux density at the center of the sample is $(3-6)\cdot 10^6$ neutrons/cm$^2\cdot$sec; the relative efficiency (the ratio of the number of interactions to the number of incident neutrons) for radiative capture by samples of U_3O_8 is $(0.5-0.9)\cdot 10^{-2}$%, and for Au samples $(0.8-2)\cdot 10^{-2}$%. The attenuation of the neutron beam by the sample in the container at energies between 350 and 1400 keV is 3.5-9%. The construction of the counters is described in [1]. The counters are filled with pure hydrogen or methane.

The cross section for the radiative capture of neutrons of energy E_n was calculated from the expression

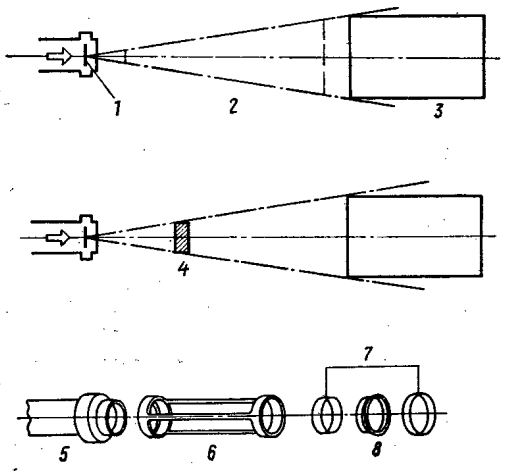

Fig. 1. Geometry of: a) measurements of neutron flux; b) bombardment of samples; c) structure of assembly for bombarding samples; 1) target; 2) location of shadow cone; 3) H-counter; 4) sample; 5) target support; 6) sample holder; 7) cadmium container; 8) sample.

Translated from Atomnaya Énergiya, Vol. 48, No. 2, pp. 87-91, February, 1980. Original article submitted April 23, 1979.

0038-531X/80/4802-0097$07.50

$$\sigma_{rad}=(E_n)=\frac{N_{\gamma 0}}{\eta N_{in}}\frac{f(\lambda, t)}{C_\varphi}\frac{n_{n.co}V_{co}}{m_{n\,sq}}\frac{C_{co}}{G_{sa}}\sigma_{co}(E_n). \quad (1)$$

Here η is the efficiency of the Ge(Li) detector; $f(\lambda, t)$, time factor; $n_{n\,co}$, number of hydrogen nuclei per cm^3; V_{co}, sensitive volume of the counter; $m_{n\,sa}$, number of activated nuclei in the sample, $\sigma_{co}(E_n)$, n – p scattering cross section [2]; $\sigma_{rad}(E_n)$, cross section for the radiative capture of neutrons; and C_φ, correction for the time variation of the neutron source strength.

The geometric factors for the counter and sample are of identical form:

$$G_{co}=\frac{\nu_{co}}{V_{co}n_{co}\sigma_{co}}; \quad (2)$$

$$G_{sa}=\frac{\nu_{sa}}{m_n\sigma_{sa}}. \quad (3)$$

In these expressions ν is the absolute efficiency of the corresponding detector. In both cases ν is calculated for an isotropic disk source of neutrons and a uniform cylindrical detector located coaxially [3].

The quantities $N_{\gamma 0}$ and N_{in} in (1) are calculated from the expressions

$$N_{\gamma 0}=\frac{N_\gamma A_\gamma}{T_{dr}}; \quad (4)$$

$$N_{in}=\frac{N_{eis}(x)}{T_{dp}A_e(x)K_n\varepsilon_p(x)}, \quad (5)$$

where N_γ is the area of the total absorption peak; T_{dr}, correction for the dead time of the analyzer recording the γ spectrum; $N_{eis}(x)$, area of the recoil proton spectrum (RPS) for the threshold $x = E_p/E_n$ [E_p, recoil proton energy; i.e., $N_{eis}(x)$, experimental integral RPS]; and T_{dp}, correction for the dead time of the analyzer recording the RPS; $K_n\varepsilon_p(x)$, integral RPS calculated by the Monte Carlo method for the chosen value of the threshold [4]. Equation (5) can also be written for the differential RPS. Problems related to the calculation of N_{in} are discussed in detail in [5].

It is important that effects in the sample $N_{\gamma 0}$ and in the counter N_{in} in Eq. (1) are produced by nearly monoenergetic neutrons. This condition is not satisfied in the bombardment of samples. The dependence of the response function on neutron energy is different for sample and counter, and therefore corrections for background effects must be introduced into the experimental results so that ultimately the values obtained correspond only to neutrons incident on the detector directly from the target.

The measured value of the background correction A_γ to the activity of a sample takes account of the effect of the room and the finite mass of the sample, container, target support, and sample holder. In addition, a correction is introduced for the anisotropy of the neutron source, and therefore the spread of neutron energies indicated in Tables 1 and 2 is produced by the thick target only. This correction is discussed in detail in [6].

The background correction $A_\varepsilon(x)$ in the experimental RPS includes the effect of the room, the walls and ends of the counter, the target support and sample holder, and the attenuation of the neutron beam by the layer

TABLE 1. Cross Sections for the Radiative Capture of Neutrons by ^{138}U

Neutron energy, keV	Radiative capture cross section, mb	Hydrogen-filled counter					Ge(Li) detector	
		type	volume, cm^3	type	pressure, $10^5 N/m^2$	RPS shape parameter	volume, cm^3	eff., %
597±16	127,1±3,9 %	I-1	112,2	H_2	1,65	0,487	32	1,66±0,03
590±23	130,8±3,6 %	K-1	99,3	H_2	2,03	0,558	32	1,66±0,03
792±22	135,7±4,2 %	K-1	99,3	H_2	2,03	0,497	32	1,66±0,03
1026±22	124,2±3,6 %	K-1	99,3	H_2	2,03	0,411	32	1,66±0,03
352±25	117,4±3,1 %	K-2	179,7	H_2	1,86	0,632	70	1,98±0,04
700±41	128,8±2,8 %	K-2	179,7	H_2	1,86	0,553	70	1,98±0,04
1192±33	87,4±3,1 %	K-2	179,7	H_2	1,86	0,375	70	1,98±0,04
348±23	119,9±2,8 %	K-1	99,3	H_2	0,90	0,586	50	1,87±0,02
348±15	122,3±3,0 %	K-1	99,3	H_2	0,90	0,586	50	1,87±0,02
603±36	114,6±2,7 %	K-1	99,3	H_2	0,90	0,456	50	1,87±0,02
1400±31	69,6±2,3 %	K-15	255,0	CH_4	3,04	0,632	50	1,87±0,02
1400±31	75,9±2,7 %	K-18	177,8	H_2	2,60	0,392	50	1,87±0,02
350±24	124,8±2,8 %	K-1	99,3	H_2	0,90	0,586	50	1,87±0,02
600±22	114,0±2,5 %	K-15	255,0	CH_4	3,04	0,677	50	1,87±0,02
1400±23	71,7±2,5 %	K-15	255,0	CH_4	3,04	0,632	50	1,87±0,02

TABLE 2. Cross Sections for the Radiative Capture of Neutrons by ^{197}Au

Neutron energy, keV	Radiative capture cross section, mb	Hydrogen-filled counter					Ge(Li) detector		$\frac{\sigma_{n,\gamma}(U)}{\sigma_{n,\gamma}(Au)}$
		type	volume, cm^3	gas	pressure, $10^5 N/m^2$	RPS shape parameter	volume, cm^3	eff., %	
597±16	126,6±3,2%	I-1	112,2	H_2	1,65	0,487	32	2,24±0,007	1,004±3,8%
590±23	131,5±3,5%	K-1	99,3	H_2	2,03	0,558	32	2,24±0,007	0,995±3,9%
352±19	212,7±3,1%	K-2	179,7	H_2	1,86	0,632	70	3,01±0,06	0,552±3,9%
700±41	121,0±2,9%	K-2	179,7	H_2	1,86	0,553	70	3,01±0,06	1,060±3,4%
1188±38	74,8±3,4%	K-2	179,7	H_2	1,86	0,375	70	3,01±0,06	1,168±3,7%
348±23	200,8±2,7%	K-1	99,3	H_2	0,90	0,586	50	2,71±0,007	0,597±3,3%
348±15	223,0±2,7%	K-1	99,3	H_2	0,90	0,586	50	2,71±0,007	0,548±3,4%
1400±27	67,7±2,7%	K-15	255,0	CH_4	3,04	0,632	50	2,71±0,007	1,028±3,0%

of air. This correction was measured for each position of the counter and neutron energy in the form of a correction spectrum for the differential or integral RPS. Figure 2 shows the measured values of $A_\varepsilon(x)$ for several values of the neutron energy. The experimental absolute value of the correction is normalized to the RPS corresponding to neutrons incident on the counter directly from the target. The data on Fig. 2 refers to a K-2 counter (cf. Tables 1 and 2) located 70 cm from the target.

Efficiency of Ge(Li) Detector. Samples of the same composition as those used in measurements at the electrostatic accelerator and two foils were bombarded simultaneously by a beam of thermal neutrons (Fig. 3). If the thermal neutron flux density is constant through the sample and foil, the efficiency can be calculated from the expression

$$\eta = Am/aM, \tag{6}$$

where M and m are, respectively, the masses of the sample and foil.

The activity A of the sample was measured with a Ge(Li) detector by the total energy absorption peaks E_γ = 74.7 keV for U_3O_8 samples and 412 keV for gold samples. The absolute activity a of a foil was determined by the $4\pi\beta - \gamma$ coincidence method.

For the arrangement shown in Fig. 3 the flux densities φ_1, $\bar{\varphi}$, and φ_2 are not identical. If we denote by C^2 the transmission of the arrangement, it can be shown that

$$\eta = \eta_1/C = C\eta_2, \tag{7}$$

where η_1 and η_2 are the efficiencies calculated for foils 1 and 2 by Eq. (6).

Consequently, from the results of bombarding the two foils and the sample, the efficiency of the Ge(Li) detector can be determined from the expression

$$\eta = \sqrt{\eta_1\eta_2}. \tag{8}$$

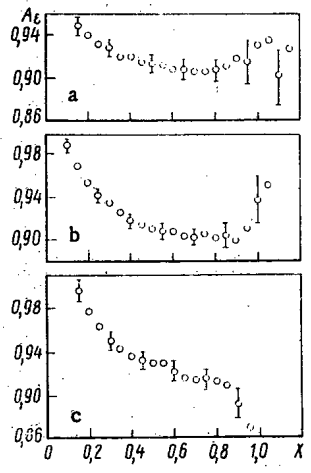

Fig. 2. Background correction $A_\varepsilon(x)$ for neutron energies of: a) 350; b) 700; c) 1200 keV.

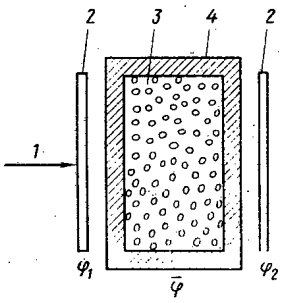

Fig. 3. Bombardment of samples by a beam of thermal neutrons: 1) neutrons; 2) foil; 3) sample; 4) container.

TABLE 3. Components of Total Random Error of ^{238}U Cross section

Quality	Error, %	
	350(keV)	1400 (keV)
Time factor $t(\lambda, t)$	0,2	0,2
Correction for const neutron source strength, C_φ	0,1	0,1
No. of hydrogen nuclei/cm^3, n_{nco}	0,2	0,2
Vol. of counter, V_{co}	0,6	0,6
No. of nuclei in sample, m_{nsa}	0,1	0,1
Geometric factor for counter, G_{co}	0,3	0,3
Geometric factor for sample, G_{sa}	0,6	0,6
np scattering cross section, σ_{co}	1,0	1,0
Eff. of Ge(Li) detector η	0,9	0,9
Total statistical error of calc. and expt.	0,6	0,6
Parameters of calc.	0,5	1,0
Bkgd. correction for counter $A_\varepsilon(x)$	0,6	0,9
Bkgd. correction for sample, A_γ	2,0	1,4
Total random error	2,8	2,7

The absolute activity of a U_3O_8 foil was measured by the method of $4\pi\beta-\gamma$ coincidences with a subsequent correction for the counting efficiency in the β channel for sources of finite thickness [7]. The absolute activity of a gold foil was found by the method of double linear extrapolation of the β counts to a value of the counting efficiency equal to unity [8]. The area of a total absorption peak in the measurement of the activity of samples by the Ge(Li) detector was determined by the trapezoid method [9].

Experimental Results. The measured values of $\sigma_{n\gamma}$ for ^{238}U are listed in Table 1, and those for ^{197}Au in Table 2. Preliminary values of some of these quantities were published in [10, 11]. Subsequently, background corrections to the activity of the samples were refined, and the present paper reports the final results. The errors indicated in the tables correspond to a 68% confidence interval.

The tables list information on the detectors employed. The use of various Ge(Li) detectors, hydrogen-filled counters, the change of composition and pressure of the filler gas, decrease the unknown systematic error connected with the parameters of these detectors and the whole set of our data introduced in using them to estimate radiative capture cross sections. The possible systematic errors of the background correction to the activity at E_n = 350 keV are from −2 to +3% for ^{197}Au, and from −1.5 to +2% for ^{238}U; for E_n = 1400 keV the limits of the ranges are approximately half as large.

In using hydrogen-filled counters it was not required that the shape of the RPS be close to that of a uniform distribution. Therefore, in using a counter over a wide range of energy the RPS differed strongly from a uniform distribution. Tables 1 and 2 list values of the RPS shape parameter for each counter. This parameter is the value of the calculated integral RPS $\varepsilon_p(x = 0.3)$ for the neutron energy under consideration. For a uniform distribution of the pulse amplitudes from x = 0 to x = 1, $\varepsilon_p(x = 0.3) = 0.7$.

Table 3 lists the random errors of all the factors in (1) for the end points of the energy range. Information is also presented on the random errors in a somewhat different form: for E_n = 350 keV the error of all quantities related to the measurement of activity is 2.4%, and for quantities referring to the hydrogen-filled counter, 1.6%. For E_n = 1400 keV these errors are 1.9 and 1.9%, respectively.

Discussion of Results and Conclusions. Figure 4a, b shows the results of our measurements with indicated random errors and the energy spread of the bombarding neutrons, and also our estimates of the radiative capture cross sections for ^{238}U [12] and ^{197}Au [13] and estimates from ENDF/B IV [2].

Our results for ^{238}U are in better agreement with estimates in [12] than with those in [2], and those for ^{197}Au differ from very close estimates in [13] and [2]. At the lower boundary of the energy range our results are higher than the estimated values by (3 ± 2)% on the average for ^{238}U, and by (15 ± 3)% for ^{197}Au. For E_n = 1.4 MeV our results are lower by (7 ± 2)% on the average for ^{238}U and by (9 ± 5)% for ^{197}Au. For $E_n \approx 1$ MeV our data for both elements on the average agree with estimates in [2, 12, 13]. Thus, for both elements the energy dependence of our data is different from that for the estimated data. We note that approximately the same energy dependence of $\sigma_{n\gamma}$ for ^{197}Au was obtained in [14] by the time-of-flight method.

This conclusion is certain. All our measured values of cross sections differ from one another in at least one of the experimental conditions: the neutron energy, the Ge(Li) detector, the counter and the pressure

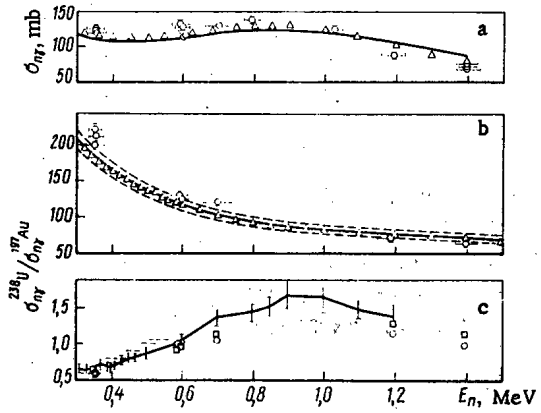

Fig. 4. Cross section for the radiative capture of neutrons by: a) ^{238}U; b) ^{197}Au, and the ratio of $\sigma_{n\gamma}$ for ^{238}U to $\sigma_{n\gamma}$ for ^{197}Au; a, b, ○) our data; △) estimated data from [12] for ^{238}U and [13] for ^{197}Au; ——) estimated from [12]; — — —) mean-square spread of estimated experimental data in [13] equal to 6.5%; c, ○) our data, □) ratio calculated from data in [2]; — — —) data from [15]; ——) data from [14].

of the gas in it, the target support. The mean-square spread of the average values at values of the energy for which experiments are repeated is 4.5%. The average random error of our data is 3.1%. The difference between these estimates of random errors clearly arises from systematic errors in the cross sections introduced by the values of η, $A_\varepsilon(x)$, $n_{n\,co}$, and V_{co} in Eq. (1).

Using the measured cross sections, the ratio of the radiative capture cross sections of uranium and gold was calculated. The errors of quantities pertaining to the recoil proton counter do not enter into the error of these ratios except statistically. Figure 4c shows our results and data from [2, 14, 15]. The values closest to our results were obtained from estimates in [2].

The necessity of reliable information on $\sigma_{n\gamma}$ for ^{238}U requires further measurements by the procedure described to decrease possible systematic errors of the results obtained. It is desirable to extend the energy range both toward lower neutron energies by using γ-ray discrimination, and toward higher energies by using methane- and hydrogen-filled counters.

LITERATURE CITED

1. S. N. Baikalov, V. S. Korolev, and V. V. Chubinskii, in: Metrology of Neutron Radiation at Reactors and Accelerators, Vol. 1, Proc. Second All-Union Conf. [in Russian], Moscow (1974), p. 58.
2. B. Maguro, ENDF/B IV Cross Section Measurement Standards, BNL-NCS-504464, August (1975).
3. N. A. Vartanov and P. S. Samoilov, Applied Gamma Spectrometry [in Russian], Atomizdat, Moscow (1969).
4. A. N. Davletshin, V. P. Platonov, and V. A. Tolstikov, in: Nuclear Constants [in Russian], No. 9, Atomizdat, Moscow (1972), p. 107.
5. A. N. Davletshin and V. A. Tolstikov, At. Energ., 42, 43 (1977).
6. A. N. Davletshin et al., At. Energ., 48, 113 (1980).
7. É. F. Garapov et al., Preprint FÉI-501, Obninsk (1974).
8. H. Menke and J. Fahland, Standardization of Radionuclides, SM-79/18, Vienna (1967).
9. IEEE Trans. Nucl. Sci., NS-19, No. 1, 155 (1972).
10. A. N. Davletshin, A. O. Tipunkov, and V. A. Tolstikov, in: Neutron Physics (Data of Third All-Union Conf. on Neutron Physics) [in Russian], Part 4, TsNIIatominform, Moscow (1976), p. 109.
11. A. N. Davletshin et al., ibid., p. 99.
12. V. N. Vinogradov et al., in: Nuclear Physics Research in the USSR [in Russian], No. 22, Atomizdat, Moscow (1976), p. 4.
13. V. N. Vinogradov et al., in: Neutron Physics (Data of Third All-Union Conf. on Neutron Physics) [in Russian], Part 1, TsNIIatominform, Moscow (1976), p. 165.
14. W. Poenitz, Nucl. Sci. Eng., 57, 300 (1975).

15. R. Spenser and F. Keappeler, in: Proc. Fourth Conf. on Nuclear Cross Sections and Technology, Vol. 2, Washington, March 3-7 (1975), p. 620.

SOLUBILITY OF NITROGEN IN WATER

Yu. A. Kalaida, Yu. D. Katkov, V. A. Kuznetsov, A. Yu. Lastovtsev, A. P. Lastochkin, and V. S. Sysoev

UDC 621.039.5.629.1

The question of the solubility of nitrogen in water at increased parameters of it has taken on great practical significance in recent years in connection with the use of nitrogen as a working body in systems of compensation for the volume in water-cooled – water-moderated reactors. This leads to an extremely substantial saturation of the coolant of the first circuit of nitrogen.

An increased nitrogen concentration in the coolant (C = 2000-3000 normal ml N_2/kg H_2O) can disrupt the normal operation and can be the cause of breakdown of circulation pumps, filters of the system of purification of heat cells, and other first circuit equipment [1-4].

An analysis of the published data on the solubility of nitrogen in water [5-12] has shown that there is a sufficiently large number of experimental data, in relatively good agreement, for low pressure and temperature, while there are few data for moderate and high pressure and temperature, and they sometimes differ substantially from one another.

One of the causes of these discrepancies, in our opinion, is the absence of an objective method of determining the limiting (equilibrium) value of the nitrogen concentration in water at various parameters. In all the studies the evaluation of the limiting solubility was to a definite degree subjective, since it depended on the experimental conditions.

In view of this, the authors of the present work undertook the following tasks:

to develop a method that would permit an objective determination of the limiting value of the nitrogen concentration in water;

to experimentally investigate the solubility of nitrogen in water in the region of moderate and increased parameters, typical of water-cooled – water-moderated reactors.

The investigations were conducted on a special stand with forced circulation, equipped with systems for compensation and air and gas removal. A peculiarity of the stand was a universal volume compensator (VC), which can be used in gas, steam, and steam – gas systems of operation. The circulation circuit included a thermally insulated sample collector of special design (capacity 1047 ± 5 ml), equipped with an autonomous cooling system. The stand and sample collector were equipped for measuring the pressure with standard manometers (error no greater than ±0.0025 MPa), standard mano-vacuummeters (error no more than ±0.001 MPa), differential transformer induction pickups with secondary indicating and recording instruments (error no more than ±0.06 MPa); and for measurement of the temperature, thermocouples (error no more than ±1°C) with the same instruments.

To find the limiting values of the nitrogen concentration in water, we developed a method of phase transformations, permitting a determination of the concentration of the solution C_i without overflow and cooling of the sample. The method was based on the phenomenon of abrupt variation of the pressure and temperature in a closed volume at the moment of phase transition of the solution from an undersaturated state to a state of limiting saturation and oversaturation.

Forced circulation of degasified water (using a VC in the steam system) or water saturated with nitrogen to some value of C_i (using a VC in a steam – gas or gas system) was carried out through the sample collector. After stabilization of the parameters, the sample collector was disconnected from the circulation circuit and the external pressure created by the VC. The change in the pressure and temperature in the disconnected

Translated from Atomnaya Énergiya, Vol. 48, No. 2, pp. 91-94, February, 1980. Original article submitted March 26, 1979; revision submitted June 27, 1979.

0038-531X/80/4802-0102$07.50

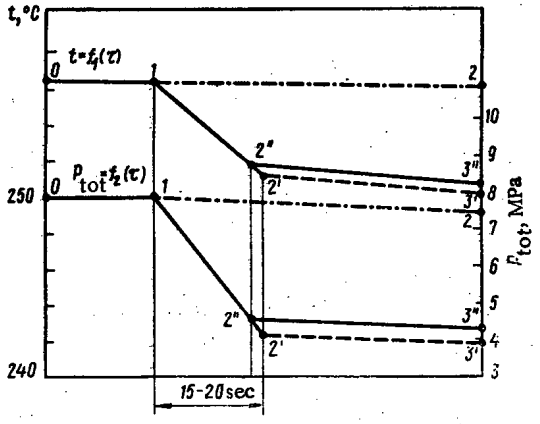

Fig. 1. Scheme of variation of the parameters in the disconnected sample collector: ——) two-phase gas – liquid mixture; — — —) degasified water ($C_i = 0$); — · —) water saturated with nitrogen ($C_i \neq 0$); time of transitional process 15-20 sec.

sample collector was recorded synchronously on the tapes of automatic recording instruments. Figure 1 shows the variation of the temperature $t = f_1(\tau)$ and pressure $P_{tot} = f_2(\tau)$ in the sample collector after it was disconnected (point 1). The processes $0-1-2'-3'$ correspond to experiments with degasified water ($C_i = 0$), the processes $0-1-2''-3''$ to experiments with water saturated with nitrogen to some value of C_i. The pressure and temperature of saturation are established at the point 2', and a pressure and temperature differing from the parameters of saturation at the point 2". The experiments show that there is an unambiguous relationship between C_i and the pressure difference at the points 2' and 2".

In our opinion, for the pressure and temperature at the point 2", the given value of C_i is the limiting, equilibrium value, i.e., $C_i = C_{lim}(P_{2''}t_{2''})$. At these parameters, the gas component of the solution is still in a bound state, at the boundary of transition to the free state. The relationship between the limiting gas content and the parameters of the solution at the moment of the phase transformation can be found according to Henry's law, keeping in mind that $P_{tot} = P_{2''}$:

$$C_{lim} = (P_{tot} - P_s)/k_{P,t}, \quad (1)$$

where $k_{P,t} = f(P_{tot}, t)$ is the solubility coefficient, dependent on the pressure and temperature of the solution, MPa · kgH_2O/normal N_2. Thus, in contrast to the methods of other researchers, in this method the limiting gas saturation is determined objectively according to the pressure jump at the moment of the phase transformation.

The method of phase transformations permits monitoring of dissolved gas without overflow of the sample according to the parameters of the phase transformation. In this case the monitoring is performed according to the nature and form of the graphs of $t = f_1(\tau)$ and $P_{tot} = f_2(\tau)$, according to the presence or absence of a "break," corresponding to the parameters of the phase transformation. The absence of a break (processes $0-1-2$ in Fig. 1) is evidence that the turned off sample collector contains a two-phase gas – liquid mixture. The phase transformations evidently cannot occur in the two-phase system. The nature of the pressure change in this case is determined by the system of cooling of the sample collector. In the case under consideration, $C_i > C_{lim}$. The same nature of the change in the pressure and temperature in the sample collector will exist when $C_i = C_{lim}$.

The presence of a break is an indication that a homogeneous medium was found in the sample collector. If the parameters of the phase transformation correspond to the parameters of water at the line of saturation, then degasified water was found in the sample collector (processes $0-1-2'-3'$ in Fig. 1). In this case $C_i = 0$. If the parameters of the phase transformation differ from the parameters of water at the line of saturation, then a homogeneous solution of gas in water was found in the sample collector (processes $0-2-2''-3''$ in Fig. 1). In this case $C_{lim} > C_i > 0$. The value of C_i can be determined according to the parameters of the phase transformation, if the solubility coefficient $k_{P,t}$ is known. Thus, for a concrete determination of the nitrogen concentration in water by the method of phase transformations without overflow of the sample, the function $k_{P,t} = f(P_{tot}, t)$ should be known.

To find this dependence we used the method of sample collection, followed by cooling. Forced circulation of water saturated with nitrogen to some value of C_i was performed through the sample collector. After stabilization of the parameters, the sample collector was disconnected from the circuit and the external pressure created by the VC. The autonomous cooling system was turned on, and the sample was cooled to 15-20°C. Then the pressure in the sample collector was measured. The gas concentration in water C_i, corresponding to the limiting parameters $P_{2''}$ and $t_{2''}$ was determined according to the difference of the specific volumes of the hot and cooled samples, considering a correction for the residual nitrogen concentration in water according to the formula

$$C_i = C_{lim}(P_{2''}, t_{2''}) = \frac{P_{tot}^{cool} - P_s}{P_0}\left[\left(\frac{v_{hot}}{1+\beta t_{hot}} - v_{cool}\right)\frac{273}{T_{cool}} + C_{res}\right], \text{ normal ml } N_2/\text{kg } H_2O, \quad (2)$$

where P_{tot}^{cool} is the total pressure in the sample collector after cooling, MPa; P_s, saturation pressure at T_{cool}, MPa; T_{cool}, temperature of the water and gas in the cooled sample collector, °K; v_{hot} and v_{cool}, specific volumes of water in the hot and cooled state, normal ml/kg; β, temperature coefficient of volume expansion of the metal of the sample collector, 1/deg; C_{res}, residual nitrogen concentration in water at P_0 = 0.1 MPa and t_{cool}, normal ml N_2/kg H_2O. The investigation was performed in the following range of parameters: $0 < P_{tot} \leq 15$ MPa, $100 \leq t \leq 340$°C, $0 \leq C_{lim} \leq 5000$ normal ml N_2/kg H_2O.

An analysis of the results showed that the relative error of the determination of the concentration C_i does not exceed ±2-3% and increases with increasing concentration of the solution.

According to the results of the experimental investigations performed, considering the previously published data, we constructed the C vs P vs t diagram of the solubility of nitrogen in water (Fig. 2). In its construction, it was assumed that in water at the line of saturation [curve of $t_s = f(P_s)$ on the P–t plane], the concentration of dissolved nitrogen is equal to zero, while at t = 0 the concentration of dissolved nitrogen is proportional to the total pressure (straight line C = A = P on the C – P plane). This is sufficiently well confirmed by the experimental data.

From Fig. 2 it follows that to each value of the pressure correspond two values of the temperature at which the limiting concentration has minimum (curve of C_{lim}^{min}) and maximum (curve C_{lim}^{max}) values. Analysis showed that the projections of the solubility isotherms onto the C – P plane are approximated with sufficient accuracy by linear functions. In this case the isotherms are tangents to the projection of the curve of C_{lim}^{max} onto the C – P plane. The normal to the P axis from the point of tangency determines the pressure P_{tot}^{max} at which a limiting nitrogen concentration in water, C_{lim}^{max}, is reached for the given temperature.

Figure 3 presents the diagram of the limiting solubility of nitrogen in water in a plot of C vs P.

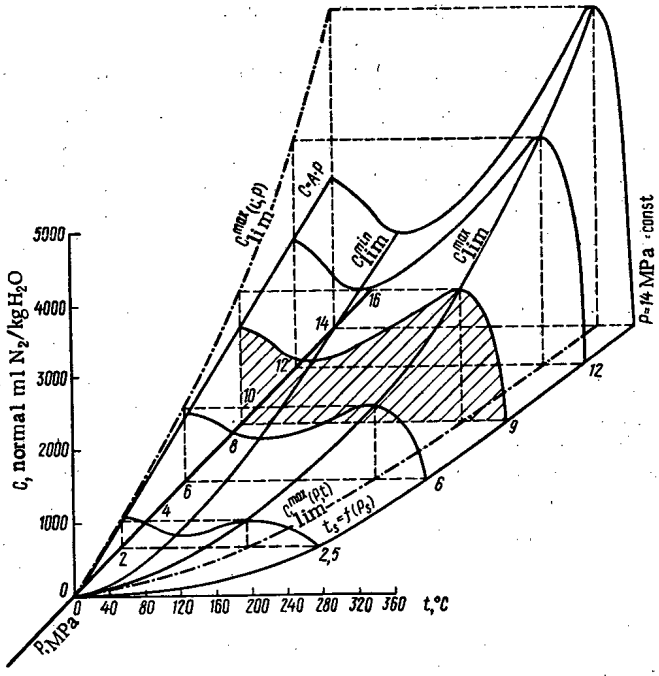

Fig. 2. C vs P vs t diagram of the limiting solubility of nitrogen in water.

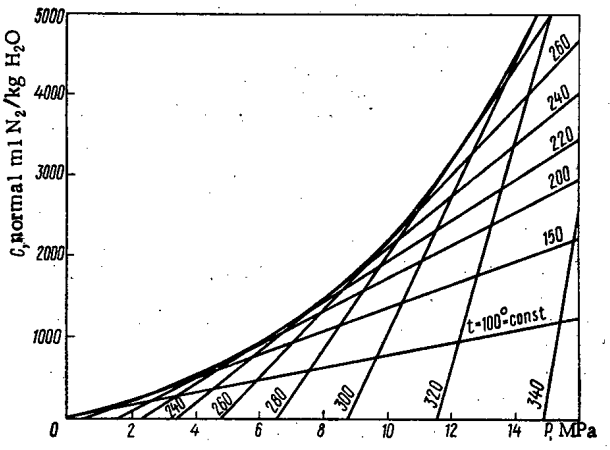

Fig. 3. C vs P diagram of the limiting solubility of nitrogen in water.

The empirical equations for the projection of the curve of C_{lim}^{max} onto the C – P plane and the isotherms were obtained in the following form:

$$C_{lim}^{max} = 0.96 P_{tot}^{max} [P_{tot}^{max} (P_{tot}^{max} + 1) + 113]; \tag{3}$$

$$C_{lim}(t) = [2.88 P_{tot}^{max} (P_{tot}^{max} + 0.67) + 108.5] P_{lim}^{i} - 1.92 (P_{tot}^{max})^2 (P_{tot}^{max} + 0.5), \tag{4}$$

where P_{tot}^{max} is the total pressure of the solution at which the maximum limiting concentration for the given temperature is reached, MPa; P_{tot}^{i}, total pressure of the solution at which the limiting concentration of the given temperature is reached, MPa.

The pressure P_{tot}^{max} is related to the temperature through the saturation pressure $P_s = f(t)$:

$$P_{tot}^{max} = y - 0.17 (1 - 3P_s), \tag{5}$$

the value of y is determined from the functions:

$$\begin{gathered} y = u + m; \\ u = (\sqrt{a^2 + b^3} - a)^{1/3}; \\ m = (-\sqrt{a^2 + b^3} - a)^{1/3}; \\ a = 4.63 \cdot 10^{-3} [(1 - 3P_s)^3 - 54 P_s (P_s + 112)]; \\ b = -2.8 \cdot 10^{-2} [12 P_s + (1 - 3P_s)^2]. \end{gathered} \tag{6}$$

From Eqs. (1) and (3) we find the solubility coefficient

$$k_{P,t} = \frac{1 - (P_s / P_{tot}^{max})}{0.96 [P_{tot}^{max} (P_{tot}^{max} + 1) + 113]}. \tag{7}$$

From the diagram of C vs P and Eq. (1) it follows that the solubility $k_{P,t}$ is numerically equal to the slope of the isotherm to the P axis in the C – P plane, i.e.,

$$k_{P,t} = \operatorname{tg} \alpha = [2.88 P_{tot}^{max} (P_{tot}^{max} + 0.67) + 108.5] \frac{M_C}{M_P}, \tag{8}$$

where M_C/M_P is the ratio of the scales along the concentration and pressure axes.

From the condition of constancy of $k_{P,t}$ at any set temperature, it follows that there is a relationship between the limiting (at the pressure P_{tot}^{i}) and maximum limiting concentration, reached at some pressure P_{tot}^{max} and set temperature:

$$C_{lim}^{(i)} = C_{lim}^{max} \frac{P_{tot}^{i} - P_s}{P_{tot}^{max} - P_s}. \tag{9}$$

The use of the method of phase transformations and the dependences obtained for $k_{P,t} = f(P_{tot}, t)$ and C_i permits a determination of the limiting concentration of nitrogen in water at moderate and high parameters without overflow of the sample and without breaking the hermetic sealing of the circulation circuit.

LITERATURE CITED

1. V. S. Sysoev, At. Energ., 26, No. 5, 461 (1969).
2. N. V. Bychkov and A. I. Kasperovich, At. Energ., 28, No. 2, 145 (1970).
3. Yu. F. Bodnar', At. Energ., 31, No. 2, 150 (1971).
4. A. I. Kasperovich, N. V. Bychkov, and V. K. Shiryaev, At. Energ., 36, No. 5, 387 (1974).
5. T. Kh. Margulova, The Water System of Thermal Electric Power Plants [in Russian], Énergiya, Moscow (1965).
6. The Chemist's Handbook [in Russian], Vol. 3, Khimiya, Moscow – Leningrad (1964).
7. Handbook of Solubility [in Russian], Vol. 1, Izd. Akad. Nauk SSSR, Moscow – Leningrad (1961).
8. K. Frölich et al., Indust. Eng. Chem., 23, 548 (1931).
9. J. Goodman and N. Krase, ibid., 401.
10. H. Pray, C. Schweikert, and B. Minnich, ibid., 44, 1146 (1952).
11. R. Wiebe, V. Gaddy, and C. Heins, ibid., 24, 927 (1932).
12. T. Anderson, Trans. Am. Nucl. Soc., 10, 507 (1967).

OPTIMIZATION OF RADIATION FACILITIES WITH ELECTRON ACCELERATORS

V. V. Krayushkin

UDC 541.15

In view of the widespread introduction of radiation technology in various branches of industry [1, 2], great importance is taken on by studies on radiation facilities (RF) by the methods of mathematical simulation. Without resorting to complex and expensive experiments, one can study the parameters of facilities which are being designed or already exist, evaluate different variants of the makeup of their apparatus, and also use mathematical methods to find optimal modes of operation and control. The present paper is devoted to problems of mathematical simulation and optimization of RF with electron accelerators, designed for radiation treatment of lumped nonmixing systems.

As in most design problems, for the optimality criterion it is advisable to take the minimum normalized expenditures [3] for the construction of the RF; these could be written as

$$\Pi = (C_a + \varepsilon_n K_{RF})/Q_{RF}, \quad (1)$$

where C_a are the annual operating costs, in rubles; K_{RF}, capital outlays for RF, rubles; ε_n, normalized coefficient of investment efficiency, year^{-1}; Q_{RF}, annual output of RF, units of output/year.

To solve the optimization problem it is necessary first of all to choose a mathematical model which would be adequate for the facility under consideration. For the model of the RF we propose to use a mathematical description of the process of irradiating objects with ionizing radiation. In this case the initial parameters of the model are the characteristics which determine the state of the object prior to irradiation while the final parameters are the physicomechanical properties (quality and state) of the final product.

When an RF with an electron accelerator is used to irradiate lumped nonmixing systems, the input parameters should include the density (ρ_o) and size of the object under irradiation. When objects are moved through the irradiation zone at constant speed, it is necessary to take account of the thickness (t_o) and width (l_o) of the objects. The totality of input parameters can be written as

$$\mathbf{x} = \mathbf{x}(\rho_o;\ t_o;\ l_o). \quad (2)$$

Since the physicomechanical properties of a material subjected to radiation treatment are determined in most cases by the absorbed dose (AD) of the ionizing radiation D, the nonuniformity Δp of the AD distribution, and in a number of cases the absorbed dose rate (ADR), P, it is expedient to take these characteristics to be the output parameters of the RF model.

Translated from Atomnaya Énergiya, Vol. 48, No. 2, pp. 94-97, February, 1980. Original article submitted July 7, 1978; revision submitted March 30, 1979.

0038-531X/80/4802-0106$07.50

The output parameters for a concrete process of radiation technology are usually found experimentally; therefore, in simulation of RF they are assumed to be determined (specified quantitatively in some interval or expressed by functions):

$$\mathbf{y} = \mathbf{y}(D;\ \Delta p;\ P). \tag{3}$$

The physical parameters of the RF are the controlling inputs: the energy E of the accelerated electrons, the radiation power (installed power of accelerator) N, the density j of the current of accelerated electrons in the irradiation zone, the characteristics of the irradiator (area S of irradiation zone, density ρ_f and thickness t_f of the absorbing filter; distance from irradiator to object under irradiation, etc.), the irradiation time τ, or the velocity v of transport of the irradiated object through the irradiation zone):

$$\mathbf{u} = \mathbf{u}(E;\ N;\ j;\ S;\ \rho_f;\ t_f;\ v). \tag{4}$$

The mathematical model of RF with electron accelerators should be written as

$$\mathbf{y} = f\{\mathbf{x},\ \mathbf{u}\}. \tag{5}$$

The dependence of the output parameters on the input and controlling actions is determined, as a rule, by the functions of AD and ADR distributions over the thickness of the object irradiated (the uniform distribution of these quantities over the length and width of the objects is ensured by uniform transport of the objects through the irradiation zone and by an electron-beam scanning system). Using methods of calculating the characteristics of the absorbed energy for several ways of irradiating nonmixing systems [1, 4-7], one can get different models for the irradiation of objects, i.e., one can determine the mathematical relations between the input parameters and the input and control actions.

To solve the optimization problem it is necessary to study the effect of the parameters of the mathematical model on the optimality criterion. The ultimate goal of this stage is to express the optimality criterion in terms of the parameters of the model, i.e., to obtain the response function as

$$\Pi = F\{\mathbf{x},\ \mathbf{u},\ \mathbf{y}\}. \tag{6}$$

To find such a relation it is necessary to study the effect of the parameters of the RF model on the quantities which appear in Eq. (1) for the normalized expenditures.

Nikulin et al. [8] presented a technique for evaluating the radiation components of the annual operating costs and the capital outlays in relation to the cost K_S of the radiation source, i.e., the electron accelerator; for foreign facilities considered by the authors these indices are linear functions of K_S. On the basis of an engineering and economic analysis of Soviet RF with electron accelerators (e.g., [9]) in much the same way as the presented method of linear approximation we obtained

$$K_{RF} = (2.4 \pm 0.3)\, K_S; \tag{7}$$

$$C_a = (0.7 \pm 0.1)\, K_S. \tag{8}$$

Comparing Eqs. (7) and (8) with analogous equations from [8], we can conclude that the capital outlays for the construction of radiation facilities in the USSR and elsewhere are roughly the same. On the basis of data about the costs of present-day domestic electron accelerators, employed in industrial and semicommercial RF we propose a formula which reflects the dependence of the cost of the accelerator on its energy parameters:

$$K_{RF} = 0.5\,(1 \pm \delta)\, E \sqrt{N},\ 10^6 \text{ rubles}, \tag{9}$$

where E is the energy of the accelerated electrons, pJ; N, accelerator power (mean power of electron beam), kW; δ, spread of cost owing to different pricing in construction enterprises.

It should be pointed out that with series fabrication of electron accelerators in our country, it is quite a complicated undertaking to make a detailed analysis; accordingly, Eq. (9) does not reflect the dependence on other factors which also affect the accelerator cost (the reliability of the units and the accelerator as a whole, the degree of automation, etc.). Nevertheless, the relation obtained provides a quite good representation of the existing situation for low-energy ($E \leq 0.32$ pJ) direct electron accelerators. Figure 1 shows how the accelerator cost depends on the electron energy for several values of accelerator power [calculated from Eq. (9) for $\delta = 0.1$].

It is known [10] that the capacity of an RF with an electron accelerator is proportional to the accelerator power and inversely proportional to the AD in the object under irradiation:

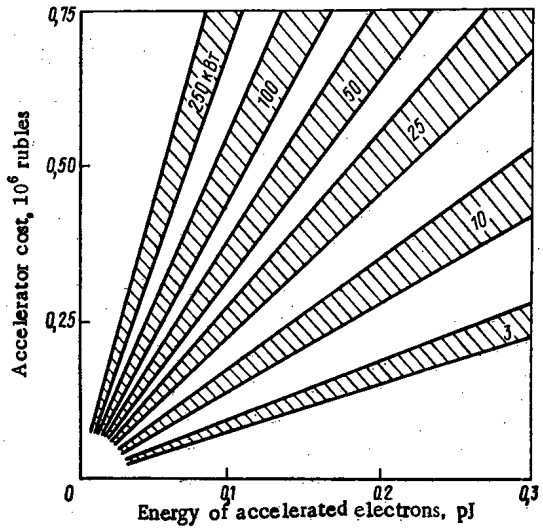

Fig. 1. Accelerator cost vs energy of accelerated electrons and beam power.

$$q = N\eta\eta^*/D_{\min} \text{ kg/sec} \tag{10}$$

or

$$Q_{RF} = 3.6qk_1k_2T_F \text{ tons/yr} . \tag{11}$$

Here η is the efficiency of radiation utilization; η^*, coefficient allowing for additional power losses by electron beam in irradiator [10] (from experience gained from the construction of domestic RF it is known that $\eta^* \approx 0.8$); D_{min}, minimum allowable AD, kJ/kg; k_1, load coefficient of facility; k_2, coefficient of utilization of operating time; T_F, operating time of facility, h/yr.

The efficiency of radiation utilization is the ratio of the power of the electron radiation required to produce the minimum allowable PD in the irradiated object, given uniform distribution of the radiation, to the total power of the accelerator, i.e.,

$$\eta = N_{\min}/N = \rho_0 t_0 D_{\min} \Big/ \int_0^R D(x)\, dx, \tag{12}$$

where D(x) is the function of AD distribution over the thickness [7]; R, maximum range of the electrons.

In the general case the efficiency of radiation utilization is a function of several variables: the energy of the accelerated electrons, the thickness and density of the object irradiated, the nonuniformity of the AD distribution, and the density and thickness of the absorbing filter:

$$\eta = \varphi(E,\ \rho_0 t_0,\ \Delta p,\ \rho\ t\ ). \tag{13}$$

When the values of the annual operating expenditures, capital outlays, and capacity of the RF, expressed in terms of the parameters of the model [see Eqs. (7)-(13)], are substituted into Eq. (1) for the normalized expenditures, we get in the general form

$$\Pi = \sigma D_{\min} E/\sqrt{N} T_F \eta, \tag{14}$$

where σ is a proportionality factor which is independent of the parameters of the RF model.

It must be pointed out that there are some radiation processes for which limitations exist as to the ADR, i.e., as follows from [7], limitations as to the current on the surface of the object irradiated. In this case the optimal value of the current density will have a value for which the condition

$$C(j_{opt}) = P_{\max} \tag{15}$$

will be satisfied. Here P_{max} is the maximum allowable value of the ADR.

For most radiation-chemical processes the dependence of the AD, which ensures the necessary quality of production, on the ADR and in the final account on the current density and the area of the exit window of the irradiator is important. When such processes are effected in an RF, the optimal values of the current

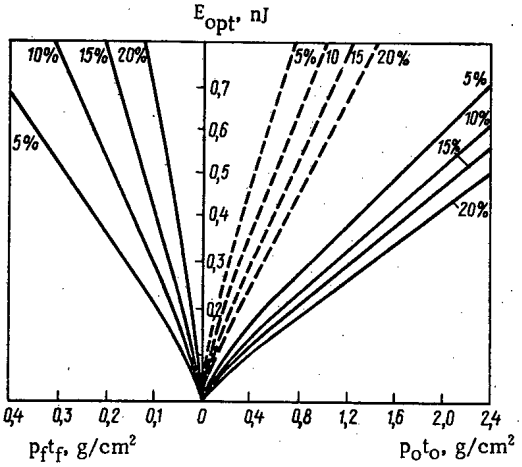

Fig. 2. Optimal energy of accelerated electrons and thickness of absorbing filter under two-sided (——) and one-sided (— — —) irradiation vs thickness of irradiated material for various values of Δp (numbers next to curves).

density and the area of the irradiation zone, which is set primarily by the area of the exit window of the irradiator, are found from the condition

$$D(j_{opt})/\sqrt{j_{opt}S_{opt}} = \min. \tag{16}$$

The normalized expenditures for the RF are reduced with a lowering of the energy as well as with an increase in the efficiency of utilization of the electron radiation. On the other hand, as the energy is decreased, the range of the electrons in the object under irradiation is shortened, thus resulting in increased nonuniformity of the AD distribution, on which stringent constraints are imposed in most cases. Therefore, the optimal electron energy is found from

$$\sqrt{E_{opt}}/\eta(E) = \min. \tag{17}$$

Let us consider in greater detail the two most common ways of irradiating objects: one- and two-sided irradiation of flat objects by a normally incident electron beam without reflecting substrates. As shown by calculations, in these cases the highest efficiency of radiation utilization with stringent requirements as to the uniformity of the AD distribution over the thickness of the irradiated object ($\Delta p \leq 0.2$) is determined by the condition that the AD be the same on the surface and on the reverse side of the object:

$$D_{surf} = D_{rev} = D_{min} \tag{18}$$

In this case the optimal values of θ are found from

$$\theta'_{opt} = \frac{1}{\rho_o t_o}\left[\pi - 2\arcsin\left(1 - \frac{4\Delta p}{1+\Delta p}\right)\right] \text{cm}^2/\text{g}\ ; \tag{19}$$

$$\theta''_{opt} = \frac{2}{\rho_0 t_0}\left[\pi - \arcsin\left(1 - \frac{4\Delta p}{1+\Delta p}\right) + \arcsin\frac{2\Delta p}{1+\Delta p}\right] \text{cm}^2/\text{g} \tag{20}$$

Here θ'_{opt} and θ''_{opt} are the optimal values of the parameter for one- and two-sided methods of irradiation.

The ratio of the thickness of the absorbing filter and the parameter θ for both methods of irradiation is found from

$$\rho_f t_f = \left[\arcsin\left(1 - \frac{4\Delta p}{1+\Delta p}\right) - 0.2\right]/\theta_{opt}. \tag{21}$$

Figure 2 shows how the optimal energy depends on the thickness of the irradiated material when condition (18) is observed.

Conclusions. On the basis of an analysis of an RF with an electron accelerator as an object of optimization in solving the problem of optimal design we found the output parameters of an RF model as well as controlling actions. As the optimality criterion we took the minimum normalized expenditures for the construction of an RF. In the general case the response function (normalized expenditures on RF) was found to depend on the parameters of the model. For two cases we constructed a nomogram which makes it possible to find the

optimal value of the energy of the accelerated electrons and the thickness of the absorbing filter.

LITERATURE CITED

1. Yu. D. Kozlov et al., Calculation of Parameters and Design of Radiation-Chemical Facilities with Electron Accelerators [in Russian], Atomizdat, Moscow (1976).
2. A. S. Shtan' and E. R. Kartashev, At. Energ., 43, No. 5, 390 (1977).
3. G. M. Ostrovskii and Yu. M. Volin, Methods of Optimizing Complex Chemical-Technological Schemes [in Russian], Khimiya, Moscow (1970).
4. K. I. Nikulin, At. Energ., 30, No. 5, 448 (1971).
5. L. V. Chepel', At. Energ., 30, No. 1, 70 (1971).
6. R. Ya. Strakovskaya et al., At. Energ., 36, No. 4, 302 (1974).
7. V. V. Krayushkin and V. P. Suminova, in: Proc. Second All-Union Meeting on Application of Charged-Particle Accelerators in the National Economy [in Russian], Vol. 1, NIIÉFA, Leningrad (1976), p. 347.
8. K. I. Nikulin et al., At. Energ., 37, No. 3, 234 (1974).
9. V. V. Krayushkin et al., in: Proc. Second All-Union Meeting on Application of Charged-Particle Accelerators in the National Economy [in Russian], Vol. 1, NIIÉFA, Leningrad (1976), p. 238.
10. Yu. S. Titkov et al., in: Radiation Chemistry [in Russian], Atomizdat, Moscow (1972), p. 446.

LETTERS

MASS TRANSFER IN SINGLE CRYSTALS OF MOLYBDENUM AND SILICON CARBIDE UNDER IRRADIATION WITH LOW-ENERGY GLOW-DISCHARGE IONS

A. A. Babad-Zakhryapin, E. V. Borisov, I. B. Savvatimova, and A. D. Senchukov

UDC 534.9.019.3

As is known [1, 2], treatment in glow-discharge plasma substantially increases the density of defects of the dislocation type in the cathode material. A hypothesis explaining this effect can be explained by using the experimental results of treatment of metallic foils in a glow discharge. Palladium foil was treated in a helium in the normal region of glow discharge at a glow potential of 300-1000 V and a current density of 20-60 mA/cm^2 for 5 min to 2 h. Considerable porosity was found to result and the initial thickness (~100 μm) of the foil was found to increase by several microns or by as much as several tens of microns. Because of the preferential swelling of the surface layers (Fig. 1) with a rise in temperature and dose of ion radiation the size of the pore in the foils increases and the density decreases. When a copper specimen 3 mm thick is treated in a helium medium the surface layer is also saturated with pores to a depth of about 80 μm (Fig. 2).

These examples permit the conclusion that the generation of defects in cathode material takes place because of swelling of the surface layers under the influence of implanted gases. This swelling results in an increase in the density of defects of the dislocation type. For example, treatment of a molybdenum single crystal with hydrogen, helium, and argon ions with a dose of more than 10^{19} ions/cm^2 at a temperature of 1400-1600°C causes the defect density in the surface layer with a depth of up to 100 μm (total specimen thickness 2-3 mm) to increase by a factor of 10 to 100. At doses above 10^{20} ions/cm^2 an increase in the defect density is observed throughout the entire volume of the material treated (Fig. 3).

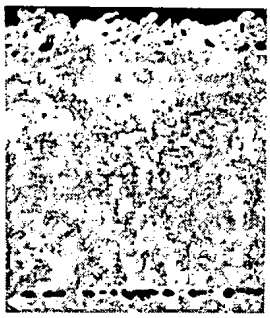

Fig. 1. Cross section of palladium foil treated with helium ions (400 V, 10^{21} ions/cm^2, 900°C (× 500).

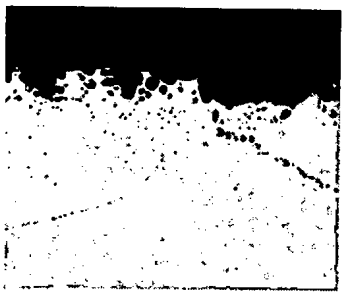

Fig. 2. Cross section of copper plate treated with helium ions (500 V, 10^{23} ions/cm^2, 900°C) (× 150).

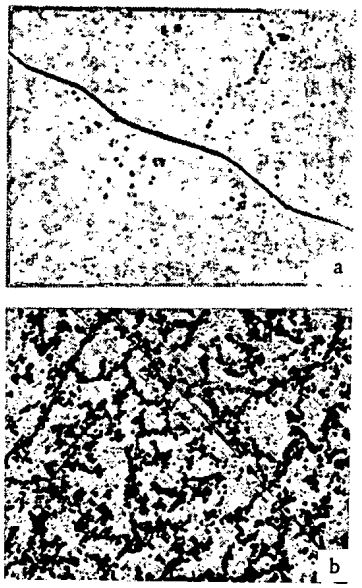

Fig. 3. Microstructure of monocrystalline molybdenum: a) original specimen; b) after treatment with hydrogen ions (10^{21} ions/cm^2, 1500°C, 500 V) (× 500).

Translated from Atomnaya Énergiya, Vol. 48, No. 2, pp. 98-100, February, 1980. Original article submitted January 30, 1978; revision submitted June 4, 1979.

0038-531X/80/4802-0111$07.50

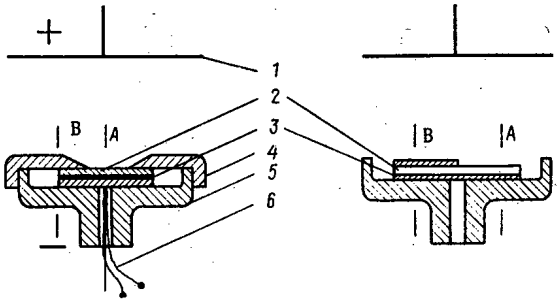

Fig. 4. Device for studying mass transfer: 1) anode; 2) material in which mass transfer is studied; 3) diffusant; 4) shield; 5) cathode; 6) thermocouple.

Defects continuously generated during treatment of a material with plasma ions should be conducive to an acceleration of mass transfer in the cathode material. To study this effect the object was placed on the cathode of a discharge device (Fig. 4). We studied plates of monocrystalline molybdenum with a thickness of about 2 mm and silicon carbide with a thickness of about 0.5 mm with layers of a diffusant deposited on them. To determine the effect of the defects we determined the change in the diffusant concentration both on segments of the specimen subjected to the action of the discharge and on segments protected by a shield or a shielding layer (see Fig. 4, zones A and B), and also made a comparison with the change in the concentration in a vacuum furnace at the same temperature and for the same length of time. The temperature was monitored with an optical pyrometer and a W – Re thermocouple. The distribution of the tungsten concentration in the molybdenum was determined by x-ray spectral microanalysis (Fig. 5). For the other materials the method used was microautoradiography. The diffusion coefficients were calculated by the familiar techniques [3-5].

It follows from the data in Table 1 that for the Mo – W pair the interdiffusion coefficient $\tilde{D}$ at high diffusant concentration (~ 50%) is practically the same for treatment in a glow discharge and in vacuum-furnace annealing. At a low diffusant concentration (≤ 3%) glow-discharge treatment increases $\tilde{D}$ roughly tenfold in comparison with the values obtained for shielded specimens and specimens heated in the vacuum furnace.

For diffusion pairs in which mass transfer was studied by the tagged-atom method (Mo – UO_2, Mo – Pm_2O_3, SiC – ^{14}C, SiC – Pm_2O_3) the values of $a^2 \cdot D_{disl}$ (where a is the diameter of the dislocation tube, D_{disl} is the coefficient of diffusion over the dislocations) for the open segments are 10 to 10^4 times those for the shielded parts. This attests to the intensification of mass transfer over the dislocations with continuous generation of structural defects in the discharge plasma, as already noted earlier [6]. The observed absence of

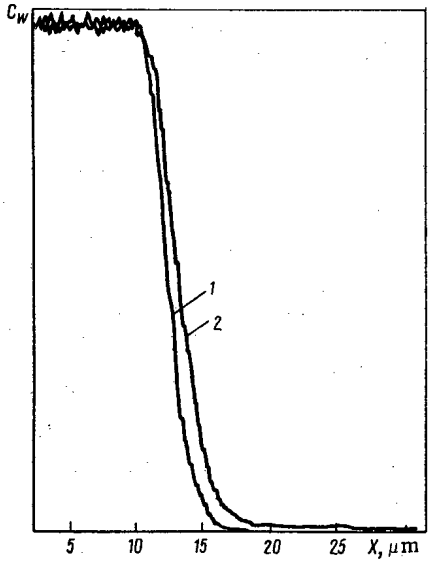

Fig. 5. Distribution of diffusant concentration in matrix: 1) after treatment in glow discharge; 2) after annealing in vacuum furnace.

TABLE 1. Diffusion Coefficients in Pairs Mo – W, Mo – Pm_2O_3, Mo – UO_2, SiC – ^{14}C, SiC – Pm_2O_3

Matrix	Diffusant	Temp.	Gas	Ion flux intensity, ion·cm^{-2}·sec	Dose, ions·cm^{-2}	Structural state of matrix	Diffusion coeff.						
								Heating in discharge			Heating in vacuum furnace		
							analysis zone	$\tilde{D}$	D_{irr}	a^2D_{disl}	$\tilde{D}$	D_{irr}	a^2D_{disl}
Mo	W	1600	H_2	$6,2\cdot10^{17}$	$3,3\cdot10^{23}$	Single crystal	A+ B+ A++ B++	$3,6\cdot10^{-14}$ $4,0\cdot10^{-14}$ $6,0\cdot10^{-13}$ $4,0\cdot10^{-14}$			$4,0\cdot10^{-14}$		
Mo	Pm_2O_3	1700	H_2	$6,2\cdot10^{17}$	$2,2\cdot10^{23}$	Single Polycrystal	A A	$1,4\cdot10^{-10}$ $8,4\cdot10^{-11}$			$2,2\cdot10^{-11}$ $3,2\cdot10^{-11}$		
Mo	UO_2	1600	H_2	$6,2\cdot10^{17}$	$1,1\cdot10^{24}$	Single crystal	A B		$2,8\cdot10^{-13}$ $2,7\cdot10^{-13}$	$4,6\cdot10^{-18}$ $4,6\cdot10^{-20}$		$4\cdot10^{-14}$	$1,0\cdot10^{-19}$
SiC	^{14}C	1450	He	$8,1\cdot10^{17}$	$1,5\cdot10^{23}$	Single crystal	A A B		$3,3\cdot10^{-11}$ $2,2\cdot10^{-10}$ $4,2\cdot10^{-11}$	$4,0\cdot10^{-15}$ $9,6\cdot10^{-15}$ $9,0\cdot10^{-15}$	No interaction		
SiC	Pm_2O_3	1450	He	$1,3\cdot10^{18}$	$4,5\cdot10^{22}$	Single crystal	A A B		$2,8\cdot10^{-10}$ $3,9\cdot10^{-10}$ $3,5\cdot10^{-10}$	$1,0\cdot10^{-16}$ $3,6\cdot10^{-16}$ $4,8\cdot10^{-20}$	No interaction		

*The values of $\tilde{D}$ and D_{irr} are given in cm^2/sec; a^2D_{disl}, in cm^4/sec; A, zone subjected to ion bombardment; B, shielded zone; + and ++, for tungsten concentration of ~ 50 and < 3%, respectively.

any appreciable variations in the volume diffusion is in accord with existing ideas concerning the effect of irradiation on diffusion processes [7, 8].

LITERATURE CITED

1. A. A. Babad-Zakhryapin and G. D. Kuznetsov, Chemical-Thermal Treatment in Glow Discharge [in Russian], Atomizdat, Moscow (1975).
2. A. A. Babad-Zakhryapin and M. I. Lagutkin, Metalloved. Term. Obrab. Met., No. 7, 70 (1976).
3. C. Matano, Jpn. J. Phys., 8, 109 (1973).
4. L. Hall, J. Chem. Phys., 21, 87 (1953).
5. P. V. Pavlov, V. A. Panteleev, and A. V. Maiorov, Fiz. Tverd. Tela, 6, No. 2, 382 (1964).
6. O. I. Butenko and Yu. M. Lakhtin, Metalloved. Term. Obrab. Met., No. 6, 21 (1969).
7. L. N. Bystrov, L. I. Ivanov, and Yu. M. Platov, in: Diffusion in Metals and Alloys [in Russian], Tulsk. Politekh. Inst., Tula (1968), p. 254.
8. A. C. Damask and G. J. Dieanes, Point Defects in Metals, Gordon and Breach (1964).

DIAGNOSTICS OF STATE OF BOR-60 REACTOR BY CALCULATION OF REACTIVITY BALANCE

V. A. Afanas'ev, V. M. Gryazev,*
V. N. Efimov, B. V. Kebadze,
N. V. Krasnoyarov, and V. A. Kachalin

UDC 621.039.514

Registration of anomalous effects by calculation of the reactivity balance (c.r.b.), which is one of the most effective methods in the diagnostics of the state of a reactor [1], is based on solving the equation of reactivity balance for the anomalous reactivity ρ_a:

$$\rho_a = \rho_k + \rho_e + \rho_r + \rho_b,$$

where ρ_k is the total reactor reactivity found by solving the equation of point kinetics; ρ_e, effect of reactivity caused by variations in the reactor parameters; ρ_r, reactivity due to displacements of the control and safety rods, and ρ_b, reactivity due to fuel burnup and swelling.

If it is borne in mind that calculations now performed in the design stage in the development of fast reactors are carried out with insufficient accuracy owing to the indeterminacy of many constants and mechanisms of the behavior of reactor components [2], then appreciable errors are involved when the reactivity balance is calculated by using the results of design calculations.

Experimental investigations on the BOR-60 reactor revealed that by using the integrated reactor parameters, measured by technological monitoring pickups, one can with relatively simple algorithms identify reactivity effects with sufficient accuracy and construct a c.r.b. system on this basis.

In particular, for BOR-60 operation with 20-30% deviation of the parameters, we obtained the following expressions [3]:

$$\rho_e = \sum_{i=1}^{5} \rho_i; \quad \tau_i \dot{\rho}_i = \tilde{\rho}_i - \rho_i,$$

where $\tilde{\rho} = \{(aN + k_1 bN/G)(k_2 bN/G)[(1 - k_1 - k_2)bN/G](k_{t_1} t_{in})(k_{t_2} t_{in})\}^T$ is a five-dimensional vector with components $\tilde{\rho}_i$ of the steady-state (asymptotic) values of the component resistivity effects associated with the thermal expansions of the reactor core, the lateral shield, the rods of the control and safety system (CSS), and the base plate of the reactor; $\rho = (\rho_1 \ldots \rho_5)^T$, vector of the dynamic values of the component reactivity effects; $\tau = (\tau_1 \ldots \tau_5)^T$, vector of time constants; a, b, k_1, k_2, empirical coefficients dividing the power reactivity coefficient $(\partial\rho_r/\partial N)$ into various components; k_{t_1} and k_{t_2}, "fast" and "slow" components of the temperature reactivity

*Deceased.

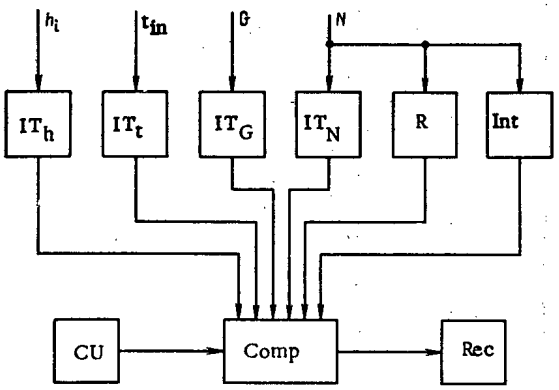

Fig. 1. Simplified block diagram of c.r.b. system of BOR-60 reactor.

Translated from Atomnaya Énergiya, Vol. 48, No. 2, pp. 100-101, February, 1980. Original article submitted September 11, 1978; revision submitted April 23, 1979.

0038-531X/80/4802-0114$07.50

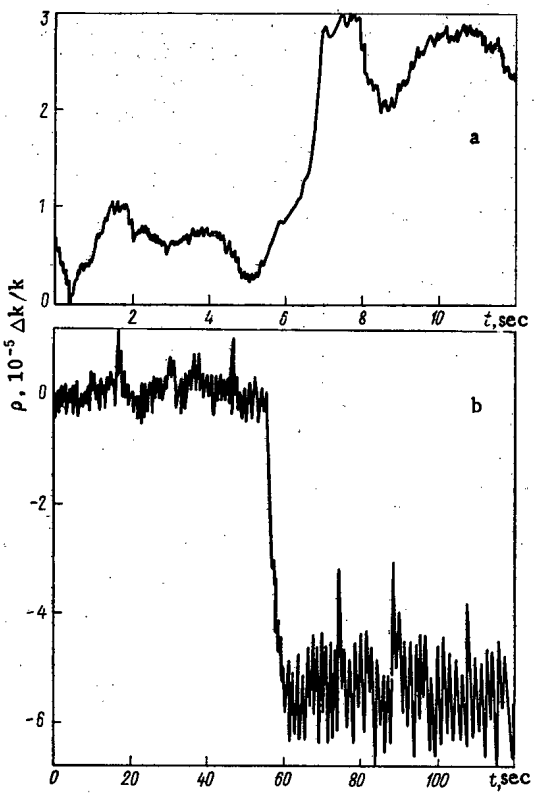

Fig. 2

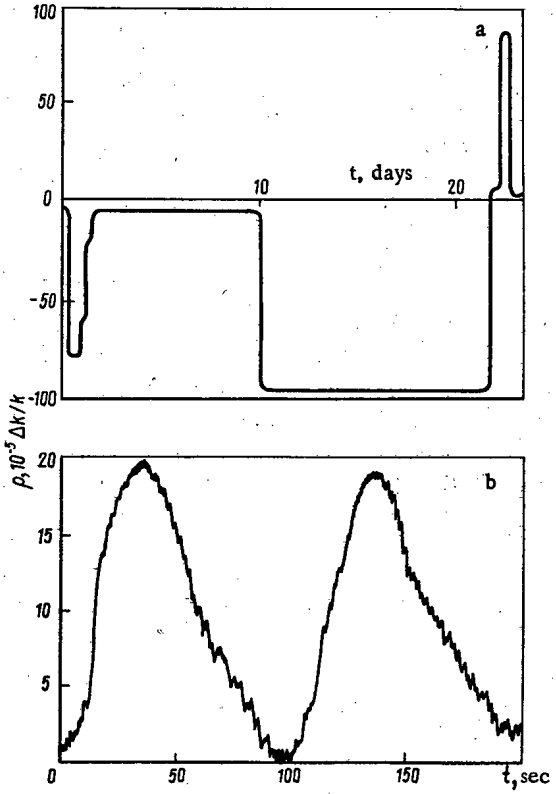

Fig. 3

Fig. 2. Variation of output signal of c.r.b. system: a) when an artificial anomalous reactivity is introduced into the reactor; b) when sodium boils up in the fuel assembly of the reactor.

Fig. 3. Anomalous changes in reactivity of BOR-60: a) when absorption rod is damaged; b) when one rod is displaced in weakened grip.

effect $(\partial\rho_r/\partial t_{in})$; and N, G, and t_{in}, the power, coolant flow rate, and coolant temperature at the reactor input.

The dependence of the efficiency of four CSS rods on their positions h_i is approximated by fifth-order polynomials. Then

$$\rho_r = \sum_{i=1}^{4} \sum_{j=0}^{5} k_{ij} h_i^j.$$

The effect of fuel burnup and swelling is

$$\rho_b = \int_0^{\tau} k_b N \, d\tau,$$

where k_b is the rate of decrease of the reactivity margin during the operating run [4]. The expression for ρ_k is the algorithm of an analog computer, i.e., a reactimeter.

In accordance with these algorithms, a system (Fig. 1) was realized for the BOR-60 reactor; this system contained input transducers with filters (IT), a reactimeter (R), an integrator (Int), an analog–digital computer (Comp) simulating the reactivity components and calculating the corresponding balance, a control unit (CU), and a recorder (Rec). Sensitivity to the appearance of anomalies should be one of the main parameters of such a system from the point of view of diagnostics. Analysis of the effect of the pickup errors, as well as the statistical errors due to the uncorrelated fluctuations of the pickup parameters and signals [5], on the sensitivity of the system demonstrated that it was possible to reliably record anomalies equivalent to $(1\text{-}2)\cdot 10^{-5}$ Δk/k. This is confirmed by an experiment with the introduction of a reactivity of $\sim 2\cdot 10^{-5}$ Δk/k in 0.3 sec as well as an experiment with local sodium boiling in the reactor core (Fig. 2).

The empirical coefficients appearing in the algorithm change with time, in view of which they should be periodically verified and corrected (roughly 2-3 times a month in the case of the BOR-60) in order to ensure the necessary sensitivity and accuracy of the system. During the reactor operation, calculating the reactivity balance allowed certain real anomalous effects to be recorded (Fig. 3). The results obtained indicate the high efficiency and sensitivity of the c.r.b. system under conditions characteristic of fast power reactors, which warrant the recommendation that such systems be developed for those reactors; in the first stage of operation, the system described here, with appropriate algorithms, could be taken as a basis.

LITERATURE CITED

1. M. Larson and I. Sackett, Nucl. Tech., 33, No. 2, 223 (1977).
2. G. Hammel and D. Okrent, Reactivity Coefficients in Large Fast-Neutron Power Reactors [Russian translation], Atomizdat, Moscow (1975).
3. V. A. Afanas'ev et al., Preprint NIIAR P-4 (338), Dimitrovgrad (1978).
4. V. A. Afanas'ev et al., At. Energ., 41, No. 4, 270 (1976).
5. B. V. Kebadze et al., At. Energ., 43, No. 1, 36 (1977).

SECONDARY SWELLING OF GRAPHITE

Yu. S. Virgil'ev, I. P. Kalyagina, E. I. Kurolenkin, and V. G. Makarchenko

UDC 621.039.532.21

As is well known, irradiation at T > 450°C with a fluence $>10^{22}$ neutrons/cm^2 causes secondary growth or swelling of graphite with the formation of vacancy pores and microcracks [1].

Since compensation for the changes in the volume by existing pores is rapidly exhausted because of the high rate of crystallite growth, it can be assumed that irradiation at room temperature also results in secondary swelling of graphite, but a substantially lower fluence. As verification, we irradiated two series of specimens of GMZ graphite to a fluence of $(2\text{-}3)\cdot10^{20}$ and $8\cdot10^{21}$ neutrons/cm^2 and then measured their properties (Table 1).

It is seen from Table 1 that the increment in the lattice constant c did not exceed 1% in the case of specimens of the first series but reached 8-10% in highly irradiated specimens of the second series, which is in

TABLE 1. Properties of Specimens before and after Irradiation at 130-170°C

Characteristic	Before irradiation	After irradiation	
		$F=(2\text{-}3)\cdot10^{20}$ neutrons/cm^2	$F=8\cdot10^{21}$ neutrons/cm^2
Rel. change in length, %	0	0,5/0,5 *	1,2/4,0
Electrical resistivity, $\Omega\cdot mm^2/m$ ($10^{-6}\ \Omega\cdot m$)	12/14	33/44	32/39
Modulus of elasticity, 10^5 kg/cm^2 ($0.98\cdot10^{10}$ P)	0,7/0,6	2,1/1,6	2,5/1,6
Lattice contant c, Å (10^{-10} m)	6,742	6,808	7,760

*Numerator, data for specimens cut parallel to extrusion axis; denominator, data for specimens cut perpendicular to that axis.

Translated from Atomnaya Énergiya, Vol. 48, No. 2, pp. 102-103, February, 1980. Original article submitted November 20, 1978.

0038-531X/80/4802-0116$07.50

TABLE 2. Change in Length of Specimens as Result of Additional Irradiation at 70°C, %

Series	Direction of cut of specimens relative to extrusion axis	After prior irradiation at 130-170°C, %	After additional irradiation* with fluence of 10^{20} neutrons/cm^2			
			5,0	8,5	11,5	18,5
First	∥	0,5	1,70	1,95	2,00	2,60
	⊥	0,5	3,30	4,15	3,80	5,90
Second	∥	1,2	0,20	0,35	0,90	—
	⊥	4,0	0,70	1,20	2,80	—

*Averaged values for several specimens. The size of the preirradiated specimens was taken for the initial value.

accordance with earlier data [2]. The increase in the length of the low-irradiated specimens of the first series did not reach the "saturation" stage. The increment in length of the parallel specimens of the second series, cut parallel to the extrusion axis, somewhat exceeded values corresponding to the saturation stage for this grade of graphite at the temperature indicated. Notwithstanding the large increment in the length of the specimens cut perpendicular to the extrusion axis, the values of the electrical resistivity and the modulus of elasticity of these specimens, as well as those of the specimens of the first series, correspond to the saturation stage characteristic of the given graphite.

To amplify the effect observed, the irradiation of the specimens studied was continued at a lower temperature of 70°C with a fluence of up to $18.5 \cdot 10^{20}$ neutrons/cm^2. In the course of long irradiation the length of low-irradiated specimens of the first series increased at a rate characteristic of GMZ graphite not subjected to previous irradiation. The saturation stage occurred when a fluence of $\sim 8.5 \cdot 10^{20}$ neutrons/cm^2 was reached, and the corresponding increment in length proved to be higher than in specimens not subjected to prior irradiation. With an additional fluence above $11.5 \cdot 10^{20}$ neutrons/cm^2 specimens were found to experience secondary swelling (Table 2) which was accompanied by a sharp increase in the electrical resistivity to $115 \cdot 10^{-6}$ Ω·m and to $140 \cdot 10^{-6}$ Ω·m, respectively, in specimens cut parallel and perpendicular to the extrusion axis.

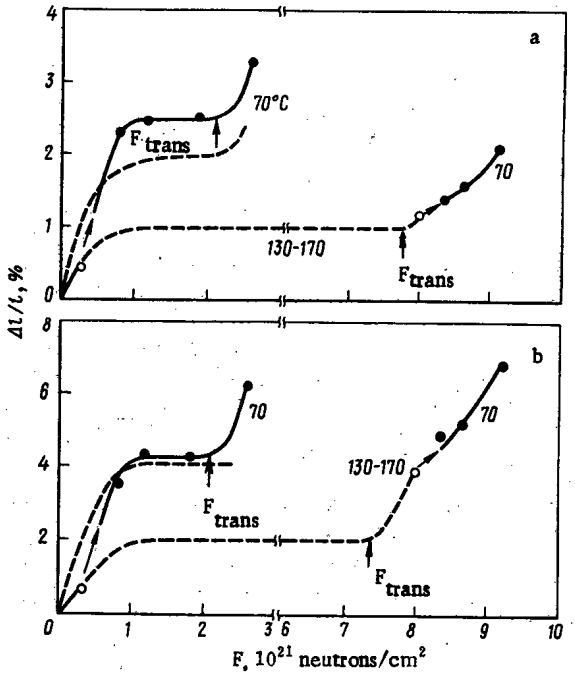

Fig. 1. Fluence-dependence of change in length of specimens cut parallel (a) and perpendicular (b) to extrusion axis: ○) initial irradiation at 130-170°C; ●) subsequent irradiation at 70°C; — — —) data for GMZ graphite at temperatures indicated, obtained earlier [2].

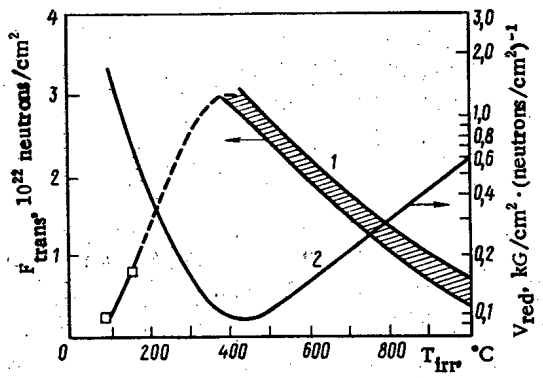

Fig. 2. Fluence F_{trans}, corresponding to onset of secondary swelling of graphite (1) and reduced velocity of steady-state radiation creep (2) [3] vs irradiation temperature: shaded strip constructed according to data of [3]; □ corresponds to F_{trans} of Fig. 1.

The specimens were covered with a dense network of macrocracks. When x-ray analyses were made the diffraction maxima proved to be completely diffused. The general increment in the length after prior and additional irradiation reached 3, 6 (Fig. 1a) and 6.5% (Fig. 2b). According to Table 2, with additional irradiation the highly irradiated specimens (second series) grow at a substantially slower rate than do the low-irradiation specimens (first series). It is seen from Fig. 1 that the value of the fluence (F_{trans}) corresponding to the onset of intensive swelling (given all the arbitrariness of this characteristic) increases as the irradiation temperature rises.

Using data on high-temperature irradiation [3] and the data obtained in the present paper, we can construct the temperature dependence of F_{trans} (Fig. 2). The curve proves to be the asymbatic curve of the temperature dependence for the reduced rate v_{red} of steady-state radiation creep [3]. Eliminating temperature in Fig. 2, we have

$$F_{trans} = Av_{red}^{-0,7}, \tag{1}$$

and when the well-known relation [4]

$$v_{red} = B(\dot{S}_c - \dot{S}_a)^{0,7},$$

is taken into account we have

$$F_{trans} = C(\dot{S}_c - \dot{S}_a)^{-0,5}, \tag{2}$$

where A, B, and C are constants; $\dot{S}_c$ and $\dot{S}_a$, growth rates of crystallographic regions along c and *a* axes,

The difference $\dot{S}_c - \dot{S}_a$ between the growth rates decreases exponentially with a rise in temperature and, therefore, mechanical interaction between growing crystallographic regions will begin at all higher values of the fluence. At a temperature above 300-350°C, however, this difference practically becomes constant and in view of this F_{trans} should not increase. To explain the descending branch of the curve f in Fig. 2 let us note that above 400°C radiation-induced vacancies experience considerable mobility. Separation of vacancies from the graphite matrix which they supersaturated and their subsequent coagulation into vacancy micropores with the latter joining up into microcracks form the basis of the mechanism proposed in [1] for secondary swelling of graphite under high-temperature irradiation. The rates of the interrelated processes mentioned above increase with the irradiation temperature (in any case, up to 1000-1100°C), after which the value of F_{trans} diminishes.

LITERATURE CITED

1. E. I. Kurolenkin and Yu. S. Virgil'ev, in: Reactor Materials Science. Proc. Conf. on Reactor Materials Science [in Russian], Vol. 2, TsNIIatominform, Moscow (1978), p. 135.
2. Yu. S. Virgil'ev, I. P. Kalyagina, and V. G. Makarchenko, At. Energ., 46, No. 3, 180 (1979).

3. V. V. Goncharov et al., Effects of Irradiation on Nuclear Reactor Graphite [in Russian], Atomizdat, Moscow (1978).
4. Yu. S. Virgil'ev et al., in: Graphite-Based Structural Materials [in Russian], No. 7, Metallurgiya, Moscow (1972), p. 73.

"POLESKOP" PHYSICAL-FIELD INDICATOR

G. N. Aleksakov and G. P. Terekhov

UDC 681.518:53.083.94

Experience from the operation of RBMK uranium – graphite channel-type reactors has shown that with the same structural dimensions the power of such reactors can be pushed up considerably without risk of a transition to the region of critical thermal loads, this being the case because of operational optimization of the energy distribution [1]. One way of solving this problem is that of improving devices for displaying the energy distribution or neutron distribution. On the one hand, these devices should provide the operator with a fuller overall picture of the distribution, while on the other hand they should simplify the choice of concrete local control actions.

The RBMK is equipped with a well-developed system of pickups for in-core monitoring. However, the electrical signal from each of these pickups gives information about the value of the monitored parameter at the site of the pickup and, therefore, for a more general picture of the energy distribution the information system should perform two functions: reproduce (reconstruct) the continuous energy distribution from sample-signals from a finite number of pickups and display the resulting energy distribution in a convenient form for perception by the operator. These operations should be carried out quite rapidly so that the operator would have time to make a decision as to the choice of corrective actions and to execute them.

The problem of reconstructing a sufficiently smooth energy distribution $g(x; y)$, prescribed by samples of values of the monitored parameter at points $g(x, y)_i$, is solved in the general case [2] by approximating the continuous function $g(x, y)$ by a series:

$$g(x;\ y) \approx g^a(x;\ y) = \sum_{i=1}^{l} g(x;\ y)_i\, \alpha_i(x;\ y), \tag{1}$$

where $\alpha_i(x; y)$ are filtration functions reflecting the interrelationship between the energy distribution at the point $(x; y)$ and the sample $g(x; y)_i$ at each point where a pickup is located. If the energy-distribution pickups are arrayed at the nodes of a lattice with square cells and are in identical conditions, then the filtration functions are the same and are determined by the position of the point $(x; y)$ relative to the point $(x; y)_i$ at which the pickup is located:

$$\alpha_i(x;\ y) = \alpha[(x;\ y) - (x;\ y)_i]. \tag{2}$$

In this case, series (1) becomes

$$g^a(x;\ y) = \sum_{i=1}^{l} g(x;\ y)_i\, \alpha[(x;\ y) - (x;\ y)_i]. \tag{3}$$

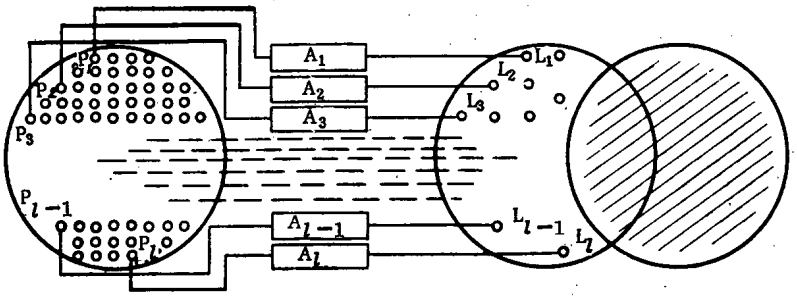

Fig. 1. Realization of method of reconstruction of two-dimensional physical fields: P) pickup; L) lamp; shaded area) screen.

Translated from Atomnaya Énergiya, Vol. 48, No. 2, pp. 103-105, February, 1980. Original article submitted January 18, 1979.

0038-531X/80/4802-0119$07.50

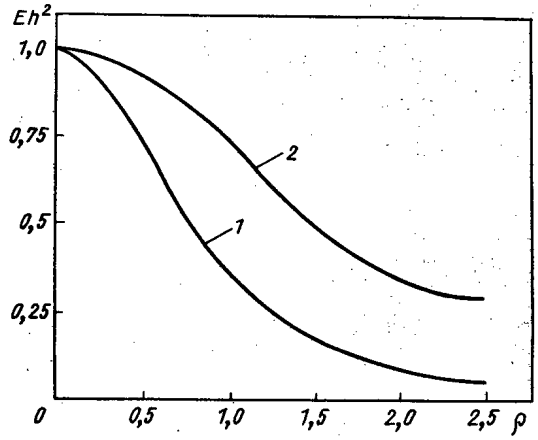

Fig. 2. Filtration function $E(\rho; h)h^2$ for: 1) h = 1; 2) h = 2.

The energy distribution according to Eqs. (1) or (3) can be reconstructed by both digital and analog computers and the results are shown on a visual display or conveyed to the operator in the form of a sequence of tables of numerical values of the energy distribution.

Optical simulation allows the operations of reconstructing the energy distribution from samples and displaying the result to be combined in the form of a light field whose illumination distribution corresponds to the distribution of the values of the monitored physical parameter. For this purpose signals from the pickup (Fig. 1) are transmitted through matching amplifiers (A) to control the brightness of light sources arranged in a plane in the same manner as the pickups in the plane of the reactor. A field of illumination is obtained on a screen set up parallel to the plane of the light sources. If the dependence of the illumination produced by each light source $g(x; y)_i$ corresponds to a filtration function $\alpha_i(x; y)$, then the illumination of each point of the screen is determined by Eq. (1). Thus, the illumination of the screen images the distribution of the monitored parameter.

Optical means can be used to obtain any form of filtration functions $\alpha_i(x; y)$. As in the case of other methods of reconstructing the distribution, the solution of the problem is simplified for a regular grid of pickups which are in identical conditions. In this case, in accordance with Eq. (3) the form of the filtration functions is the same for all samples. Constructionally, it is simplest to make the characteristic of the light source approximate a point source for which the dependence of the illumination E on the distance h to the screen and the radius vector ρ from the projection of the source on the screen to the point (x; y) on the screen is given by

$$E(\rho;\ h)=I\frac{h}{(h^2+\rho^2)^{3/2}}, \tag{4}$$

where I is the intensity of the light source.

Equation (2) can be rewritten as

$$E(\rho;\ h)=\frac{I}{h^2}\frac{1}{\left(1+\frac{\rho^2}{h^2}\right)^{3/2}}=\frac{I}{h^2}\frac{1}{(1+r^2)^{3/2}}, \tag{5}$$

where $r = \rho/h$ is the relative distance of the point (x; y) from the projection of the source. The section of this function by the plane passing through the projection of the source is shown in Fig. 2. By varying the distance h we can regular the "sharpness of filtration" of the function $E(\rho, h)$ for h = par. This choice makes it possible to minimize the error of the reconstruction of the distribution

$$R(x;\ y)=g(x;\ y)-g^{\alpha}(x;\ y) \tag{6}$$

for any reasonable functions g(x; y). Numerically, the magnitude of the error can be estimated with

$$\Delta_{qu}=\frac{\int\limits_{x;\ y\in S} R^2(x;\ y)\,dx\,dy}{\int\limits_{x;\ y\in S} g^2(x;\ y)\,dx\,dy} \tag{7}$$

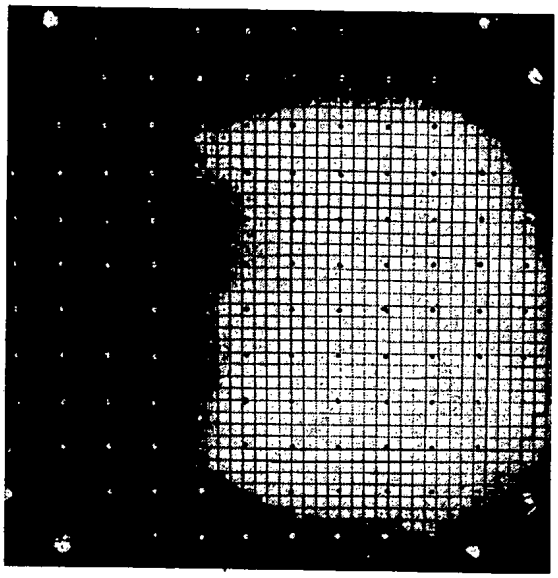

Fig. 3. Screen with grid of markers for one distribution.

or

$$\Delta_{\text{mod}} = \frac{\int\limits_{x;\ y \in S} |R(x;\ y)|\, dx\, dy}{\int\limits_{x;\ y \in S} g(x;\ y)\, dx\, dy}, \tag{8}$$

where the integrals are taken over the entire monitored region S.

Calculations and experiments show that minimization of the error of reconstruction is attained for m = $a/h = 0.7$ (a is the pitch of the grid of point sources of light). With such a relative pitch the filtration functions of the point sources are "sufficiently smooth" for the equalized energy distribution not to have any visible nonuniformities in the illumination while at the same time being sharp enough for reliably recording, e.g., dips in the distribution corresponding to the disconnection of one of the lamps.

The human eye makes a good distinction between the illumination of neighboring segments with a clearly expressed boundary. The sensitivity threshold under these conditions is 0.2-0.5%, depending on the level of illumination. To utilize this feature of vision, a grid of markers is combined with the screen; the markers have the same brightness which can be regulated simultaneously within the limits 0-100% relative to the maximum brightness of the screen. The markers are placed at points corresponding to the positions of the control rods (Fig. 3).

The brightness of the markers characterizes the monitored parameter. If the value of the parameter is below the nominal level, the markers are bright against a dark background and if the value of the parameter is higher than the nominal, they are dark against a bright background, whereas in the zone with nominal distribution the markers disappear. The algorithm for the actions of the operator in forming the specified energy distribution consists in moving the control rods in such a way as to cause all markers to disappear.

The system of markers can be used to measure the monitored parameter at a concrete point in the reactor. In this case, the brightness of the markers is adjusted until the marker at the given point disappears. The monitored parameter is measured by the value of the electrical signal controlling the marker brightness. The sensitivity of this method of measurement is no less than 0.5% and the accuracy is determined by the errors of reconstruction of the distribution, measurement of the electrical signal, and calibration of the electrical signal in units of the monitored parameter.

The Poleskop physical-field indicator can find application in physical experiments and in systems of manual and semiautomatic control of various objects with distributed parameters. The formulation of this problem was the result of discussions on the problems of control of the energy distribution in reactors with a number of workers of Scientific-Research and Design Institute of Power Engineering (NIKIÉT). The attention and support of I. Ya. Emel'yanov were conducive to the development of the work. The authors are indebted also to Ya. V. Shevelev for his support and invaluable comments.

LITERATURE CITED

1. N. A. Dollezhal', At. Energ., 44, No. 5, 203 (1978).
2. J. W. Goodman, Introduction to Fourier Optics, McGraw-Hill (1968).

RADIATION STABILITY OF PHOSPHORUS-CONTAINING CATIONITES

S. B. Makarova, A. V. Smirnov,
A. S. Telegin, N. V. Bychkov,
and B. S. Roginskaya

UDC 541.15

The radiation stability of phosphorus-containing (phosphonic) cationites is inadequate for their use in sorption of radioactive elements [1]. In the present paper, phosphonic (KRF) and methylene phosphonic (KRMF) cationites based on copolymers of styrene with 2 and 5% divinyl benzene are used as an example to study the effect of the production technology and structure of phosphorus-containing cationites and their radiation stability.

KRF cationites were obtained by phosphorylation of copolymers of phosphorus trichloride in the presence of anhydrous aluminum chloride with subsequent hydrolysis and oxidation with 25% nitric acid or 20% hydrogen peroxide [2] while KRMF was obtained by phosphorylation of chloromethylate copolymers with phosphorus trichloride with subsequent hydrolysis (Fig. 1).

Specimens of cationites were irradiated under a layer of water in a ^{60}Co source in the range 200-1200 Mrad. The irradiated cationite was washed to remove destruction products with no less than 5 volumes of water and the volume of the cationite was recorded before and after irradiation. After conditioning in the $Na^+ - H^+$ cycle, the exchange volume was determined with respect to 0.1 N NaOH. Potentiometric titration of the cationites in the H-form was carried out by the method of separate weighed portions, while the pH of the equilibrium solutions was measured on a pH-262 instrument (weighed portion of 0.3 g, total volume of 0.1 N NaOH and NaCl was 50 ml). The IR spectra were recorded with a double-beam UR-20 spectrometer. Specimens were prepared by pressing 2 mg of cationite with 150 mg of anhydrous potassium bromide. Thermogravimetric curves were obtained on a deviatograph of the OD-101 deviatograph in a nitrogen atmosphere at a heating rate of 6 deg/min.

It was found that the cationites KRF-2p and KRF-5p have the lowest radiation stability; nitric acid had been used in the oxidation stage in obtaining these cationites. At a dose of 500 Mrad the cationite KRF-2p completely breaks down, while KRF-5p does so at a dose of 1200 Mrad. A substantially higher stability is displayed by KRMF cationites and by cationite KRF-5p which was obtained by using hydrogen peroxide as an oxidant (see Table 1).

The low radiation stability of KRF cationites is evidently due to their treatment with nitric acid: When the acid is replaced with a softer oxidant the stability of KRF phosphonic cationites increases considerably, although it still remains lower than that of KRMF. The enhanced stability of the latter is probably due to the

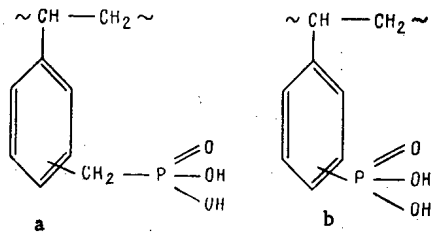

Fig. 1. Structure of elementary monomer unit of: a) KRMF; b) KRF cationites.

Translated from Atomnaya Énergiya, Vol. 48, No. 2, pp. 105-106, February, 1980. Original article submitted January 24, 1979.

0038-531X/80/4802-0122 $07.50

TABLE 1. Variation of Physicochemical Parameters of Cationites in H^+-Form as Functions of Irradiation Dose

Cationite	Irradiation dose, Mrad	Vol. of specimen, ml	Capacity, mg-equ/ml of initial	Phosphorus content, %	Loss of capacity, % of initial
KRMF-2p	0	20,0	3,1	9,5	—
	200	19,0	3,08	—	0,6
	500	18,0	2,84	—	8,4
	800	17,5	2,76	—	11,0
	1200	17,3	2,72	—	12,3
KRMF-5p	0	20,0	3,18	8,5	—
	800	17,9	2,80	—	12,0
	1200	17,8	2,70	—	15,1
KRF-5p	0	15,0	4,26	12,7	—
	800	13,3	3,57	—	16,2
	1200	12,7	3,03	—	28,9

fact that there is no oxidation treatment in their technology since because of their structure (methylene bridge between aromatic ring and phosphonic group) they should have a lower radiation stability [3].

In the IR spectra of KRMF cationites the most characteristic absorption bands (in the region of 1205 and 1020 cm^{-1}) are conserved without change and no new bands are observed. The curves from potentiometric titration of the original and irradiated cationites are identical ($pK_{a_1} = 3.24$, $pK_{a_2} = 8.07$). The thermogravimetric data for KRMF cationites irradiated with doses of 500 and 1200 Mrad coincide up to 420°C. At 500°C the loss of mass by a cationite irradiated with a dose of 1200 Mrad is 10% higher than at 500 Mrad, which is indicative of a great breakup of the skeleton at high irradiation doses.

LITERATURE CITED

1. E. V. Egorov et al., in: Ion Exchange and Chromatography [in Russian], Part 2, Voronezh State Univ. (1971), p. 49.
2. S. B. Makarova et al., Byull. Izobret., No. 45, 92 (1977).
3. V. G. Plotnikov, Opt. Spektrosk., No. 4, 593 (1969).

ANALYSIS OF THE COMPOSITION OF A MIXTURE OF ^{249}Bk + ^{249}Cf ON THE BASIS OF X RAYS

G. V. Buklanov and Yu. P. Kharitonov

UDC 543.422.8.002.5

In studies on the synthesis of transfermium elements and the investigation of their properties [1] ^{249}Bk and ^{249}Cf are often used as targets for irradiation with heavy ions; ^{249}Bk is a relatively short-lived β emitter, and the daughter product ^{249}Cf accumulates rapidly in it. When these nuclides are separated and purified and the targets are prepared, the monitoring of the absolute and relative concentrations is complicated by the fact that ^{249}Cf has a specific α activity $1.6 \cdot 10^2$ times as high and a γ activity $8 \cdot 10^3$ times as high as ^{249}Bk. Therefore, an admixture of as little as 10-15% Cf in the Bk makes it practically impossible to determine the berkelium from the α radiation, and the situation is even worse for the γ radiation.

The principal methods for the determination of ^{249}Bk are the measurement of its β activity [2] and that of the accumulation of the α activity of the daughter product Cf in a Bk specimen [3]. Both methods require the preparation of thin specimens for measurements. In addition, the measurements by the second method take a long time (3-5 days).

However, during the α and β decay of transuranium elements at low excited levels (30-50 keV) of daughter nuclei through the conversion of γ radiation there usually arises a fairly intensive characteristic L-type

Translated from Atomnaya Énergiya, Vol. 48, No. 2, pp. 106-108, February, 1980. Original article submitted January 30, 1979.

0038-531X/80/4802-0123 $07.50

x radiation. The energy of the L series of elements with Z = 95-100 is 15-25 keV; elements with neighboring values of Z are separated by a "gap" of 340-360 eV with respect to the L_α lines and 500-620 eV with respect to the L_β lines. Under these conditions the use of a semiconductor spectrometer may be very effective. It is known that x-ray spectrometry has been used for identifying extremely small quantities of transuranium elements by α-L_X coincidence [4].

Using a silicon spectrometer with a resolution of ~170 eV (for E = 5.9 keV) and ~300 eV (for E = 26.4 keV) [5], Zubareva et al. studied the possibility of using x-ray spectrometry to analyze a mixture of ^{249}Bk + ^{249}Cf.

Preparation of a ^{249}Bk Reference Source. For quantitative measurements a reference source of ^{249}Bk was preared; the ^{249}Bk and the accumulated daughter product ^{249}Cf were separated by the method of extraction chromatography in a D2ÉGFK system (polyethylene – nitric acid with prior oxidation of the berkelum to the tetravalent state with potassium bromate) [6]. In one extraction-chromatographic cycle the Cf content of the Bk fraction was reduced below 0.1%. The Bk yield by this method was usually ~97%. After carefully removing the Cf and ballast impurities from the Bk, a quantity of nitric acid solution of Bk was applied to a glass backing and dried under an infrared lamp. The quality of the resulting source was good enough to obtain [with an Si(Au) detector) ^{249}Bk and ^{249}Cf α spectra with a resolution of ~25 keV and with a number of counts in the low-energy "tail" that amounted to no more than 1% of the principal peak.

To determine the initial quantity of ^{249}Bk in the reference source, for 7 days after its preparation we made periodic measurements (14 times) of the absolute α activity of the ^{249}Bk and the increasing α activity of the ^{249}Cf, as well as of the activity ratio $R = A_{Cf}/A_{Bk}$. Within the limits of the measurement time $\lambda_{Bk}t \leqslant 0.015$, and therefore we can write with sufficient accuracy:

$$A_{Cf}(t) = N_{Bk}(0)\,\lambda_{Bk}\lambda_{Cf}t + N_{Cf}(0)\,\lambda_{Cf}; \quad (1)$$

$$R(t) = \frac{\lambda_{Cf}}{\alpha_{Bk}}t + \frac{N_{Cf}(0)}{N_{Bk}(0)}\,\frac{\lambda_{Cf}}{\lambda_{Bk}\alpha_{Bk}}, \quad (2)$$

where t is the time elapsed after the purification of the Bk; $N_{Bk}(0)$, initial number of Bk nuclei; $N_{Cf}(0)$, amount of Cf remaining in the Bk after purification; α_{Bk}, fraction of ^{249}Bk nuclei decaying by α radiation; λ_{Bk}, decay constant of ^{249}Bk.

The values of the parameter α_{Bk} given in [7] differ by more than 50%, and therefore we determined it independently in our measurements.

From the experimental values of A_{Cf} and R, using the method of least squares, we found the best values of the slopes of the lines (1) and (2), and from these we determined the initial amount of Bk in the source: $m_{Bk} = 1.05 \pm 0.06$ μg and α_{Bk} ^{249}Bk $= (1.48 \pm 0.10)\cdot 10^{-5}$, which practically coincides with the result $\alpha_{Bk} = (1.45 \pm 0.08)\cdot 10^{-5}$ obtained by Milsted et al. [3]. From the measured absolute α activity of ^{249}Bk and the value obtained for α_{Bk}, we again obtained the initial amount of Bk: $m_{Bk} = 1.02 \pm 0.08$ μg. In the calculation it was assumed that the half-lives of ^{249}Bk and ^{249}Cf are 314 days [3] and 366 years [8], respectively.

X-Ray Yield in the Decay of ^{249}Bk and ^{249}Cf. In the decay of ^{249}Bk and ^{249}Cf, x rays may be emitted by three elements: Am L_X as a result of the α decay of Bk, Cm L_X from the α decay of Cf, and Cf L_X from the β decay of ^{249}Bk if it goes to excited levels. We may expect the yield of the Am L_X series to be small in comparison with the Cm L_X because the α activity of ^{249}Bk is only 1/160 that of ^{249}Cf. Concerning the β decay of ^{249}Bk we know only that in 99% of the cases it goes to the ground state of ^{249}Cf and the fraction of $\beta + \gamma$ coincides < 1% [7]. However, direct measurement (without coincidences) of the x-ray spectrum of the Bk + Cf mixture showed that in addition to L series of Cm it also contains an L series of Cf with a comparable yield (see Fig. 1a).

Figure 1 shows the spectrum of the reference source 128 days after it was prepared (a). The amounts of Bk and Cf in the specimen at this time were 0.78 and 0.25 μg, respectively. As was to be expected, the yield of the Am L series is insufficient for observation.

The presence of the L series of Cf in the spectrum cannot be explained by self-excitation of the Cf as a result of α activity: in a specimen of the Cf fraction from which the Bk has been removed, we do not observe any Cf line (see Fig. 1b). Moreover, in the case of self-excitation by both α and β particles, the spectrum of the reference source should, in addition to the L series of Cf, also contain the L series of Bk, of which there is 3 times as much in the specimen as there is of Cf. We cannot exclude the possibility that the effects of self-excitation may appear when we work with amounts $\gg 1$ μg, since when the amount of a substance is increased by a factor of n, the fluorescence yield due to self-excitation increases by a factor of n^2 (the power of

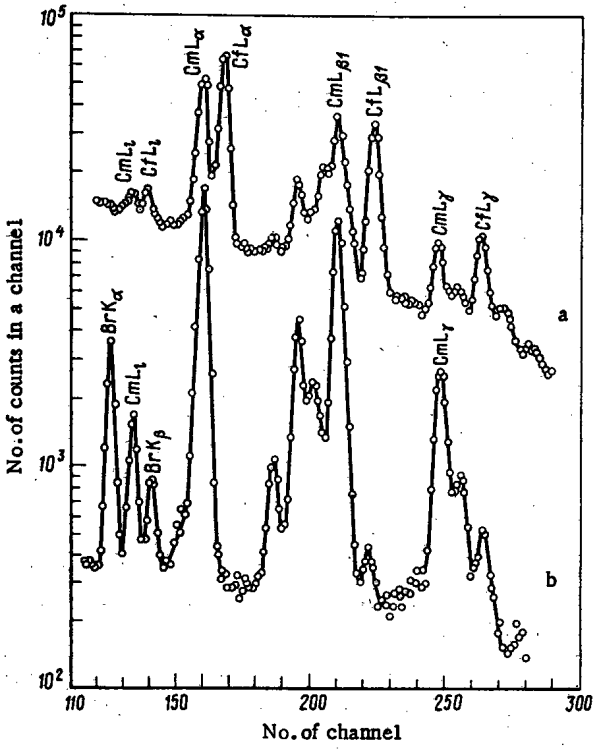

Fig. 1. a) X-ray spectra of reference source containing 0.78 μg of ^{249}Bk and 0.25 μg of ^{249}Cf at the time of measurement; b) the californium fraction after the separation of berkelium.

the exciting source becomes n times as great, and so does the number of excited nuclei). This possibility of the excitation of fluorescence in the source is indicated by the presence in the spectrum of the Cf fraction (see Fig. 1b) of the K series of bromine, which was present in the oxidizer when the Bk and Cf were separated. When the Bk content of the specimen was <1 μg (the measurements were made with specimens weighing 0.3-1.0 μg), a proportionality is observed between the amount of ^{249}Bk and the L_X radiation of Cf.

Thus, we can conclude that the L series of Cf in the spectrum of the mixture of ^{249}Bk + ^{249}Cf appears as a result of β decay of ^{249}Bk, and in this case the Cf L lines can be used for relative and absolute measurements of the ^{249}Bk.

From the spectra in Fig. 1 it can be seen that the Cm L_α, Cf L_α, and Cf L_β lines are most suitable for analysis. The yields of these lines per disintegration, on the basis of a number of specimens with known Bk and Cf content, were for Bk, $\omega(\text{Cf } L_\alpha) = (5.5 \pm 1.10) \cdot 10^{-5}$ (β disintegration)$^{-1}$; $\omega(\text{Cf } L_\beta) = (2.7 \pm 0.7) \cdot 10^{-5}$ (β disintegration)$^{-1}$; for Cf, $\omega(\text{Cm } L_\alpha) = (5.3 \pm 1.1) \cdot 10^{-2}$ (β disintegration)$^{-1}$.

The errors in the given values of ω resulted from the large error in the determination of the absolute efficiency of the spectrometer because there were no well-calibrated sources for energies of 10-30 keV. The relative intensity of the count of the Cf L_α and Cm L_α lines in the spectrum of the reference specimen is independent of the efficiency of the spectrometer and of the initial amount of Bk:

$$\frac{N(\text{Cf } L_\alpha)}{N(\text{Cm } L_\alpha)} = \frac{\exp(-\lambda_{Bk} t)}{1-\exp(-\lambda_{Bk} t)} \frac{\lambda_{Bk}}{\lambda_{Cf}} \frac{\omega(\text{Cf } L_\alpha)}{\omega(\text{Cm } L_\alpha)}. \quad (3)$$

Therefore, the ratio $\omega(\text{Cf } L_\alpha)/\omega(\text{Cm } L_\alpha)$ can be determined with better accuracy. According to our measurements, it is $(1.03 \pm 0.05) \cdot 10^{-3}$. This means that for equal amounts of ^{249}Bk and ^{249}Cf in the mixture the ratio of the intensities of the corresponding L_α lines is 0.44 ± 0.02.

Limits of Detection of an Admixture of ^{249}Bk in ^{249}Cf. After experimentally determining the counting rate of the analytic line of Bk, $I_{e.f}(\text{Cf } L_\alpha) = 2.1 \cdot 10^3$ counts/min · μg Bk, and the background counting rate in the region of this line in the spectrum of the Cf fraction, $I_b = 2.2 \cdot 10^2$ counts/min · μg Cf, we can estimate the limit of detection of ^{249}Bk and ^{249}Cf. To do this, we make use of the generally accepted criterion $N_{e.f} = 3\sqrt{N_b}$. After some simple transformations, we obtain

$$\left(\frac{m_{Bk}}{m_{Cf}}\right)_{min}=\frac{3\sqrt{I_{ef}}}{I_b\ (Cf\ L_\alpha)\sqrt{m_{Cf}t}}\approx\frac{2\cdot10^{-2}}{\sqrt{m_{Cf}t}},$$

where m_{Cf} is the amount of ^{249}Cf, in which the Bk is determined, in micrograms; t is the measurement time, in min. Thus, for a measurement time of ~5 min, the detection threshold of ^{249}Bk in 1 μg of ^{249}Cf is ~0.01 μg. It should be emphasized that the estimate obtained is valid for specific measurement conditions: the resolution of the spectrometer for the L_α lines of Cm and Cf is ~0.01 μg. It should be emphasized that the estimate obtained is valid for specific measurement conditions: the resolution of the spectrometer for the L_α lines of Cm and Cf is ~300 eV, and the absolute efficiency is ~1%.

Conclusion. The results of the study enable us to conclude the following: the β decay of ^{249}Bk is accompanied by an L series of x rays from the daughter product Cf. The yield of this radiation is low: $\omega(L_\alpha + L_\beta + L_\gamma) \approx 10^{-4}$ (β disintegration)$^{-1}$, but because of the high specific β activity of ^{249}Bk, 1 μg of this isotope emits $\sim 3.7\cdot10^5$ x-ray quanta per minute. This enables us to detect a fairly small amount of Bk (~0.01 μg) on the basis of x rays in a period of 5-10 min. The rapid accumulation of the daughter product ^{249}Cf does not interfere with the determination of the ^{249}Bk on the basis of x rays. Even when the mixture contains equal numbers of Bk and Cf nuclei, the ratio of the L_α lines corresponding to them is 0.46. Therefore the composition of a mixture of ^{249}Bk + ^{249}Cf can be determined on the basis of x rays over broad ranges of variation of the relative concentrations of Bk + Cf, roughly from 0.03 to 80. It is important to note that for relative measurements it is not necessary to prepare special specimens, since x rays with energies of 15-20 keV are not strongly absorbed in the solution and in the walls of the chemical vessel.

The authors wish to express their gratitude to G. N. Frelov for formulating the problem; we are grateful to I. Zvare and V. N. Kosyakov for their guidance and for consultations on the chemical part of the work, and also to V. A. Druin and V. G. Subbotin for their valuable comments.

LITERATURE CITED

1. V. A. Druin et al., At. Energ., 43, No. 3, 55 (1977).
2. V. M. Glazov, R. I. Borisova, and A. I. Shafiev, NIIAR Preprint P-181, Dimitrovgrad (1973).
3. J. Milsted et al., J. Inorg. Nucl. Chem., 31, 1561 (1969).
4. C. Bemis et al., Phys. Rev. C, 16, No. 3, 1146 (1977).
5. A. M. Zubareva et al., JINR Preprint R13-10430, Dubna (1977).
6. G. M. Kozakova, V. N. Kosyakov, and E. A. Erin, Radiokhimiya, 17, No. 2, 311 (1975).
7. V. M. Gorbachev, Yu. S. Zamyatnin, and A. A. Lbov, Basic Characteristics of Isotopes of Heavy Elements. A Handbook [in Russian], Atomizdat, Moscow (1975).
8. V. G. Polyukhov et al., Radiokhimiya, 19, No. 4, 460 (1977).

DETERMINATION OF EQUILIBRIUM PARAMETERS OF SODIUM – OXYGEN – HYDROGEN SYSTEM

Yu. V. Privalov

UDC 621.039.534

The development of effective method for removing impurities and monitoring them and an understanding of corrosion processes in sodium coolant necessitate the study of equilibrium Na – O – H systems. Notwithstanding the large number of experimental investigations, no computational method has hitherto been presented for determining the equilibrium parameters of that system.

Analysis of [1-4] shows that the following phases exist in the Na – O – H system: liquid molecular solution L_1 based on Na with dissolved NaOH, NaH, and Na_2O components, liquid molecular solution L_2 based on NaOH with dissolved NaH and Na_2O, solid sediments of NaH and Na_2O, solid solutions αL_1 and βL_2 based on the α and β modifications of NaOH, and gaseous hydrogen H_2.

The following reversible reactions occur among the five components of the system:

$$2Na + NaOH \rightleftarrows NaH + Na_2O; \quad (1)$$

$$Na + NaOH \rightleftarrows 1/2H_2 + Na_2O; \quad (2)$$

$$Na + 1/2H_2 \rightleftarrows NaH; \quad (3)$$

$$NaOH + NaH \rightleftarrows H_2 + Na_2O, \quad (4)$$

whose equilibrium constants K_1^{ol}, K_2^{ol}, K_{f3}^0, and K_4^{ol}, respectively, are related by $K_2^{ol} = K_1^{ol}/K_{f3}^0$ and $K_4^{ol} = K_1^{ol}/(K_{f3}^0)^2$. The numerical values of the constants K^{ol} and K_{f3}^0 calculated from new data on the properties of the substances, in selecting which we were guided mainly by the recommendations of [5], were approximated in the temperature range from 371 to 840°K by the functions

$$\lg K_1^l = 2.687 + 2805/T - 2.389 \lg T;$$

$$\lg K_{f3}^0 = -5.198 + 3120/T + 0.250 \lg T.$$

In our calculations of K_1^{ol}, for the standard state of NaOH at T ≤ 592°K we took the state of the supercooled liquid while for the other components we took the basic standard state. The melting points of Na, NaOH, and NaH are 371, 592, and 840°K, respectively.

In addition to the reaction constants, for equilibrium calculations it is necessary to know the activity of the components; in solutions L_1 and L_2 this activity was determined according to the modified Van Laar theory [6]. Assuming that components with similar molecular volumes have identical coordination numbers in the liquid state and that the coordination number for all the molecules of the components of the solution is determined by the solvent, on the basis of that theory we get the following approximate expressions for the activity of the components in the temperature interval from 371 to 840°K for the solution L_1:

$$a_1 = x_1 \exp\{[x_2(1-x_1)u_{12} + x_3(1-x_1)u_{13} + x_4(1-x_1)u_{14} - x_2x_3u_{23} - x_2x_4u_{24} - x_3x_4u_{34}]/RT\}; \quad (5)$$

$$a_2^l = x_2 \exp\{[\Delta_2 + x_1(1-x_2)u_{12} - x_1x_3u_{13} - x_1x_4u_{14} + x_3(1-x_2)u_{23} + x_4(1-x_2)u_{24} - x_3x_4u_{34}]/RT\}; \quad (6)$$

$$a_3 = x_3(K_{f3}^0/k) \exp\{[-x_1x_2u_{12} + x_1(1-x_3)u_{13} - u_{13} - x_1x_4u_{14} + x_2(1-x_3)u_{23} - x_2x_4u_{24} + x_4(1-x_3)u_{34}]/RT\}; \quad (7)$$

$$a_4 = (x_4/s_4) \exp\{[-x_1x_2u_{12} - x_1x_3u_{13} + x_1(1-x_4)u_{14} - x_2x_3u_{23} + x_2(1-x_4)u_{24} + x_3(1-x_4)u_{34}]/RT\} \quad (8)$$

and for the solution L_2:

$$a_2^l = y_2 \exp\{[y_3(1-y_2)u_{23} + y_4(1-y_2)u_{24} - y_3y_4u_{34}]/RT\}; \quad (9)$$

$$a_3 = y_3(K_{f3}^0/k) \exp\{[\Delta_3 - u_{13} + y_2(1-y_3)u_{23} - y_2y_4u_{24} + y_4(1-y_3)u_{34}]/RT\}; \quad (10)$$

$$a_4 = (y_4/s_4) \exp\{[\Delta_4 - y_2y_3u_{23} + y_2(1-y_4)u_{24} + y_3(1-y_4)u_{34}]/RT\}, \quad (11)$$

Translated from Atomnaya Énergiya, Vol. 48, No. 2, pp. 108-109, February, 1980. Original article submitted February 22, 1979; revision submitted July 9, 1979.

0038-531X/80/4802-0127$07.50

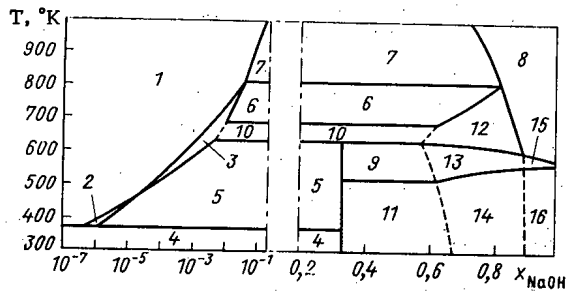

Fig. 1. Phase diagram of Na – NaOH at P = 1.2 bar: 1) L_1; 2) L_1 + NaH; 3) L_1 + Na_2O; 4) Na^T + NaH + Na_2O; 5) L_1 + Na_2O + NaH; 6) L_1 + L_2 + Na_2O; 7) L_1 + L_2; 8) L_2; 9) Na_2O + NaH + αL_2; 10) L_1 + Na_2O + L_2; 11) Na_2O + NaH + βL_2; 12) L_2 + Na_2O; 13) αL_2 + Na_2O; 14) βL_2 + Na_2O; 15) αL_2; 16) βL_2.

where the subscripts 1, 2, 3, 4 pertain to Na, NaOH, NaH, and Na_2O; x(y), molar fraction of the component in the solution $L_1(L_2)$; k, Sievertz constant for the solution of hydride in sodium, taken according to the equation $\log k = -2.183 - 175/T$, which the present author obtained by interpreting the experiments of [7, 8]; s_4, solubility of the oxides in the sodium, as taken from the equation $\log s_4 = 0.318 - 2372/T$ [9]; a_2^l, activity of the alkali, referred at $T \leq 592°K$ to the state of the supercooled liquid, and at $T \geq 592°K$, just as the activities a_1, a_2, and a_3 at any values of the temperature, to the basic standard state; and u and Δ, constants of interaction between components, J/mole. Equations (6), (10), and (11), unlike the Van Laar equations, contain an additional term Δ for components with a molecular volume different from that of the solvent. By solving the systems of equations relating the measured equilibrium parameters for a number of particular cases of the Na – O – H system [2-4, 10] and the activities (5)-(10), with allowance for reactions (1)-(4), we found the values of the constants in Eqs. (5)-(11): $u_{12} = 27840$; $\Delta_2 = 6660 - 14.492\ T$; $u_{13} = 26340$, $u_{14} = 0$; $u_{23} = -13{,}040$; $\Delta_3 = 22{,}110 + 38.165\ T$; $u_{24} = 17{,}190$; $\Delta_4 = -53{,}510 + 16.978\ T$; $u_{34} = 15{,}600$

Thus, all the necessary quantities for calculating the equilibrium parameters of the Na – O – H system (pressure, phase boundaries, concentration, activity, etc.) have been found by the ordinary methods of chemical thermodynamics. Comparison of the calculations and practically all published measurements of the equilibrium parameters [2-4, 11-13] showed that the discrepancies lie within the limits of the error of measurement. This allows the equilibrium concept discussed to be recommended for solving various problems of sodium technology. Thus, e.g., of great interest for sodium technology RBN as well as for the production of sodium, sodium hydride, and potassium by alkali exchange, etc., is the Na – NaOH phase diagram published in part earlier [3, 4] for high NaOH concentrations. A more complete diagram (Fig. 1) was constructed by incorporating the data of [4] on the temperature of phase transitions of the solutions αL_2 and βL_2.

LITERATURE CITED

1. Yu. V. Privalov, Preprint NIIAR P-16(310), Dimitrovgrad (1977).
2. Yu. V. Privalov, Preprint NIIAR P-6(300), Dimitrovgrad (1977).
3. É. M. Mitkevich and B. A. Shikhov, Zh. Neorg. Khim., 11, No. 3, 633 (1966).
4. B. A. Shikhov, Zh. Neorg. Khim., 12, No. 4, 545 (1967).
5. V. A. Likharev, Preprint FÉI-612, Obninsk (1975).
6. E. A. Melvin-Hughes, Physical Chemistry [Russian translation], IL, Moscow (1962), p. 675.
7. H. Katsuta and K. Furukawa, Nucl. Technol., 31, No. 2, 218 (1976).
8. D. Vissers et al., Nucl. Technol., 21, No. 3, 235 (1974).
9. K. Claxton, in: Proc. Int. Conf. on Liquid Metal Technology in Energy Production, Champion, Penn., May 3-6 (1976), Paper VB6.
10. K. Myles and F. Cafacco, J. Nucl. Mater., No. 67, 249 (1977).
11. H. Uhlmann et al., in: Problems of Technology and Corrosion in Sodium Coolant and Protective Gas [in Russian], Central Institute of Nuclear Research, Dresden, German Democratic Republic (1977), Vol. 1, p. 16.
12. F. A. Kozlov et al., in: Proc. Engineering Physics Institute [in Russian], Atomizdat, Moscow (1974), p. 120.
13. R. Pulham and P. Simm, in: Proc. Conf. Brit. Nucl. Energy Soc., Nottingham, April 4-6 (1973), p. 5.

NONSTEADY TEMPERATURE IN NUCLEAR-REACTOR CHANNEL

A. S. Trofimov and A. V. Sobolev

UDC 621.039.517.5

As is well known [1], in calculating the nonsteady temperature in elements of the active region with definite relations between the fuel-element and heat-carrier parameters, a quasisteady representation of the temperature distribution over the fuel-element cross section is possible. At the same time, it is necessary to take into account its distribution over the height. When the heat-carrier flow rate and the heat-transfer coefficient are variable over time, it is impossible to obtain an analytical solution of this problem. Consider one of the methods of approximate solution applied to a multilayer rod fuel element and a single-phase heat carrier [2]. In this case, the thermal processes may be described, in dimensionless form, by the following system of equations:

$$\begin{cases} \dfrac{\partial\theta}{\partial\tau}+G(\tau)\dfrac{\partial\theta}{\partial z}=ku+(1-G)\eta(z),\ 0\leqslant z=\dfrac{\chi}{H}\leqslant 1; \\ \dfrac{\partial u}{\partial\tau}+\xi(\tau)\dfrac{\partial\theta}{\partial\tau}+\delta(\tau)u=\Psi(\tau)\eta(z)q(\tau),\ 0\leqslant\tau; \\ \tau=0,\ u=\theta=0,\ z=0,\ 0=\theta_+(\tau), \end{cases} \tag{1}$$

where $u(\tau, z)$ and $\theta(\tau, z)$ are the relative temperatures of the fuel elements and heat carrier, respectively [2]; $G(\tau) = W(\tau)/W(0)$, relative heat-carrier flow rate; $\eta(z)$, relative energy-liberation distribution in the channel, normalized to the mean value; $q(\tau) = [N(\tau) - N(0)]/N(0)$, change in reactor power; k, ξ, δ, Ψ, factors [2] which, in the general case, depend on the time when the change in heat-transfer coefficient is taken into account.

For unchanging flow rate $G(\tau)$, or stepwise change in flow rate, Eq. (1) is solved analytically [2] for any perturbations of the power $q(\tau)$ or the input temperature $\theta_+(\tau)$. For arbitrary $G(\tau)$, only an approximate solution may be obtained.

Integrating the second relation in Eq. (1) gives the result

$$\frac{\partial\theta}{\partial\tau}+G\frac{\partial\theta}{\partial z}=\eta(z)\int_0^\tau\delta(\tau')q(\tau')\exp\left[-\int_{\tau'}^{\tau}\delta(\tau'')\,d\tau''\right]\times$$

$$\times d\tau'+(1-G)\eta(z)-\varepsilon(\tau)\theta(\tau;\ z)+\int_0^\tau\left[\frac{\partial\varepsilon}{\partial\tau'}+\varepsilon\delta(\tau')\right]\theta(\tau';\ z)\exp\left[-\int_{\tau'}^{\tau}\delta(\tau'')\,d\tau''\right]d\tau', \tag{2}$$

where $\varepsilon(\tau) = k\xi(\tau)$.

To estimate the last term, $\theta(\tau'; Z)$ may be written in the form of an expansion in Taylor series in the vicinity of the point $\tau' = \tau$

$$\theta(\tau';\ z)\approx\theta(\tau;\ z)+(\tau'-\tau)\frac{\partial\theta(\tau;\ z)}{\partial\tau}+(\tau'-\tau)^2\frac{\partial^2\theta(\tau;\ z)}{\partial\tau^2}+\ldots.$$

Substituting this into the integral of Eq. (2) offers the possibility of solving the problem with any degree of accuracy. To obtain an analytic solution, only the first two terms of the series are retained. This allows the integrodifferential Eq. (2) to be transformed to a first-order partial differential equation with variable coefficients

$$\gamma_*(\tau)\frac{\partial\theta}{\partial\tau}+G(\tau)\frac{\partial\theta}{\partial z}+m(\tau)\theta=[1-G(\tau)+\varphi(\tau)]\eta(z), \tag{3}$$

where

$$\gamma(\tau)=1+\int_0^\tau(\tau-\tau')\left(\frac{\partial\varepsilon}{\partial\tau'}+\varepsilon\delta\right)\exp\left[-\int_{\tau'}^{\tau}\delta\,d\tau''\right]d\tau';$$

Translated from Atomnaya Énergiya, Vol. 48, No. 2, pp. 109-110, February, 1980. Original article submitted March 12, 1979.

0038-531X/80/4802-0129 $07.50

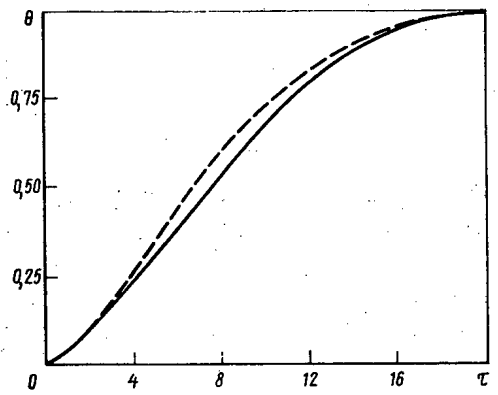

Fig. 1

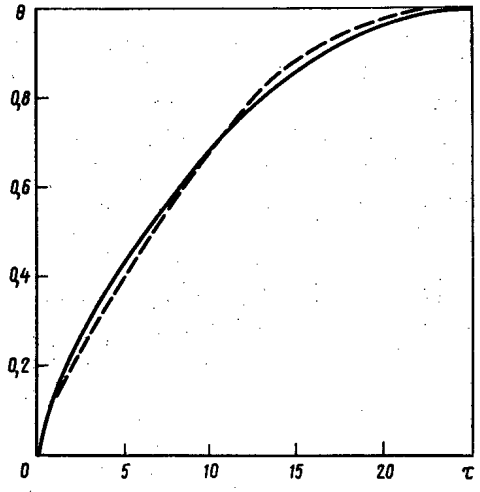

Fig. 2

Fig. 1. Temperature change at reactor outlet with stepwise power change: —) accurate solution; — — —) approximate solution.

Fig. 2. Temperature change at reactor outlet with stepwise change in heat-carrier flow rate (notation as in Fig. 1).

$$m(\tau)=\varepsilon-\int_0^{\tau}\left(\frac{\partial\varepsilon}{\partial\tau'}+\varepsilon\delta\right)\exp\left[-\int_{\tau'}^{\tau}\delta\,d\tau''\right]d\tau';$$

$$\varphi(\tau)=\int_0^{\tau}\delta q\,\exp\left[-\int_{\tau'}^{\tau}\delta\,d\tau''\right]d\tau'.$$

It is sufficiently simple to solve Eq. (3) by using a Laplace transformation over the spatial coordinate z, which leads to the following calculational formula

$$\theta(\tau;\ z)=\int_{\tau_*}^{\tau}\frac{1-G+\varphi}{\gamma}\,\eta\left(z-\int_{\tau'}^{\tau}\frac{G}{\gamma}\,d\tau''\right)\exp\left(-\int_{\tau'}^{\tau}\frac{m}{\gamma}\,d\tau''\right)d\tau'+\theta_+(\tau_*)\exp\left(-\int_{\tau_*}^{\tau}\frac{m}{\gamma}\,d\tau'\right),\qquad(4)$$

where

$$\tau_*=\begin{cases}\displaystyle\int_0^{\tau_*}\frac{G}{\gamma}\,d\tau=\int_0^{\tau}\frac{G\,d\tau'}{\gamma}-z;\\ 0\ \text{for}\ z\geqslant\displaystyle\int_0^{\tau}\frac{G\,d\tau}{\gamma}.\end{cases}$$

The function $\tau_*(\tau)$ determines the thermal momentum transfer over the active region due to heat-carrier motion, taking account of the thermal lag determined by $\gamma(\tau)$. Setting $0 \leq z \leq 1$, the change in heat-carrier temperature $\theta(\tau; z)$ in any cross section over the height of the active region may be determined. Knowing $\theta(\tau; z)$, it is simple to calculate the fuel-element temperature

$$u(\tau;\ z)=\eta(z)\int_0^{\tau}\psi q\exp\left(-\int_{\tau'}^{\tau}\delta\,d\tau''\right)d\tau'-\int_0^{\tau}\xi\frac{\partial\theta}{\partial\tau'}\exp\left(-\int_{\tau'}^{\tau}\delta\,d\tau''\right)d\tau'.\qquad(5)$$

It is impossible to estimate the accuracy of the approximate solution in general form. Analysis of the static relations for the initial and final reactor conditions shows complete identity of the accurate and approximate models. The quality of the model in dynamic terms was verified by comparing accurate and approximate solutions with differential stepwise perturbations. The curves in Fig. 1 show the change in temperature at the outlet of a reactor with the parameters $\delta = 0.8462$; $\varepsilon = 10.15$; $\eta(z) = 1.2\cos 2.05(z - 0.5)$ for unit power step $q = 1$ and unchanging heat-carrier flow rate $G = 1$, $\theta = 0$. In Fig. 2, analogous curves are shown for $q = \theta_* = 0$ and change in the heat-carrier flow rate from $G = 1$ to $G = 0.5$.

It follows from Eq. (2) that the accuracy of the model is determined mainly by the value of δ: the larger δ, the less the error due to curtailing the series. Analysis shows that Eq. (4) for stepwise perturbations with

$\delta \geqslant 0.4$ gives good accuracy of the calculations: the discrepancy is no more than ~6%. This provides the basis for recommending the approximate model for practical calculations, which allows the laborious procedure of numerical solution of Eq. (1) to be avoided. The integrals in Eqs. (4) and (5) are sufficiently simple to calculate on a computer. Graphoanalytic methods may also be used.

LITERATURE CITED

1. A. Ya. Kramerov and Ya. V. Shevelev, Engineering Calculations of Nuclear Reactors [in Russian], Atomizdat, Moscow (1964).
2. A. S. Trofimov and B. F. Gromov, Inzh.-Fiz. Zh., 7, No. 8, 31 (1964).

A β-RADIATION SOURCE BASED ON POLYSTYRENE CONTAINING TRITIUM

V. M. Gul'ko, E. I. Knizhnik, V. K. Rudishin, and A. I. Yashchuk

UDC 539.124.03:546.11.023:078.046

The important advantages of tritium over other radionuclides – low toxicity [1, 2], relatively long half-life, relatively simple methods of introducing it into compounds [3, 4] – has led to the wide use of tritium sources [3-5]. The design and characteristics of the usual tritium sources have been discussed in [3, 5]. A matter of considerable interest is the use in a source of tritium in a chemically bound state, e.g., in a hydrogenous polymer. Such a source will have a more uniform distribution of tritium, small mass, and no bremsstrahlung from the tritium-bearing layer; furthermore, it will be possible to prepare a source of arbitrary shape.

In the present paper we present the first results of a study of characteristic sources of β radiation based on polystyrene (PS) containing tritium. To prepare the sources, we used PS-7,8 ^{3}H in a benzene solution [6] with a specific activity of 600 mCi/ml or 682 mCi/g of solution (or 31 Ci/g of polymer) and a PS concentration of 19 mg/ml. The layer of PS was applied to a molybdenum backing 1.0 mm thick which had a titanium layer 0.8 μm thick sprayed onto it. The ionization current of the source was measured by means of an ionization chamber and a U5-6 electrometric amplifier. The desorption of tritium from the source was determined by accumulation in a spherical chamber, for 1 h, of the gas emitted by the source, followed by pumping it into the ionization chamber of a "Biota" radiometer with fixed volume, and measuring the concentration. The thickness of the PS layer was determined by weighing on a VLM-20M balance.

Table 1 shows the characteristics of a group of six sources; for 6 months after preparation, the ionization current remained practically unchanged. It can be seen that the desorption increases with time, and for sources with a higher current the desorption increases more rapidly. Evidently, this is related to the radiolysis of the PS under the action of the characteristic β radiation.

The dose absorbed by the PS was calculated by the formula [4]:

$$D = 1.6 \cdot 10^{-14} NEM^{-1}. \quad (1)$$

TABLE 1. Characteristics of the Sources

No. of source	Thickness of PS layer, 10^{-4} g/cm^2	Ionization current, 10^{-10} A/cm^2	Desorption, 10^{-8} Ci/cm^2·h	
			after preparation	6 months later
1	3	3,2	0,6	2,8
2	3	3,1	2,1	3,2
3	2	2,0	0,4	1,3
4	2	2,5	0,8	1,1
5	5	3,0	2,2	4,4
6	2	2,1	—	3,2

Translated from Atomnaya Énergiya, Vol. 48, No. 2, p. 111, February, 1980. Original article submitted April 12, 1979.

0038-531X/80/4802-0131 $07.50

For a source with a specific activity S = 31 Ci/g the number of disintegration per half-year was $N \approx 1.8 \cdot 10^{19}$. Then for an average β-particle energy of E = 5700 eV and a mass of M = 1 g, the dose amounts to 1640 Mrad. According to the data of [7], the working capacity of the PS should remain practically undiminished (without taking account of the isotope effect).

The expected degree of decomposition of the PS (K) was estimated by the formula [4]:

$$K = \{1 - \exp[-FESG(-M)\,6.14 \cdot 10^{-16} t]\}\ 100\%. \quad (2)$$

The degree of decomposition of the tritium-bearing PS, taking account of the absorption by the PS of the characteristic β radiation (F = 1), the half-year period of operation $t = 1.57 \cdot 10^7$ sec, E = 5700 eV, and S = 31 Ci/g, was 1.7, 8.8, 16.8, 24.1, and 20.8% when the number of irreversibly damaged molecules per 100 eV of absorbed energy G(–M) was equal to 0.1, 0.5, 1.0, 1.5, and 2.0, respectively.

It is expedient to use PS-based sources when the use of the traditional tritium emitters is less effective or is completely impossible.

Neutralization of Electrostatic Charges. In the neutralization of static electricity it is very important that the ions should be formed as close as possible to the zone of generation of the electrostatic charges. However, it is practically impossible to construct a usual type of tritium source in an arbitrary shape. On the other hand, a PS source is technologically convenient and is easily applicable to the surface of various materials. This makes it possible for each specific case to construct a source of the necessary shape and place it in the immediate vicinity of the spot where the charges will appear, in particular on the surface of machinery and mechanisms.

X-Ray Structural Analysis. In multicomponent x-ray structural analysis, we require a source of characteristic x-ray emission from which several lines are emitted simultaneously. If tritium-bearing PS is applied to a backing which contains the elements being analyzed, then under the action of β particles from the tritium, the backing will emit characteristic x rays which can pass easily through a thin layers of PS. Such a system makes it possible to obtain practically any line of any element, and the PS film itself will not have any bremsstrahlung, so that the background level will be considerably reduced; this is an advantage which distinguishes such a source from the traditional kind.

Calibration of β Spectrometers. The method described in [8] makes it possible to prepare polymer tritium sources with a controlled thickness from 5 to 30 $\mu g/cm^2$ with a high degree of uniformity, which are used for calibrating β spectrometers. They are distinguished by a relatively high and stable yield of β particles and by satisfactory radiation safety.

Atomic Batteries. Polymer tritium sources are promising for use in atomic batteries. They can be made very thin, which makes it possible to concentrate in a small volume a considerable surface emitting electrons. In addition, such batteries will be much lighter than the usual kind.

LITERATURE CITED

1. Basic Rules of Hygiene for Work with Radioactive Substances and Other Sources of Ionizing Radiation, OSP-72 [in Russian], Atomizdat, Moscow (1973), p. 18.
2. Norms of Radiation Safety, NRB-76 [in Russian], Atomizdat, Moscow (1976), p. 22.
3. G. D. Gorlovoi and V. A. Stepanenko, Tritium Emitters [in Russian], Atomizdat, Moscow (1965).
4. E. Evans, Tritium and Its Compounds [Russian translation], Atomizdat, Moscow (1970).
5. A. Manin, Bull. Inf. Sci. Tech. CEA, No. 178, 65 (1973).
6. V. M. Kaloshin et al., Compounds and Products Containing Radioactive Isotopes. A Catalogue [in Russian], V/O "Izotop," Moscow (1975), p. 14.
7. D. Bopp and W. Parkinson, in: The Effect of Radiation on Organic Materials [Russian translation], Atomizdat, Moscow (1965), p. 445.
8. R. Davis and C. St. Pierre, Nucl. Instrum. Methods, 64, 348 (1968).

COMPARISON OF THE RESULTS OF CALCULATING FAST-NEUTRON PASSAGE THROUGH HYDROGEN AND CARBON LAYERS

É. B. Brodkin, A. N. Kozhevnikov, V. G. Madeev, V. A. Utkin, and A. V. Khrustalev

UDC 539.125.5.17.52

Although our theoretical understanding of radiation transfer is now sufficiently complete, and the possibility now exists of realizing even the most rigorous method of solving transfer equations, the problem of reliability of the results obtained arises in calculating the protection of power reactors by a single program. The simplest method of estimating the indeterminacy of the calculation is to compare the results obtained using several programs, preferably of different classes, using independent systems of constants.

As experiments show, the main causes of discrepancy in the results are the initial microconstants used in the calculation, the methods of transforming them, and the model adopted to describe radiation transfer. The aim of the present work is to analyze the effect of these factors on the results. This analysis is best carried out in conditions of the simplest radiation-source geometry, so that the effect of other more significant factors is eliminated. In the present work, the dependence of the fast-neutron flux density on the thickness of hydrogen and carbon layers is calculated.

The hydrogen (ρ = 0.111 g/cm^3) and carbon (ρ = 1.65 g/cm^3) media are represented in the form of an infinite plate of thickness 120 cm, and the neutron source in the form of an infinite plate of thickness 1 cm with isotropic sources $\rho_I = 10^{-4}$ g/cm^3 uniformly distributed over the volume. The neutron energy distribution of the source corresponds to the fission spectrum. The programs used in the calculations are described briefly below.

Program ROZ-5 [1] is intended for the solution, in the multigroup approximation, of problems on the passage of neutrons (neutron problems), primary (arising in the fission of uranium) and secondary (formed in the capture and inelastic scattering of neutrons) γ radiation in one-dimensional plane geometry, and also for the solution of corresponding combined problems and the calculation of perturbation-theory functionals. ROZ-5 is based on the discrete-ordinate method. Finite-difference equations are solved by an iterative method, using accelerated convergence according to the mean-flux method. Calculations using the ROZ-5 program were carried out with the ARAMAKO-2F system of constants, providing for the representation of the elastic-scattering cross section in the P_5 approximation. The neutron energy range (from thermal to 10.5 MeV) was represented in the form of 26 groups.

The MOKDIF program [2] is intended for the calculation of the spatial – energy distribution of neutrons in a heterogeneous medium of one-dimensional geometry (a sphere, infinite cylinder, or plate). The program algorithm is based on a combination of the Monte Carlo method and the spherical harmonic method (P_1 approximation). The program is combined with the NEDAM system of group (52 groups) constants [3] for Monte Carlo calculations (at an energy > 0.1 MeV) and a 21-group system (for an every $\leq$ 0.1 MeV).

The SABINE-3 program [4] is intended for the calculation of the spatial – energy distribution of neutrons and γ quanta in a heterogeneous medium of one-dimensional geometry (sphere, cylinder, plate).

The algorithm of the neutron problem is based on diffusion as the method of introduction. The introduction flux density is calculated in 19 energy groups by numerical integration over the source volume. The diffusion equations for each of the 26 groups are solved by the method of factorizing the second-order linear operator, with several typical boundary conditions. In solving the γ problem, the method used was integration over the source volume with exponential attenuation and an accumulation factor. The program is added to the existing library, containing the nuclear constants for reactions between neutrons and γ quanta for 33 elements.

Translated from Atomnaya Énergiya, Vol. 48, No. 2, pp. 112-113, February, 1980. Original article submitted March 23, 1979.

0038-531X/80/4802-0133 $07.50

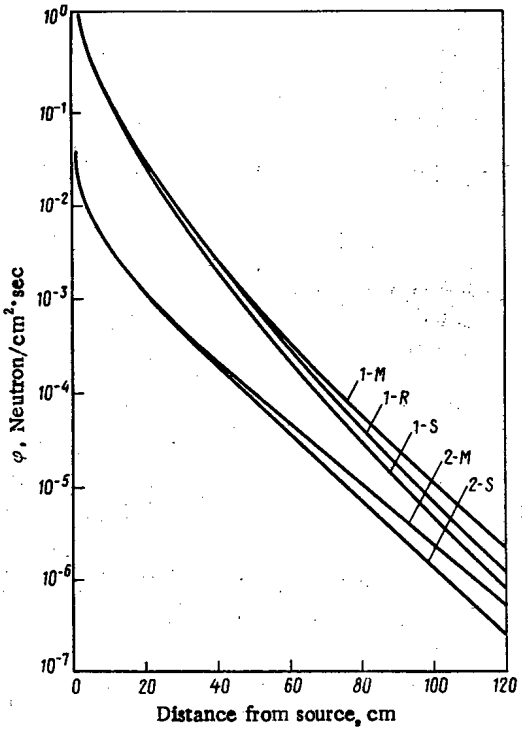

Fig. 1. Spatial distribution of neutron flux in hydrogen: 1) E < 0.1 MeV; 2) E > 6.5 MeV; M) calculation by the MOKDIF program with vacuum conditions at the boundary to the left of the source; R) calculation by the ROZ-5 program, with the same conditions; S) calculation by the SABINE-3 program with "reflection" conditions at the source – medium boundary.

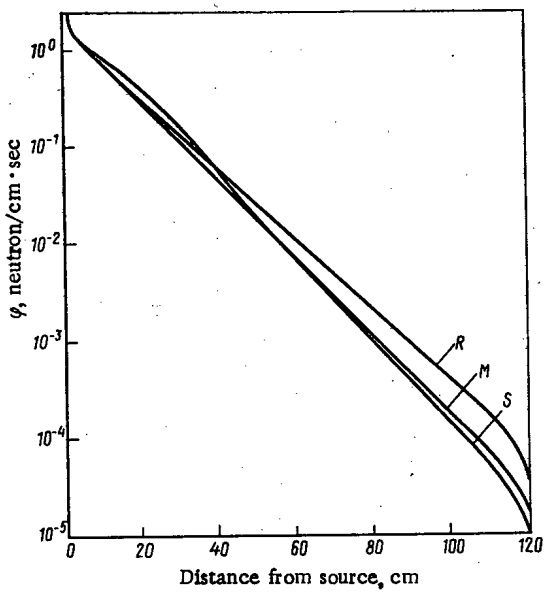

Fig. 2. Spatial distribution of neutron flux density in carbon at E > 0.1 MeV: M) calculation according to the MOKDIF program, with vacuum conditions at the boundary to the left of the source; R) calculation by the ROZ-5 program with the same conditions; S) calculation by the SABINE-3 program, with "reflection" conditions at the source – medium boundary.

The results calculated for the spatial distribution of neutrons of different energy groups in hydrogen and carbon for the same formulation of the problem according to the above programs are shown in Figs. 1 and 2. It is evident that the results of calculations for the two materials differ with increase in thickness (by more than a factor of two for a thickness above 100 cm). As was assumed, the cause of the discrepancy in the results can be analyzed sufficiently thoroughly for the case of hydrogen, since the neutron interaction cross section is known with good accuracy for this element over practically the whole of the given energy range, neutrons are scattered only elastically, and the differential scattering cross section is expressed by a simple formula.

In the initial calculation by the ROZ-5 program, an 8-group representation of the neutron spectrum was used in the range 0.1-10.5 MeV, in accordance with the ARAMAKO-2F system of constants. Since the neutron flux density calculated by ROZ-5 with this representation of the energy distribution was found to be less than the same neutron flux density as calculated by the MOKDIF program, it was concluded that 8 groups are insufficient for the representation of the spectrum in this range.

To verify this conclusion, the ROZ-5 program was used to calculate the spatial distribution of the neutron flux density in the energy range 0.1-13.5 MeV in a 30-group representation and in the range 6.5-13.5 MeV in an 11-group representation. The total group interaction cross sections were calculated on the basis of the cross sections used in the MOKDIF program. The group scattering indices were determined from the analytic formula for elastic scattering. Comparison of the results obtained by the MOKDIF and ROZ-5 programs with the same system of constants (Fig. 1) shows that they are in good agreement over the whole of the thickness range (0-120 cm). This indicates that the reason for the discrepancy in results obtained using programs realizing more rigorous models of radiation transfer should be sought primarily in the system of constants used together with the computational program.

Analysis of the reason for the discrepancy is complicated, of course, when the comparison is of results obtained using programs in which different degrees of rigor are adopted in modeling the neutron-transfer process, or when there are several types of interactions of the neutrons with nuclei of the medium, and their cross sections cannot be expressed by simple dependences. This is the case when comparing results obtained using the SABINE-3, ROZ-5, and MOKDIF programs, both for hydrogen (in comparing SABINE-3 with ROZ-5 and MOKDIF) and for carbon (in comparing any pair of programs). As yet, it has not been possible to perform a sufficiently complete analysis of the discrepancy in the results for the calculated versions of the spatial distribution in carbon. However, in view of the significance of the results in themselves, it seemed useful to present them here.

In conclusion, note that analysis of the identity of results obtained from different programs using some system of constants is one of the most urgent, and inadequately solved, problems in the investigation of all possible radiation-field characteristics.

LITERATURE CITED

1. T. L. Germogenova et al., in: Problems of Reactor Protection Physics [in Russian], No. 4, Atomizdat, Moscow (1972), p. 22.
2. A. N. Kozhevnikov et al., Preprint IAÉ-2877, Moscow (1977).
3. L. N. Zakharov et al., Preprint IAÉ -2994, Moscow (1978).
4. P. Niks, G. Perlini, and K. Ponti, in: Physical Problems of Reactor Protection [Russian translation], Atomizdat, Moscow (1971), p. 5.

ANALYSIS OF ACTIVATION METHOD FOR MEASURING FAST-NEUTRON INTERACTION CROSS SECTIONS

A. N. Davletshin, A. O. Tipunkov,
S. V. Tikhonov, and V. A. Tolstikov

UDC 539.125.5

Data obtained by various experimenters using various methods, even for such well-studied nuclides as ^{238}U and ^{197}Au, show appreciable divergences. This is particularly true for energies $\gtrsim 1$ MeV. Not only are these differences in data obtained by time-of-flight and activation methods, but even the results obtained by various experimenters using the activation method show divergences. We are convinced that these differences result from an incorrect account of the background corrections for the effects of neutron scattering.

In irradiating samples at an electrostatic accelerator it is necessary to determine the activity $N_{\gamma 0}$ induced in a sample by neutrons reaching it directly from the target. However, some neutrons leave the target and undergo various interactions in structural elements before reaching the sample. The spectrum of these neutrons may be considerably different from that of neutrons arriving directly from the target. These background neutrons induce activities in the sample which we shall call sample backgrounds. There are also other reasons why the measured effect differs from $N_{\gamma 0}$.

We describe briefly the sources of sample backgrounds and methods of measuring them.

1. Room Background A_{B1}. This background is the result of neutron scattering from the walls of the laboratory, and is assumed constant far from the walls.

For long half-lives it is convenient to determine this background by comparing the activities of samples irradiated simultaneously under normal conditions (~4 cm from the target) and at a distance of ~2-3 m from the target, or by measuring the activity of the sample as a function of the distance from the target. By extrapolating this relation to an infinite distance, we obtain the value of A_{B1}.

2. Sample Background A_{B2}. Most of the neutrons which interact with the sample undergo elastic and inelastic scattering. The mean free path of these neutrons after scattering in a disk sample is appreciably longer than the sample thickness. Such neutrons can increase the activity of the sample as a result of radiative capture. This effect can be determined by using samples of various masses and extrapolating the experimental values of the cross section to zero mass. Since this background amounts to less than 2% of the activity of the sample, it was calculated.

3. Container Background A_{B3}. A U_3O_8 sample is usually packed in a nickel container. In addition, it is also packed in a cadmium container to decrease the room and target support backgrounds. This leads to a decrease in the neutron flux incident on the sample. At the same time, neutrons scattered in the containers cause further activation of the sample. The combination of these effects leads to an increase in the activity of the sample. The value of this background is determined by measuring the activities for containers of various masses.

4. Target Support Background A_{B4}. The target support is a very massive structure, and is located close to the sample. Its main elements affecting the activation conditions of the sample are a layer of cooling water and a brass cover. Neutrons leaving the target outside the solid angle subtended by the sample are scattered and cause additional activation when they strike the sample. This effect is decreased to a certain extent because of the attenuation of the direct neutron flux in the target support. This background is also determined by measuring the activity for target supports of various masses.

5. Background Resulting from the Anisotropy of the Neutron Source A_{B5}. The activation of the sample by neutrons from the target is a linear function of the geometric factor G_{sa}, which depends on the dimensions of the source and sample, and the distance between them. Measurements of the activity of the sample for various distances from the target showed that at distances < 5 cm the activity of the sample is lower than it

Translated from Atomnaya Énergiya, Vol. 48, No. 2, pp. 113-115, February, 1980. Original article submitted April 23, 1979; revision submitted July 10, 1979.

0038-531X/80/4802-0136 $07.50

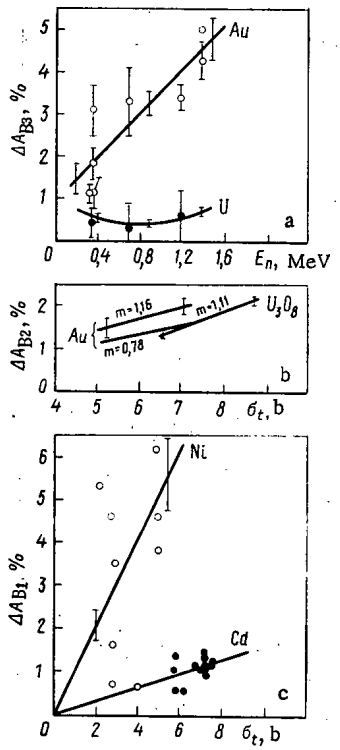

Fig. 1

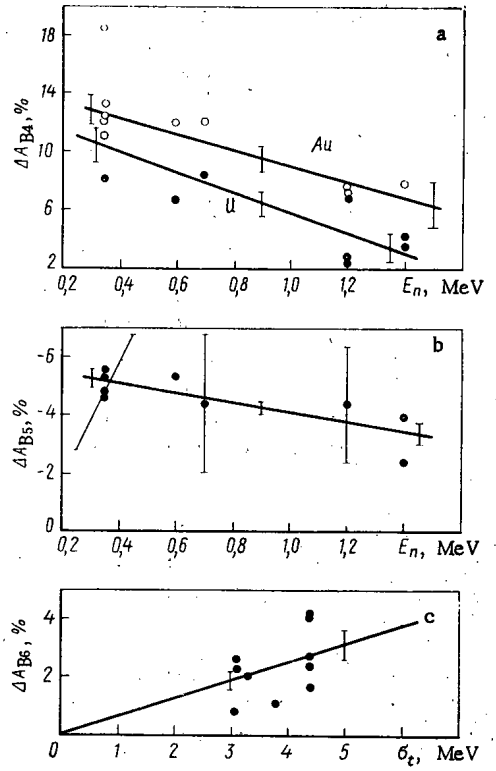

Fig. 2

Fig. 1. Relative values of backgrounds of: a) room ΔA_{B_1}; b) sample ΔA_{B_2}; c) containers for U_3O_8 and Au samples ΔA_{B_3}. Here and in Fig. 2: ○) experiment; ——) least squares average.

Fig. 2. Relative values of backgrounds of target support ΔA_{B_4}, anisotropy of neutron source ΔA_{B_5}, and sample holder ΔA_{B_6} for U_3O_8 and Au samples.

should be for a linear law. There are two reasons for this. First, the differential cross sections for the $T(p, n)^3He$ and $^7Li(p, n)^7Be$ reactions decrease with increasing angle of departure of the neutrons. Second, neutrons emerging at larger angles are more strongly attenuated by the target support structure. At the same time, this effect is partially compensated by neutrons which emerge at larger angles and have lower energies than neutrons which emerge at 0°. The background A_{B_5} is measured as follows: The sample is irradiated at the normal distance of 4 cm from the target and at a distance of 6 cm, for which the linear law of variation of activity with G_{sa} is still valid. The difference between the normalized activities is the background sought.

6. Sample Holder Background A_{B_6}. Some of the neutrons scattered by the brass sample holder fall on the sample and give rise to further activation. The value of this background can be determined by using sample holders of various masses.

Figures 1 and 2 show the results of measurements of various sample backgrounds in the form of the relative contribution ΔA_{Bj} for 350–1400 keV neutrons. If the background is different for U_3O_8 and Au samples, the results are shown on separate graphs. The backgrounds of the containers and sample holder are shown as functions of the total microscopic cross section of the corresponding element, and normalized to unit mass. This is convenient in view of the presence of resonances in the cross sections.

The value of ΔA_{B_1} for uranium was calculated from the estimate of ΔA_{B_1} for gold samples. In addition, this background was determined for three values of the neutron energy from the dependence of the activity of the uranium samples on the distance from the target. These values with errors are also shown on the graph. The calculated and measured values are in complete agreement.

The ΔA_{B_4} background is larger for gold than for uranium, although the energy dependences are similar. This results from the fact that neutrons scattered in the target support and falling on the sample have substantially lower energies than neutrons incident at 0°. The probability of their capture by a gold nucleus is larger, since the resonance integral for gold is 5.5 times as large as that for uranium.

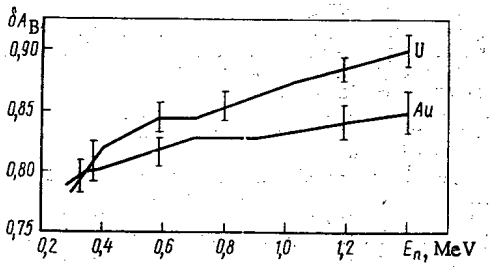

Fig. 6. Total background correction as a function of neutron energy for U_3O_8 and Au samples.

Most of the experimental values of the background ΔA_{B5} were measured as described above. ΔA_{B5} for uranium was determined for three values of the neutron energy from the dependence of the activity of the samples on distance (2-40 cm). These values and the experimental errors were plotted. Agreement with the remaining data is good.

Using the background estimates obtained, the total background correction δA_B was calculated for the experimental radiative capture cross sections of ^{238}U and ^{197}Au. The calculated results are shown in Fig. 3. In the neutron energy range considered the total random errors of the corrections vary from 1.4 to 1.9% for gold, and 1.3-2% for uranium.

The main contribution to the total random error comes from ΔA_{B4}. The conditions of measurement of this background are such that it may have an appreciable systematic error. An estimate shows that for E_n = 350 keV this error for gold (ΔA_{B4} = 12.5%) may reach 3%. The reason is that the target support makes a large contribution to the background, and cooling it with water does not decrease it significantly. In addition, added background mass cannot be distributed in the same way relative to the target as the main mass. It follows from the above that it is necessary to lighten the target support as much as possible and to cool it with gas in order to lower the contribution of the background ΔA_{B4} and to decrease its systematic error appreciably.

Thus, taking careful account of background corrections changes the value of the experimental capture cross section appreciably, even for neutrons with energies less than 1.5 MeV. There is no mutual compensation of the scattering corrections in activation measurements. An underestimate of the effects investigated in this paper can cause the difference in values reported by various experimenters.

YIELD AND ANGULAR DISTRIBUTIONS OF PHOTONEUTRONS FROM THICK LEAD TARGETS

A. P. Antipenko, V. G. Batii, V. Ya. Golovnya, V. I. Kasilov, N. I. Lapin, L. A. Makhnenko, and S. F. Shcherbak

UDC 539.172.284:539.124.162.6

The purpose of this study is to investigate the yield and angular distributions of photoneutrons from lead targets of different thicknesses in the impinging-electron energy range of 60-200 MeV.

The measurements were made by the activation method on a beam from the LUÉ-300 linear electron accelerator. We used the reaction $^{27}Al(n, p)^{27}Mg$ with $T_{1/2} = 9.8$ min. Threshold detectors, which were aluminum disks 48 mm in diameter and 4 mm thick, were placed at a distance of 50 cm from a lead target over a range of angles from 0 to 165° with the axis of the impinging electron beam, spaced 15° apart. The activity of the detectors was measured with a scintillation γ spectrometer which had an NaI(Tl) crystal measuring 63 × 63 mm.

Data on the integral neutron flux were obtained with an error of ±10% by the method of effective threshold cross sections [1]. The total integral neutron flux was determined from the relation

$$\Phi = K\varphi\,(E_{\text{eff}},$$

where K is a coefficient taking account of the contribution made by the neutrons with energies less than the effective reaction threshold. A value of $K \approx 12$ was obtained from an estimate of the shape of the photoneutron spectrum given in [2]. The error in determining Φ was ±20%.

Figure 1 shows the variation of the fast-neutron flux density ($E_n > 4.5$ MeV) at different angles as a function of the thickness of the lead target for an electron energy of 200 MeV. The diameter of the target was constant, equal to 43 mm. It can be seen that for a thickness of more than 18 radiation lengths (1 radiation length equals 5.6 mm) there is practically no increase in the neutron yield at all angles. In the rest of our study we used a lead-target thickness of 100 mm for the measurement of the angular and energy variations.

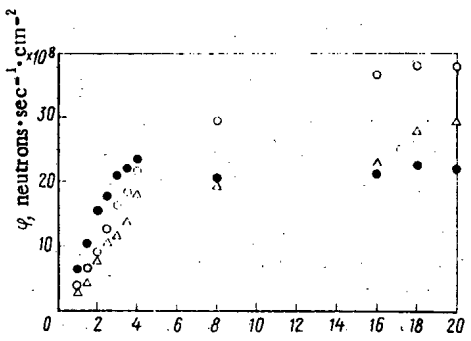

Fig. 1

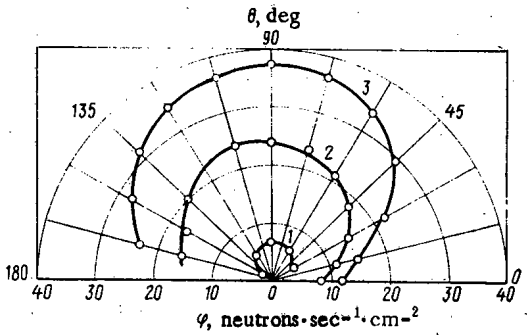

Fig. 2

Fig. 1. Fast-neutron flux density as a function of target thickness at angles of 30° (●), 90° (○), and 150° (Δ) at a distance of 1 m from the center of the target, with an electron-beam current of 1 μA.

Fig. 2. Angular variation of the fast-neutron flux density for an impinging-electron energy of 60 (1), 125 (2), and 200 (3) MéV and a beam current of 1 μA.

Translated from Atomnaya Énergiya, Vol. 48, No. 2, pp. 115-116, February, 1980. Original article submitted April 23, 1979.

0038-531X/80/4802-0139 $07.50

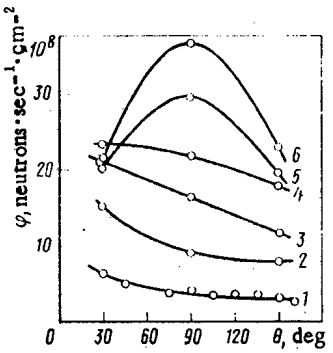

Fig. 3

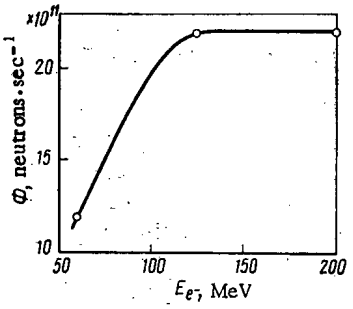

Fig. 4

Fig. 3. Variation in the shape of the graph of fast-neutron flux density vs angle as the target thickness is varied (electron-beam current 1 μA, distance from center of target 1 m): 1) d = 1; 2) 2; 3) 3; 4) 4; 5) 8; 6) 16 radiation lengths; ○) experimental points.

Fig. 4. Neutron flux as a function of impinging-electron energy at an electron-beam power of 1 kW.

Figure 2 shows the angular distributions of fast neutrons, which demonstrate the anisotropy of the neutron yield, with a maximum at 90°. In a number of earlier experimental studies [3-5] measurements were made on the angular distributions of fast photoneutrons from targets with a thickness of $\geqslant 10$ radiation lengths with $E_{\gamma max}$ = 22-55 MeV. The investigators also observed anisotropy of the neutron yield, with a maximum at angles close to 90°. This effect can be explained essentially by the small contribution of the statistically emitted neutrons in the energy region $E_n > 4.5$ MeV. The angular distributions of such neutrons are usually described by the sum of the first Legendre polynomials [3, 6, 7].

Figure 3 shows the variation in the shape of the graph of the fast-neutron flux density vs angle for different lead-target thicknesses, with an electron energy of 200 MeV. For a target thickness of 1 to 4 radiation lengths we observe a striking anisotropy, with a maximum at small angles. For a target thickness greater than 4 radiation lengths, the neutron yield at 90° increases considerably.

The absence of a 90° maximum in the angular distribution and the presence of an anisotropy in the forward direction when the target thickness is less than 4 radiation lengths is explained by the attenuation of the neutron flux by the target material at angles close to 90° (by a factor of ≈ 1.6, according to our estimates); the flux of neutrons flying forward remains practically unattenuated, and the flux of the neutrons flying backward is attenuated only slightly (for a target with a thickness of only 1 radiation length and $\theta = 165°$ the attenuation factor is about 1.1). It is also apparent that for a small target thickness the bremsstrahlung spectrum is harder, and consequently the contribution of the reactions which yield isotropy, e.g. $(\gamma, 2n)$ and others, is greater [8].

Figure 4 shows the variation of the total neutron flux from a lead target 100 mm thick as a function of the impinging-electron energy calculated per unit beam power. It can be seen that the specific neutron yield for an electron energy of more than 100 MeV reaches its maximum value of $2.2 \pm 0.4 \cdot 10^{12}$ neutrons/sec·kW, and for higher electron-energy values it remains practically constant. This value is in good agreement with the results of the calculations in [9] for a lead target 102 mm thick and 50 mm in diameter, which showed $1.6 \cdot 10^{12}$ neutrons/sec·kW (using the cross section obtained by Harvey et al.) and $2.8 \cdot 10^{12}$ neutrons/sec·kW (using the cross section obtained by Miller et al., and also with the data of an experimental study [10] for a lead target 60 mm thick and 25 mm in diameter, which showed $(2.7 \pm 0.8) \cdot 10^{12}$ neutrons/sec·kW.

The above experimental results may be useful in the design of fast-neutron sources based on linear electron accelerators.

LITERATURE CITED

1. E. A. Kramer-Ageev et al., Activation Methods of Neutron Spectrometry [in Russian], Atomizdat, Moscow (1976).
2. D. Gaythor and P. Goode, J. Nucl. Energy, 21, No. 9, 733 (1967).

3. G. Price, Phys. Rev., 93, 1279 (1954).
4. G. Reinhardt and W. Whitehead, Nucl. Phys., 30, No. 2, 201 (1962).
5. F. R. Allum et al., ibid., 53, No. 4, 545 (1964).
6. R. Baker and K. McNeill, Can. J. Phys., 39, 1158 (1961).
7. J. Rawlins et al., Nucl. Phys., A122, 128 (1968).
8. K. McNeill et al., Can. J. Phys., 46, 1974 (1968).
9. R. Alsmiller and H. Moran, Nucl. Instrum. Methods, 48, 109 (1967).
10. V. I. Noga, KhFTI Preprint, No. 78-34, Khar'kov (1978).

A NEW SYSTEM OF GROUP CONSTANTS FOR THE CALCULATION OF FAST REACTORS

L. N. Abagyan, N. O. Bazazyants, M. N. Nikolaev, and A. M. Tsibulya

UDC 621.039.51.134

A good deal of work is now being done on a new version of the BNAB-78 system of group constants, which now includes data for 17 elements and isotopes: for fuel materials – ^{235}U, ^{238}U, ^{239}Pu, and ^{240}Pu; for structural and technological materials – Fe, Cr, Ni, Mn, Na, O, C, and ^{4}He; for materials of the control components – ^{10}Bu and Eu; and also for D, ^{3}He, and Er. Efforts to extend this system are being made. In the study of isotopes for which new group constants have not yet been prepared, data from the earlier version of the system of constants [1, 2] can be used.

The work on the BNAB-78 was carried on in two stages. The first stage took account of the data published in 1977 for differential microscopic experiments alone. The result of this stage was the development of a system of constants which has come to be known as BNAB-MIKRO. The choice of the variation of the cross sections of ^{235}U, ^{239}Pu, and ^{240}Pu as functions of energy was based on estimates made by Kon'shin et. al. [3-5]; in the case of Fe, Ni, and Cr the choice was based on estimates made at the Nuclear Data Center [6-8]. The results of these estimates were corrected, taking account of newly obtained experimental information. The constants for carbon and ^{10}B were based on estimates taken from the ENDF/B library [9]. The remaining data were obtained from the results of our own estimates.

The second stage consisted in an analysis of the divergences between the results of experiments conducted on fast critical assemblies and the results of calculations by BNAB-MIKRO system. We considered data obtained on 21 assemblies with uranium fuel and 13 assemblies with plutonium fuel; in five cases these experiments related to media with $k_\infty = 1$.

We observed a contradiction between the new experimental data on the excitation cross section for inelastic scattering of the 47 keV level of ^{238}U [10, 11] and the results of measurements of the ratios of the fission and capture cross sections in ^{238}U to the fission cross section of ^{235}U in a medium of metallic uranium with 5.56% enrichment and $k_\infty = 1$. These measurements were independently made by different methods in the USSR, the Federal Republic of Germany, France, and Great Britain [12, 13] and led to very exact results (1%) which were in excellent agreement. To explain these data, we had to reduce the cross section of inelastic scattering by ^{238}U for an energy of hundreds of keV to the level of the earlier results obtained by Smith [14] (which served as the basis for the earlier version of the BNAB constants [1]). The capture cross section of ^{238}U used in BNAB-MIKRO [15] in the region from 2 to 40 keV also had to be reduced to the level of the estimate made by Tolstikov [16]. The results of the analysis of macroexperiments also indicated a need to increase the fission cross section of ^{239}Pu by 1.5%, which was done. Unlike the change in the cross sections of ^{238}U, this change is completely consistent with the latest experimental data [17], which were not taken into account in the BNAB-MIKRO system.

The system of constants with the indicated changes in the cross sections of ^{238}U and ^{239}Pu has been given the name of BNAB-78. In addition to the groups of the BNAB-70 system of constants, the BNAB-78 system includes a group 0 (10.5-14 MeV) and a group –1 (14-14.5 MeV); it includes data on the characteristics of

Translated from Atomnaya Énergiya, Vol. 48, No. 2, pp. 117-118, February, 1980. Original article submitted May 8, 1979.

0038-531X/80/4802-0141 $07.50

TABLE 1. Divergences between Calculation and Experiment in the Criticality Coefficients, Cross-Sectional Ratios, and Reactivities of Small Specimens in the Centers of the Active Zones of Fast Critical Assemblies, %

Characteristic	No. of experiments	Divergence				Accuracy		Divergence		
		BNAB 70	BNAB-MIKRO	BNAP-M*	BNAP-78	of one expt.	av.	ENDF/B-IV	JAERI FAST	JENDL-1
$k_{3\Phi}$ (^{235}U)	16	—0,4	—0,9	—0,1	—0,1	0,8	0,2	0,4	0,4	0,7
$k_{3\Phi}$ (^{239}Pu)	12	—2,6	—1,9	—1,0	—0,2	0,9	0,3	—0,3	—0,3	0,1
$\bar{\sigma}_f$ (^{238}U)/$\bar{\sigma}_f$ (^{235}U)	32	—0,7	2,2	1,3	1,4	5,3	0,9	2,8	2,9	—0,1
$\bar{\sigma}_c$ (^{238}U)/$\bar{\sigma}_f$ (^{235}U)	17	2,4	3,9	0,3	0,3	2,3	0,6	—2,6	—1,8	—1,4
$\bar{\sigma}_f$ (^{239}Pu)/$\bar{\sigma}_f$(^{235}U)	30	—4,7	—2,1	—2,0	—0,5	3,3	0,6	—0,7	—1,9	—3,1
$\bar{\sigma}_f$ (^{240}Pu)/$\bar{\sigma}_f$ (^{235}U)	13	—0,8	2,6	2,1	2,4	9,9	2,8	7,3	6,8	1,2
ρ (^{238}U)/ρ (^{235}U)	13	—4,4	—0,8	—2,8	—1,6	9,1	2,5	—5,1	—0,8	6,7
ρ (^{239}Pu)/ρ (^{235}U)	20	—3,2	—2,4	—2,0	—0,2	3,6	0,8	—1,8	—0,4	—3,1
ρ (^{10}B)/ρ (^{235}U)	19	—22	—16	—14	—13	11	2,5	—17	—9,7	—8,6
ρ (Fe)/ρ (^{235}U)	12	—11	6	6	6	27	8	8	1,4	—15
ρ (Ni)/ρ (^{235}U)	10	—5	17	19	20	12	4	8	15	9
ρ (Cr)/ρ (^{235}U)	9	—3	19	20	21	16	5	28	31	—8

*BNAB-M differs from BNAB-MIKRO only in the change of the ^{238}U cross sections; the fission cross section of ^{239}Pu remains the same.

delayed fission neutrons; the resonance structure is described both with the aid of self-shielding factors and in the subgroup representation; the anisotropy of inelastic scattering is described to within the P_5 approximation; group cross sections are given for the most important reactions: (n, 2n), (n, p), (n, α), and others.

Table 1 contains data on the average divergences between calculation and experiment in the characteristics of critical assemblies obtained by different versions of the BNAB constants and also by the foreign systems of constants ENDF/B IV [18], JAERI-FAST, and JENDL-1 [19]. It also shows estimates of the errors in the results of individual experiments (according to the mean-square distribution and the errors of the average divergences between calculation and experiment (less by a factor of $\sqrt{N}$ than the error of an individual experiment; N is the number of experiments of a given type). The latter relate only to the results of the calculation using the BNAB constants, since the calculations by the foreign systems of constants were carried out only for some of the critical assemblies we considered. The data show that the use of BNAB-78 ensures the calculation of the characteristics which determine the neutron balance, to within experimental errors.

The calculated reactivity of ^{10}B is found to be too low regardless of what system of constants is used. We assume that the reason for this lies in some still unidentified methodological errors in the experiments and/or the calculations. The same cause may be responsible for the considerable divergences in the reactivities of Cr and Ni: in the experiment on the KBR-3-3 assembly [20], in which these reactivities were measured and calculated most reliably, the divergences between calculation and experiment are small.

The BNAB-78 system of constants is recommended for use in physical calculations for fast reactors and neutron shielding. According to our estimates, the errors obtained with it for the calculated prediction of k_{eff} and the coefficient of reactivity of a large plutonium breeder reactor with partly burned-up fuel are 1%, 2%, and 3%, respectively. These errors are due to the inaccuracy of the data on the cross sections of parasitic capture (chiefly in fragments), and in the case of the coefficient of reactivity they are also due to inaccuracies in the value of α.

It should be noted that at the time of publication of this paper, the BNAB-78 system has been supplemented by revised group constants for ^{7}Li, ^{11}B, Al, Si, Ca, Cd, Cd, and Pb. For all the materials, tables of the formation of γ quanta in neutron reactions (for 15 γ groups) have been formulated, so that we can recommend these constants for the calculations of radiation shields as well.

LITERATURE CITED

1. L. N. Abagyan et al., Group Constants for the Calculation of Nuclear Reactors [in Russian], Atomizdat (1964).
2. L. V. Antonova et al., in: Proceedings of the Trilateral Soviet – Belgian – Dutch Symposium on Some Problems in Fast-Reactor Physics [in Russian], Vol. 1, Report 18, Moscow (1970).
3. G. V. Antsipov et al., in: Problems in Atomic Science and Technology. Nuclear Constants Series [in Russian], Part 2, No. 20, Izd. TsNIIatominform, Moscow (1975), p. 3.

4. V. A. Kon'shin et al., ibid., No. 16, 329 (1974).
5. G. V. Antsipov et al., in: Nuclear-Physics Research in the USSR. A Collection of Abstracts [in Russian], No. 21, Obninsk (1976), p. 45.
6. V. M. Bychkov et al., in: Problems in Atomic Science and Technology. Nuclear Constants Series [in Russian], Part 1, No. 20, Izd. TsNIIatominform (1975), p. 46.
7. V. M. Bychkov and V. I. Popov, in: Problems in Atomic Science and Technology. Nuclear Constants Series [in Russian], No. 25, Izd. TsNIIatominform, Moscow (1977), p. 55.
8. V. M. Bychkov et al., in: Neutron Physics. Materials of the Fourth All-Union Conference on Neutron Physics [in Russian], Part IV, Moscow (1977), p. 91.
9. B. Magurno, ENDF/B IV Cross Section Measurements Standards. Inform. Analysis Center Report. BNL-11973, Upton, New York (1975).
10. P. Guenther and A. Smith, in: Proc. of the Washington Conf. "Nuclear Sections and Technology," Vol. II, NBS (1975), p. 862.
11. P. Guenther, D. Havel, and A. Smith, Fast Neutron Excitation of the Ground-State Rotational Band of ^{238}U. Report ANL/NDM-16 (1975).
12. M. Darrouzet et al., in: Proc. Int. Symp. on Physics of Fast Reactors, Vol. I, Tokyo (1973), p. 537.
13. J. Chaudat, M. Darrouzet, and E. Fisher, Experiment in Pure Uranium Lattices with Unit k_∞. Assemblies: SNEAK-8/8Z, UK 1 and UK 5 in ERMINE and HARMONIE. KFK-1865 (CEA-R-4552) (1974).
14. A. Smith, Nucl. Phys., 47, No. 4, 333 (1963).
15. G. N. Manturov and M. N. Nikolaev, Preprint FÉI-666, Obninsk (1976).
16. V. A. Tolstikov and V. S. Shorin, in: Problems in Atomic Science and Technology. Nuclear Constants Series [in Russian], Part 2, No. 20, Atomizdat, Moscow (1975), p. 61.
17. In: Proc. of the NEANDC/NEACRP Specialists Meeting on Fast Neutron Fission Cross Sections of ^{233}U, ^{235}U, ^{238}U, and ^{239}Pu, Argonne, June 28-30, 1976, ANL-7690.
18. R. Hardie, R. Schenter, and R. Wilson, Nucl. Sci. Eng., 57, No. 3, 222 (1975).
19. I. Otake, in: Proc. Specialists Meeting on Neutron Data of Structural Materials for Fast Reactors, Geel, December 5-8, 1977, Report IA-6.
20. V. I. Golubev et al., in: Problems in Atomic Science and Technology. Nuclear Constants Series [in Russian], No. 28, Izd. TsNIIatominform, Moscow (1978), p. 41.

COLLATION OF SEVERAL METHODS OF PULSED γ-RAY DOSIMETRY

Yu. P. Bakulin, V. N. Kapinos, A. P. Korotovskikh, and Yu. A. Medvedev

UDC 539.12.08

At the present time devices are being developed [1-5] for measurements of the dose and dose rates of pulsed ionizing radiation, but they do not include standard means of measurement. It is therefore of great interest to compare the results of dosimetric investigations carried out by various methods. Such a comparison is made in the present paper for γ-ray pulses with a duration of roughly several tens of nanoseconds and a characteristic leading edge of about 10 nsec.

The experiments were performed with a highly stable pulsed source of bremsstrahlung, ensuring a maximum dose rate of $8 \cdot 10^6$ A/kg. In our collation we compared the shape of the dose-rate pulses recorded by high-frequency [2, 5, 6] and scintillation [7] methods and integral doses measured by high-frequency and thermoluminescent [8] methods.

To record the pulse shapes by high-frequency methods we used a detector with a dynamic range of $2.5 \cdot 10^3$-$8 \cdot 10^5$ A/kg. The choice of precisely this detector was due to the fact that the upper limit of its dynamic range corresponded to the upper limit ($\sim 2.5 \cdot 10^5$ A/kg) of the range of the scintillation counter used in the collation.

Translated from Atomnaya Énergiya, Vol. 48, No. 2, pp. 118-119, February, 1980. Original article submitted July 3, 1979; revision submitted August 27, 1979.

0038-531X/80/4802-0143 $07.50

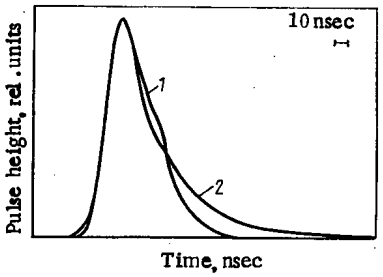

Fig. 1. Normalized copies of oscillographic records of γ-ray dose-rate pulses recorded by high-frequency (1) and scintillation (2) detectors with pulse duration of 40 nsec.

TABLE 1. Bremsstrahlung Doses Recorded by High-Frequency and Thermoluminescence IKS-A Dosimeters

Expt. No.	$D \cdot 10^9$, C/kg	$D \cdot 10^9$, C/kg	D/D'	Expt. No.	$D \cdot 10^9$, C/kg	$D \cdot 10^9$, C/kg	D/D'
1	2,2	2,0	1,1	6	3,0	2,5	1,2
2	2,4	2,0	1,2	7	25	20	1,3
3	2,3	3,3	0,7	8	28	30	0,9
4	2,3	2,2	1,0	9	38	34	1,1
5	3,0	2,7	1,1				

We compared the shapes of pulses recorded by high-frequency and scintillation methods (Fig. 1). The pulse duration τ at half-height (FWHM) was 41 and 36 nsec, respectively. Analysis of the normalized curves indicates good agreement between the shapes of dose-rate pulses, A(t) and A'(t), recorded by high-frequency and scintillation detectors, respectively. The value of the integral dose was found from the readings of the high-frequency and scintillation detectors, D and D', by using the relation

$$D = kA_{\max}\tau, \tag{1}$$

where A_{max} is the maximum value of A(t) and k is the form factor of the dose-rate pulse, as given by

$$k = \int_0^\infty A(t)\,dt/D'. \tag{2}$$

The results of comparisons of the integral doses are given in Table 1. In the plot corresponding to the thermoluminescence method the values given for the doses are averaged over the readings of two or three IKS-A thermoluminescent dosimeters arranged on the cylindrical surface of the high-frequency detector. The doses of the pulsed ionizing radiation, found from the readings of the high-frequency and thermoluminescence detectors, agree to within 30%.

Since there was practically no distinguishable spread of the readings of the high-frequency detector when the experiments were repeated many times, the deviations given in Table 1 for the readings of the high-frequency and thermoluminescence detectors are entirely due to the spread of the readings of the thermoluminescence dosimeters.

Analysis of the normalized curves of the time dependence of the γ-ray dose rate, recorded by high-frequency and scintillation detectors, showed that the observed difference lies within the limits of experimental errors which are determined primarily by the error of the oscillograph recorder ($\sim 10\%$). The slower decay of the pulse at the output of the scintillation detector is explained by the existence of slow components in the pulse characteristic of the plastic scintillator [7] and, possibly, by the energy dependence of the detectors tested. In conclusion, let us point out that the time resolution of the high-frequency method is estimated to be roughly 10 nsec [5].

LITERATURE CITED

1. V. N. Kapinos et al., Metrol. Tochnye Izm., No. 2, 21 (1970).
2. V. N. Kapinos and Yu. A. Medvedev, in: Int. Sci.-Tech. Conf. of COMECON Member-Countries on Scientific Instruments "Nauchpribor SÉV-78," Digest of Papers [in Russian], Izd. TsNII Priborostroeniya, Moscow (1978), pp. 170, 172.
3. V. N. Kapinos et al., in: Digest of Papers, All-Union Sci.-Tech. Conf. "State of the Art and Prospects for Development of High-Speed Photography and Cinematography and Metrology of Fast Processes" [in Russian], Atomizdat, Moscow (1978), p. 118.
4. V. N. Kapinos, Yu. A. Medvedev, and B. M. Stepanov, in: Digest of Papers, All-Union Sci.-Tech. Conf. "State of the Art and Prospects for Development of High-Speed Photography and Cinematography and Metrology of Fast Processes" [in Russian], Atomizdat, Moscow (1978), p. 120.
5. V. N. Kapinos et al., in: Digest of Papers, All-Union Sci.-Tech. Conf. "State of the Art and Prospects for Development of High-Speed Photography and Cinematography and Metrology of Fast Processes" [in Russian], Atomizdat, Moscow (1978), p. 121.

6. V. N. Kapinos and Yu. A. Medvedev, At. Energ., 46, No. 2, 112 (1979).
7. Z. A. Al'bikov, A. I. Veretennikov, and O. V. Kozlov, Pulsed-Radiation Detectors [in Russian], Atomizdat, Moscow (1978), p. 63.
8. K. K. Shvarts et al., Thermoluminescence Dosimetry [in Russian], Zinatne, Riga (1968), p. 56.

CORRECTIONS TO NEUTRON FLUX MEASUREMENTS BY GOLD FOIL METHOD

G. M. Stukov and I. A. Yaritsyna

UDC 539.125.5.08

We have determined highly accurate corrections to the perturbation of the thermal neutron flux density in water by the gold foil method under specific conditions of measurement. At the same time, we have found the correction to the gold activity measured by the $4\pi\beta-\gamma$ coincidence method for foils of finite thickness when the β-counting efficiency (ε_β) is less than unity. The foils used in the experiment were 20 mm in diameter and of nine different thicknesses from 1.6 to 47 mg/cm^2. The mass of each foil was determined to within 0.05%. A foil of each thickness was irradiated twice (with and without a cadmium cover 0.7 mm thick) in a tank of distilled water with a neutron source at the center. The activity of the foils was measured with a standard $4\pi\beta-\gamma$ coincidence counter. The correction to the gold activity $(1+\alpha)$ was first determined as a function of the parameter $f=(1-\varepsilon_\beta)/\varepsilon_\beta$ [1], which was varied by shielding with very thin unactivated gold foils of various thicknesses. This varied ε_β from 85 to 42%. The results of the experiment are shown in Fig. 1. The least-squares method was used to find the required correction to the activity for any value of $(1-\varepsilon_\beta)/\varepsilon_\beta$ (the straight line in Fig. 1). The relation obtained was used later to find the true activity of gold foils in measurements with a $4\pi\beta-\gamma$ coincidence counter.

The specific activity (A_T) of ^{198}Au induced by thermal neutrons was determined for each foil from the usual formula for the cadmium difference, and the required correction for the perturbation for each foil thickness can be calculated from the expression

$$K=A_T/A_0, \tag{1}$$

where A_0 is the specific activity of an infinitely thin foil corresponding to an unperturbed thermal neutron flux density. The value of A_0 can be determined by extrapolating the available values of A_T, to zero foil thickness $t=0$. It is convenient, however, to extrapolate to $t=1/A_T$, since in this case the approximating function is linear, and the least-squares method can be used. In accord with [2] we have

$$K=\frac{A_T}{A_0}=\frac{\bar{\varphi}_0}{2\bar{\mu}at}\frac{1+\varepsilon}{1+(\varphi_0/2)\,g}; \tag{2}$$

$$\frac{\bar{\varphi}_0}{2\mu at}\approx\frac{\varphi_0(\mu at)}{2\mu at}; \tag{3}$$

$$\varphi_0(\mu at)\approx\frac{2\mu at}{1+2\mu at}\ (\text{for } \mu at<1). \tag{4}$$

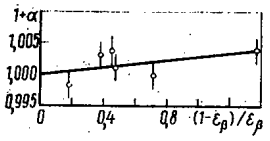

Fig. 1

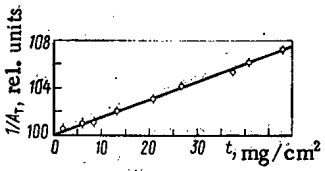

Fig. 2

Fig. 1. Correction to gold activity as a function of $(1-\varepsilon_\beta)/\varepsilon_\beta$.

Fig. 2. Reciprocal of specific activity of gold foil as a function of foil thickness.

Translated from Atomnaya Énergiya, Vol. 48, No. 2, pp. 119-120, February, 1980. Original article submitted June 26, 1979.

0038-531X/80/4802-0145$07.50

Substituting Eqs. (3) and (4) into (2) we obtain

$$1/A_T = (1/A_0) + Bt, \tag{5}$$

where t is the foil thickness and B is a proportionality factor.

Applying Eq. (5), the results were processed by the least-squares method (Fig. 2). The value of A_0 was determined to within 0.1%.

Thus, the correction to the perturbation of the thermal neutron flux density by gold foils in water was determined under conditions frequently encountered in practice, when the flux density varies within the distance between source and foil. The error of this correction is reduced considerably. Thus, e.g., for foils 20 μm (39 mg/cm^2) thick, the thickness most frequently used in measuring neutron fluxes at the UÉN-3, amounts to 0.2%. The decrease in the error of this correction led to a significant increase in the accuracy of the absolute measurement of the neutron flux by the method of activation of gold foils.

LITERATURE CITED

1. A. Baerg, Metrologia, 2, 23 (1966).
2. K. Beckurts and K. Wirtz, Neutron Physics, Springer-Verlag, New York (1964).

DETERMINATION OF THE LANTHANUM, CERIUM, PRASEODYMIUM, AND NEODYMIUM CONTENT OF SOLUTIONS BY AN X-RAY SPECTRAL METHOD USING THE SRF-5 INSTRUMENT

I. M. Krasil'nikov, I. D. Skorova, A. V. Sholomov, P. A. Konstantinov, and A. P. Matyushin

UDC 621.039.66.667

The automatic regulation of processes for the extractive separation of complex mixtures of rare-earth elements (REE) provides for high-speed checking of the amounts of three or four different REE at specified stages of the technological process.

An x-ray spectral method [1] was used for conducting such a check. The measurements were made on the SRF-5 x-ray fluorescent spectrometer on the basis of the K series of the characteristic radiation of the REE, since the small energy values of the characteristic radiation of the L series (4.6-7.6 eV) would have made the high-speed analysis much more difficult [2]. The advantages of using the characteristic radiation of the K series for the analysis of the REE were noted earlier in [3]. In order to avoid the accumulation of "tails" in determining one of the REE (the range of measured concentrations is 0.05-30 g/liter, and the total amount varies from 1 to 300 g/liter), a high resolution is required in the spectrometric device, and the SRF-5 instrument provides such high resolution. Although the SRF-5, in order to take account of the matrix effect, is equipped with an obturator device, which makes it possible to use the standard-and-background method, in the present case it could not be used, since the specific intensity of the signal and the background does not vary uniformly when the composition of the matrix varies. For example, determination of lanthanum, cerium, and praseodymium by the standard-and-background method leads to a deviation of 35-55% between the analysis results and the true values. The study of the components of the background radiation requires separate consideration. However, the relatively high energy of the characteristic radiation of the K series of lanthanum, cerium, neodymium, and praseodymium and the similarity of their absorption characteristics were prerequisites for making corrections in the measurement results by using an estimate for the variation of the absorbing properties of the samples investigated and of the standard specimens.

Such an estimate is made by means of an additional scintillation counter, which records a narrow beam (1.5 mm in diameter) of the primary emission of the x-ray tube and transilluminates the cuvette with the solution

Translated from Atomnaya Énergiya, Vol. 48, No. 2, pp. 120-121, February, 1980. Original article submitted June 25, 1979.

0038-531X/80/4802-0146$07.50

TABLE 1. Coefficient of Variation in the Determination of the Concentration of Various REE by the x-Ray Spectral Method, Taking Account of Matrix Effects, %

Element	Concentration g/liter	Coefficient of variation	Element	Concentration g/liter	Coefficient of variation
Ce	27	4	Nd	0,62	3
La	13	5	Pr	3	3
Nd	8	3		0,22	6

being analyzed. The elctrical signals from the scintillation counter are discriminated by a one-channel amplitude analyzer in the ~40 keV energy range and are transmitted to a counting device. If we take account of the fact that the energy resolution of a scintillation counter with an NaI(Tl) crystal (thickness 10 mm) is 30-40% for an energy of ~35 keV, we can take it that the counter registers radiation with an energy of 30-40 keV. The characteristic radiation of the K_{α_1} lines of cerium, lanthanum, praseodymium, and neodymium falls into this energy range. Thus, using an additional counter, we can determine the variation in the absorptive properties of the samples investigated in the range of energy of the characteristic radiation of the elements being analyzed.

The measurement of the intensity of the K_{α_1} lines of REE on the SRF-5 and the additional transillumination required 2.5 min and 40 sec, respectively, i.e., the total analysis time is not increased.

An analysis of the solutions for the amounts of the listed REE was conducted on the basis of one standard specimen with a known content of each element being analyzed. The concentration of the relevant REE in the sample was calculated by the formula

$$C_{\text{det}} = C_0 B \frac{I_{\text{samp}}}{I_0},$$

where C_{det} is the concentration of the element being determined in the sample; C_0, concentration of the element determined in the standard specimen; B, ratio of the values of the intensity of the radiation which passed through the sample and through the standard specimen, measured with an additional scintillation counter; I_{samp}, intensity of the K_{α_1} line of the determined element in the sample being studied; I_0, intensity of the K_{α_1} line of the element being determined in the standard specimen. The accuracy of the method is characterized by the variation coefficients obtained (Table 1). The lower threshold of sensitivity of the determination of the concentration of lanthanum, cerium, praseodymium, and neodymium, calculated by the 3σ criterion, is 0.02 g/liter.

The above-described method was successfully used in practice in an analytical laboratory and enabled us to carry out high-speed checks without preliminary preparation of the sample (analysis time ~5 min) on the lanthanum, cerium, neodymium, and praseodymium content in liquid products of the extractive separation of REE. This method can be used for determining the amounts of other REE, in particular samarium, europium, and gadolinium, which makes possible the high-speed checking of the entire technological process of REE separation.

LITERATURE CITED

1. S. M. Barskii and N. I. Komyak, Apparatura i Metody Rentgenovskogo Analiza, No. 11, 76 (1972).
2. G. I. Rekhkolainen and A. P. Kosinov, ibid., No. 10, 134.
3. G. V. Bondarenko and M. A. Blokhin, Zavod. Lab., No. 4, 531 (1967).

AXIAL STABILITY OF VVÉR-1000 REACTOR WITH CONTROL WITH MINIMUM STANDARD DEVIATION

A. M. Afanas'ev and B. Z. Torlin

UDC 621.039.56

The xenon height stability of the neutron field in the VVÉR-1000 reactor with the rods of the automatic controller (AC) inserted to various depths and with pickups at various locations was studied in [1]. The present paper gives the results of investigations on the stability of a reactor which, in addition to an automatic controller, has a height distribution regulator (HDR) based on an auxiliary control rod (CR) or a special shortened absorption rod (SAR). The HDR was controlled by using either a special ionization chamber (IC), generating an imbalance signal which sets the CR in motion, or two ionization chambers whose difference signal causes a displacement of the SAR. Since data from numerous pickups can be used to control the height field of the VVÉR-1000, it is of interest to analyze how this would affect the stability of the reactor.

The analysis was carried out with the improved IRINA programs [2, 3], making it possible to calculate the influence function of each CR or SAR on the neutron field as well as to calculate the complex values of the frequencies of xenon oscillations over a wide range of variation of their real parts. In the calculations we used the same reactor parameters as in [1] and also deviated somewhat from the calculated [4] power coefficients of reactivity (local α_l and integral α_i) to reduce their absolute values. The resulting decrease in stability made the reactor more sensitive to the effects studied and permitted a more definite observation of the tendencies in the behavior of the neutron field under a change in the number or position of the pickups.

The reactor stability will be characterized by the die-away time T of the least stable (first) axial normal mode [2]. In all the examples considered the dying-away process was oscillatory [2]. The period of the oscillations varied from variant to variant and averaged 33 h (with a spread of ±5 h). The algorithm for the operation of the rods was determined by the requirement that the following condition be fulfilled:

$$\sum_{i=1}^{M} a_{ji}\varphi_i = 0, \quad j = 1, 2, \ldots, N, \tag{1}$$

where M and N, respectively, are the numbers of pickups and rods; φ_i, deviation of the neutron flux from the steady-state value at the location of the i-th pickup; and a_{ji}, weighting factors. It can be shown that $\min \sum_{i=1}^{M} \varphi_i^2$, i.e., the minimum standard deviation of the neutron flux from its steady-state distribution is attained if for a_{ij} we take Ψ_{ji}, the value of the influence function of the j-th rod at the site of the i-th pickup. It is precisely this kind of control of a neutron field with an AC and SAR that Table 1 gives the values of T for various numbers of pickups, uniformly arranged over the height of the reactor core. The end of the AC rod and the center of the SAR, whose absorbing part is equal to half the height of the reactor core, are at the middle of the reactor.

TABLE 1. Values of T for Optimal Control with AC and SAR, h

α_l	α_i	$M = 3$	$M = 4$	$M = 8$	$M = 3$ *
—0,005	—0,0045	17,2	11,2	11,3	29,0
—0,005	0	17,9	11,0	10,6	55,2
—0,002	0	23,1	12,4	10,7	—36,4 †

*Here and in Table 2 the pickups were located at 1/3, 1/2, and 2/3 of the height of the reactor core.

†Here and in Table 2, the time constant of the oscillations of the neutron field.

Translated from Atomnaya Énergiya, Vol. 48, No. 2, pp. 121-122, February, 1980. Original article submitted July 9, 1979.

0038-531X/80/4802-0148$07.50

TABLE 2. Values of T for Nonoptimal Control with AC and SAR, h

α_l	α_i	$M = 3$	$M = 4$	$M = 7$	$M = 3$ *
—0,005	—0,0045	10,5	—	—	28,6
—0,005	0	11,2	9,0	8,0	30,4
—0,002	0	15,6	10,8	9,1	—69,4 †
0	0	23,5	—	—	—

TABLE 3. Values of T for Optimal Control with Two CR, h

α_l	α_i	$M = 2$	$M = 5$	$M = 3$
—0,005	—0,0045	10,9	8,3	7,2
—0,005	0	11,5	8,3	7,1
—0,002	0	17,4	9,2	7,7

Table 2 gives the values of T for the same variants as in Table 1, but here the weighting factors in Eq. (1) for AC were taken to be unity instead of Ψ_{ji}. The data of Table 2 permit the conclusion that increasing the number of pickups not only can improve the quality of the transient process, but can also have a positive influence on the speed of the control system. The data in the last columns of Tables 1 and 2 are interesting in that they were obtained with the pickup arranged most closely to each other in the central part of the reactor core. It is easily seen that this resulted in a loss of stability. When $\alpha_l = -0.002$, the reactor even proved to be unstable. However, if in this variant the central pickup is disconnected, the system immediately becomes stable with an oscillation die-away time of T = 18.9 h. The system can be made even more stable if the remaining pickups are moved to the edges of the reactor. Thus, with the pickups placed at 1/4 and 3/4 of the height of the reactor core, the die-away time is reduced to 6.9 h. An example of an unsuccessful use of pickups was mentioned in [1]: the AC rod is actuated by the IC placed in the central part of the reactor core; the SAR is controlled by a difference signal from the upper and lower IC. In this case, even with $\alpha_l = -0.005$ and $\alpha_i = -0.0045$ the system is unstable with a xenon-oscillation time constant of 44.1 h.

In conclusion, we look briefly at the stability characteristics of a reactor with two CR which ensure control of the neutron field with minimum standard deviation and which are placed at 1/3 and 2/3 of the height of the reactor core. Table 3 gives the die-away time T for variants with two and five pickups, arranged uniformly over the height, and with three pickups, one of which is at the center and the other two are at a distance of 1/6 of the core height from the core edges. The data of Table 3 also indicate that increasing the number of pickups uniformly arranged over the height is conducive to improving the stability and that a noticeable effect in enhancing the stability can be achieved by moving the pickups closer to the edges of the reactor core.

LITERATURE CITED

1. A. M. Afanas'ev and B. Z. Torlin, At. Energ., 44, No. 6, 530 (1978).
2. A. M. Afanas'ev and B. Z. Torlin, At. Energ., 44, No. 6, 487 (1978).
3. A. M. Afanas'ev and B. Z. Torlin, Preprint ITÉF-2, Moscow (1978).
4. I. Ya. Emel'yanov, P. A. Gavrilov, and B. N. Seliverstov, Control and Safety of Nuclear Power Reactors [in Russian], Atomizdat, Moscow (1975).

YIELDS OF ^{181}Re, ^{182m}Re, ^{182}Re, ^{183}Re, ^{184m}Re, ^{184}Re, AND ^{186}Re IN THE BOMBARDMENT OF TUNGSTEN BY PROTONS AND DEUTERONS, AND TANTALUM BY α PARTICLES

P. P. Dmitriev and G. A. Molin

UDC 539.172.12

Radionuclides of rhenium are obtained with a high yield in "carrier-free" form in the bombardment of tungsten by protons and deuterons, and tantalum by α particles. We have measured the dependence of the ^{181}Re, ^{182m}Re, ^{182}Re, ^{183}Re, ^{184m}Re, and ^{184}Re yields on particle energy for a thick tungsten target bombarded with protons and deuterons with energies up to 22.3 MeV, and tantalum bombarded with α particles with energies up to 43 MeV. Theoretical yield curves were calculated for ^{186}Re. In measuring the yields of radionuclides the following values of half-lives, energies, and quantum yields of γ lines were adopted: ^{181}Re (20 h, 365.5 keV, 56.4% [1]), ^{182m}Re (64 h, 1121.28 keV, 23% [2]), ^{182}Re (12.7 h, 1121.28 keV, 31.9% [2]), ^{183}Re (700 days, 291.72 keV, 3.31% [3]), ^{184m}Re (165 days, 920.93 keV, 8.3% [4]), ^{184}Re (38 days, 792.07 keV, 37.4% [4]). The half-lives of the radionuclides are convenient for research and applications.

Stacks of foils were bombarded in the deflected beam of the FÉI cyclotron. The tungsten foil was 98 mg/cm^2 in thickness, and the tantalum 36 mg/cm^2. The energy of the particles after passing through each foil was determined from data in [5]. The average energy of the particles was determined to within 1.5% by

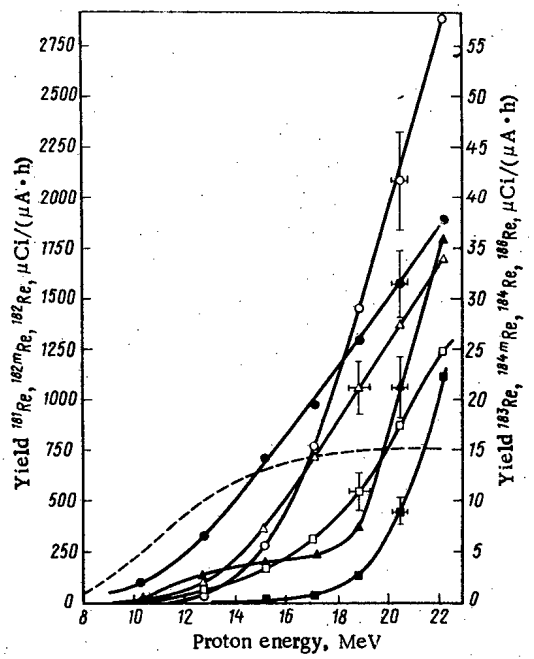

Fig. 1

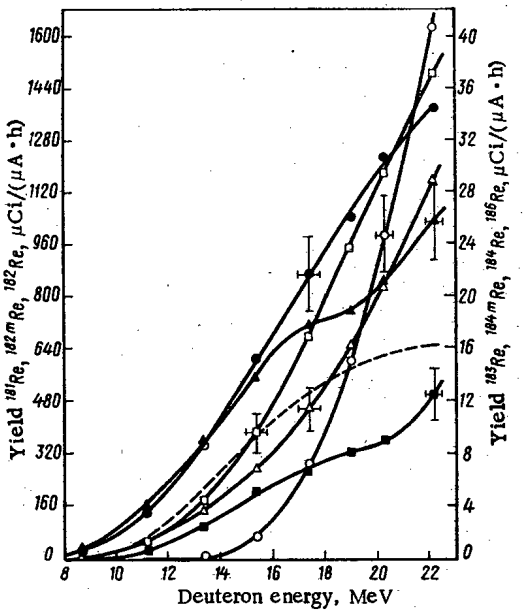

Fig. 2

Fig. 1. Yields of ^{181}Re, ^{182m}Re, ^{182}Re, ^{183}Re, ^{184m}Re, ^{184}Re, and ^{186}Re as functions of proton energy for a thick tungsten target: ○) ^{181}Re; □) ^{182m}Re (× 5); ●) ^{182}Re; △) ^{183}Re; ■) ^{184m}Re (× 25); ▲) ^{184}Re; — — —) ^{186}Re.

Fig. 2. Yields of ^{181}Re, ^{182m}Re, ^{182}Re, ^{183}Re, ^{184m}Re, ^{184}Re, and ^{186}Re as functions of deuteron energy for a thick tungsten target: ○) ^{181}Re (× 2); □) ^{182m}Re (× 5); ●) ^{182}Re; △) ^{183}Re; ■) ^{184m}Re (× 20); ▲) ^{184}Re; — — —) ^{186}Re (: 10).

Translated from Atomnaya Énergiya, Vol. 48, No. 2, pp. 122-124, February, 1980. Original article submitted July 9, 1979.

0038-531X/80/4802-0150$07.50

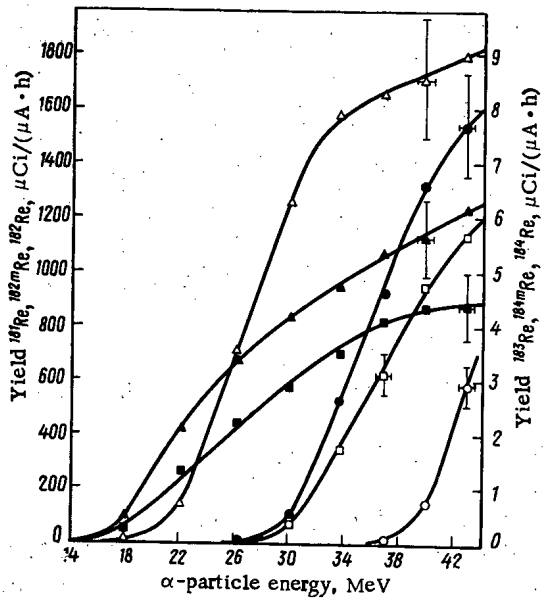

Fig. 3. Yields of ^{181}Re, ^{182m}Re, ^{182}Re, ^{184m}Re, and ^{184}Re as functions of α-particle energy for a thick tantalum target: ○) ^{181}Re (×2); ○) ^{182m}Re (×5); ●) ^{182}Re; △) ^{183}Re; □) ^{184m}Re (×100); △) ^{184}Re (×10).

measuring the absorption of the beam current in aluminum. The radionuclides were identified by γ energies and half-lives. The activity of the nuclides was measured by the photopeaks of selected γ lines (in measuring the activity of ^{184}Re the small contribution of the ^{184m}Re – ^{184}Re decay branch was taken into account). The photopeaks were measured on a γ spectrometer with a DGDK-50 A1 Ge(Li) detector having a resolving power (FWHM) of 3.2 keV at 1332.51 keV (^{60}Co) and 1.7 keV at 122.06 keV (^{57}Co). The photoefficiency of the detector was found with a set of OSGI radiators. The integrated beam current was determined from the ^{65}Zn activity in copper monitor foils 18 mg/cm^2 thick. From an analysis of the data of [6-8] and our measurements of the relative behavior of the excitation functions, the following values of the monitor reactions were adopted:

$$^{65}\mathrm{Cu}(pn)^{65}\mathrm{Zn},\ \sigma = 46\ \mathrm{mb},\ E_p = 22.5\ \mathrm{MeV};$$
$$^{65}\mathrm{Cu}(d2n)^{65}\mathrm{Zn},\ \sigma = 525\ \mathrm{mb},\ E_d = 22.5\ \mathrm{MeV};$$
$$^{63}\mathrm{Cu}(\alpha,\ pn + 2n),\ \sigma = 325\ \mathrm{mb},\ E_\alpha = 44\ \mathrm{MeV}.$$

Figures 1-3 show the experimental values of the nuclide yields. The error in measuring the yields is 12-14%, and is due mainly to systematic errors in measuring the activity and integrated current. Strong interference of the ^{182}Re γ lines of nearly the same energy prevented the measurement of the ^{186}Re activity by the photopeak of the 137.15 keV γ lines, and therefore the ^{186}Re yield curves were calculated theoretically as in [9] (r_0 = 1.3 fermi).

When tungsten is bombarded with protons and deuterons ^{186m}Re ($T_{1/2} = 2.0 \cdot 10^5$ years) is formed also. The spins of ^{186m}Re and ^{184m}Re are both 8^+, and an estimate of the ^{186m}Re yield from the ^{184m}Re yield [only for the (p, n) and (d, 2n) reactions] gives a ^{186m}Re yield of $2.7 \cdot 10^{-8}$ μCi/μAh for protons and $8.9 \cdot 10^{-7}$ μCi/μA·h for deuterons, both at 22 MeV.

Some data on yields and cross sections with the formation of rhenium nuclides are given in [10-13]. Hermes et al. [10] measured the excitation functions of the ^{181}Ta(α, 2n)^{183}Re reaction up to E_α = 48 MeV, ^{181}Ta(α, 3n)$^{182(m+g)}$Re up to E_α = 58 MeV, and ^{181}Ta(α, 4n)^{181}Re up to E_α = 80 MeV. Integration of the excitation functions gives 10.8 and 263 μCi/μAh, respectively, for the ^{183}Re and ^{181}Re yields at E_α = 43 MeV, which are in satisfactory agreement with our results. At E_α = 80 MeV the ^{181}Re yield is 2900 μCi/μA·h. Since the (α, 3n) cross sections for ^{182m}Re and ^{182}Re are not reported separately in [10], we cannot compare these data with ours.

The excitation functions of the ^{186}W(d, 2n)^{186}Re reaction were measured by Pement and Wolke [11] at energies up to 14 MeV, and by Nassiff and Münzel [12] for energies up to 16.7 MeV. The values of the cross sections in [12] are approximately twice as large. Our theoretical calculations are in good agreement with data in [11]. For example, the cross section at the maximum of the excitation function is 380 mb according to our data, and 350 and 647 mb, respectively, according to [11, 12]. Nassiff and Münzel measured the activity

of ^{186}Re by the photopeak E_γ = 137.15 MeV, and the overestimate is possibly related to the background of ^{182}Re γ lines of nearly the same energy. Pement and Wolke bombarded a W target enriched to 97.2% in ^{186}W, and measured the ^{186}Re activity by β radiation. The yield curves for ^{183}Re and ^{184}Re in the bombardment of tungsten by 22 MeV protons and deuterons given in [13] differ appreciably from our results. It is difficult to indicate the reasons for these differences, since it is stated in [13] that the values of the quantum yields of γ lines in the measurements of the activity of ^{183}Re and ^{184}Re were taken from [14], but only the relative intensity of the γ radiation for ^{183}Re and ^{184}Re is given in [14].

The authors thank Z. P. Dmitrieva for performing the calculations.

LITERATURE CITED

1. N. G. Gusev and P. P. Dmitriev, Quantum Radiation of Radioactive Nuclides [in Russian], Atomizdat, Moscow (1977).
2. M. Schmorak, Nucl. Data Sheets, 14, 559 (1975).
3. A. Artna-Cohen, Nucl. Data Sheets, 16, 267 (1975).
4. M. Martin and P. Stelson, Nucl. Data Sheets, 21, 1 (1977).
5. C. Williamson, J. Boujot, and J. Picard, Rapport CEA-R, 3042 (1966).
6. P. P. Dmitriev et al., At. Energ., 24, 279 (1968); R. Colle et al., Phys. Rev., C9, 1819 (1974).
7. P. P. Dmitriev and N. N. Krasnov, At. Energ., 18, 184 (1965); C. Fulmer and I. Williams, Nucl. Phys., A155, 40 (1970); D. Williams and J. Irvine, Phys. Rev., 130, 265 (1963).
8. N. Porile and D. Morrison, Phys. Rev., 116, 1193 (1959); F. Houck and J. Miller, Phys. Rev., 123, 231 (1961).
9. P. P. Dmitriev et al., At. Energ., 32, 426 (1972).
10. F. Hermes et al., Nucl. Phys., A228, 165 (1974).
11. F. Pement and R. Wolke, Nucl. Phys., 86, 429 (1966).
12. S. Nassiff and H. Münzel, Radiochim. Acta, 19, 97 (1973).
13. I. O. Konstantinov et al., At. Energ., 44, 183 (1978).
14. W. Bowman and K. MacMurdo, Atomic Data, Nucl. Data Tables, 13, 285 (1974).

NEW RUSSIAN JOURNALS

IN ENGLISH TRANSLATION

BIOLOGY BULLETIN
Izvestiya Akademii Nauk SSSR, Seriya Biologicheskaya

The biological proceedings of the Academy of Sciences of the USSR, this prestigious new bimonthly presents the work of the leading academicians on every aspect of the life sciences—from micro- and molecular biology to zoology, physiology, and space medicine.
Volume 7, 1980 (6 issues) $195.00

SOVIET JOURNAL OF MARINE BIOLOGY
Biologiya Morya

Devoted solely to research on marine organisms and their activity, practical considerations for their preservation, and reproduction of the biological resources of the seas and oceans.
Volume 6, 1980 (6 issues) $115.00

WATER RESOURCES
Vodnye Resursy

Evaluates the water resources of specific geographical areas throughout the world and reviews regularities of water resources formation as well as scientific principles of their optimal use.
Volume 7, 1980 (6 issues) $215.00

HUMAN PHYSIOLOGY
Fiziologiya Cheloveka

A new, innovative journal concerned *exclusively* with theoretical and applied aspects of the expanding field of human physiology.
Volume 6, 1980 (6 issues) $195.00

SOVIET JOURNAL OF BIOORGANIC CHEMISTRY
Bioorganicheskaya Khimiya

Features articles on isolation and purification of naturally occurring, biologically active compounds; the establishment of their structure, methods of synthesis, and determination of the relation between structure and biological function.
Volume 6, 1980 (12 issues) $245.00

SOVIET JOURNAL OF COORDINATION CHEMISTRY
Koordinatsionnaya Khimiya

Describes the achievements of modern theoretical and applied coordination chemistry. Topics include the synthesis and properties of new coordination compounds; reactions involving intraspheral substitution and transformation of ligands; complexes with polyfunctional and macromolecular ligands; complexing in solutions; and kinetics and mechanisms of reactions involving the participation of coordination compounds.
Volume 6, 1980 (12 issues) $255.00

THE SOVIET JOURNAL OF GLASS PHYSICS AND CHEMISTRY
Fizika i Khimiya Stekla

Devoted to current theoretical and applied research on three interlinked problems in glass technology; the nature of the chemical bonds in a vitrifying melt and in glass; the structure-statistical principle; and the macroscopic properties of glass.
Volume 6, 1980 (6 issues) $145.00

LITHUANIAN MATHEMATICAL JOURNAL
Litovskii Matematicheskii Sbornik

An international medium for the rapid publication of the latest developments in mathematics, this quarterly keeps western scientists abreast of both practical and theoretical configurations. Among the many areas reported on in depth are the generalized Green's function, the Monte Carlo method, the "innovation theorem," and the Martingale problem.
Volume 20, 1980 (4 issues) $175.00

PROGRAMMING AND COMPUTER SOFTWARE
Programmirovanie

Reports on current progress in programming and the use of computers. Topics covered include logical problems of programming; applied theory of algorithms; control of computational processes; program organization; programming methods connected with the idiosyncrácies of input languages, hardware, and problem classes; parallel programming; operating systems; programming systems; programmer aids; software systems; data-control systems; IO systems; and subroutine libraries.
Volume 6, 1980 (6 issues) $115.00

SOVIET MICROELECTRONICS
Mikroelektronika

Reports on the latest advances in solutions of fundamental problems of microelectronics. Discusses new physical principles, materials, and methods for creating components, especially in large systems.
Volume 9, 1980 (6 issues) $160.00

Send for Your Free Examination Copy

PLENUM PUBLISHING CORPORATION, 227 West 17th Street, New York, N.Y. 10011
In United Kingdom: 88/90 Middlesex Street, London E1 7EZ England
Prices slightly higher outside the U.S. Prices subject to change without notice.